Understanding variability and drivers of seawater inorganic carbonate chemistry across temperate nearshore marine systems in the U.S. Mid-Atlantic

Carly LaRoche
Charlottesville, VA

B.S. Environmental Science, American University, 2018

A Dissertation presented to the Graduate Faculty of the University of Virginia in Candidacy for the Degree Doctor of Philosophy

Department of Environmental Sciences
University of Virginia
May 2024

Committee:
Scott Doney (advisor)
Peter Berg
Emily Rivest
Matt Reidenbach
Lisa Colosi-Peterson

Table of Contents

Abstract

In nearshore marine ecosystems, extreme seawater inorganic carbonate system variability is regulated by biogeochemical, hydrodynamic, and thermodynamic drivers. Rising CO_2 emissions and other anthropogenic perturbations have led to shifting coastal carbon cycles. Given a backdrop of global change, resolving regional uncertainties in drivers and variability of seawater carbonate chemistry in nearshore systems can improve out understanding of how these systems fit into critical climate issues. This dissertation will discuss the results of three projects investigating coastal carbonate chemistry at different spatial and temporal scales in the U.S. Mid-Atlantic. (1) A publicly available inventory of Mid-Atlantic seawater carbonate system sampling sites, including all locations sampling pCO_2, pH, Dissolved Inorganic Carbon (DIC), and Total Alkalinity (TA), was created to better understand the spatial distribution of regional monitoring. (2) Seasonal and spatial DIC and TA dynamics were assessed across spatially diverse sites in the Virginia Coast Reserve (VCR). Drivers of patterns were assessed across lagoonal, inlet, and marsh adjacent sites. (3) South Bay in the VCR was examined at a higher temporal and spatial frequency to determine pH patterns in a seagrass meadow and a marsh influenced lagoon.

Acknowledgements

I am extremely grateful to the many people who have provided guidance, support, and community throughout my time as a student in the Department of Environmental Sciences at UVA. I'd like to first thank my advisor, Scott Doney, for his wisdom and guidance as I navigated new skills and research questions. I am also deeply appreciative of the support of my committee, Peter Berg, Emily Rivest, Matt Reidenbach, and Lisa Colosi-Peterson.

During my time at UVA, it was a privilege to work alongside and learn from other VCR-LTER researchers. Thank you also to VCR-LTER staff past and present. Cora, Donna, Sophia, Tom, Jonah, and Buck: thank you for your endless support in and out of the field. I will forever have fond memories of water quality wings and times spent at the CRC because of the welcoming community you all have worked to foster there. I'm also extremely grateful for my field-mates, including Lauren Brideau, Luke Groff, and Paola Granados. A special shoutout and thank you goes to Kayleigh Granville, who spent countless hours in South Bay with me.

I'm extremely grateful for my experiences with the MACAN community. Thank you to Avalon Bristow, Kirstin Wakefield, and Janet Reimer, for your guidance and support. A huge thank you to past and present collaborators at VIMS, including Hunter Walker, Iris Anderson, and Emily Rivest (and other members of the Rivest Lab!), who all patiently helped me through field preparations and lab work. I'd also like to acknowledge the guidance and unwavering support of past and present Doney Lab members. Thank you to Emma Brahmey, Mary Stack, Joy Ferenbaugh, Liz Tatham, Darren McKee, Eleanor Lawrence, Wiley Wolfe, Alana Menendez, and Savannah Hartman. Overall, the graduate student community I found in the Department of Environmental Sciences is unmatched: thank you especially to my friends Madeline Miles and Zoe Bergman who have been by my side throughout this journey.

Finally, I couldn't have done this without the love and encouragement from my family, friends, and partner, Mac. I am eternally grateful for your support.

Chapter 1: Introduction: Seawater inorganic carbonate chemistry in the coastal zone

1.1 Introduction

Brought on by anthropogenic CO_2 emissions, atmospheric CO_2 and oceanic pCO_2 have been rising in consort since the Industrial Revolution (Gruber et al., 2023; Jewett and Romanou, 2017). Air-sea CO_2 gas exchange mediates the transfer of excess atmospheric carbon dioxide into the surface ocean, equilibrating CO_2 concentrations between the sea surface and the overlying atmosphere (Wanninkhof et al., 2014). The ocean is responsible for the uptake of 30-40% of anthropogenic CO_2 emissions to date (Le Quéré et al., 2018). The large inorganic carbon storage capacity of the ocean is a consequence of carbon dioxide's high propensity for dissociation in seawater. In accordance with dissociation equilibria, CO_2 entering the water column is distributed across three inorganic species (Zeebe and Wolf-Gladrow, 2001). While ocean CO_2 absorption mitigates climate change by decreasing atmospheric CO_2 concentrations, it also alters seawater inorganic carbonate chemistry (Doney et al., 2009; Gattuso et al., 2015). Alongside increasing the partial pressure of carbon dioxide, (pCO_2,) surface ocean pH has fallen 0.1 units since the Industrial Revolution, reflecting a 30% increase in acidity (Jewett and Romanou, 2017; Khatiwala et al., 2013).

Encompassing estuaries, tidal wetlands, and coastal bays, the nearshore coastal marine environment exhibits significant spatial and temporal seawater carbonate system variability from varied natural and anthropogenic influences (Cai et al., 2011; Lowe et al., 2019; Wallace et al., 2014). Heterogeneity in seawater carbonate chemistry is introduced via biogeochemical processes, air-sea exchange, lateral exchange, freshwater inputs, and gradients in physical seawater properties (Feely et al., 2010; Wallace et al., 2014). In biogeochemical hotspots like intertidal salt marshes and subtidal seagrass meadows, net ecosystem metabolism can be a driving force in determining local seawater carbonate chemistry conditions (Gattuso et al., 1999; Lowe et al., 2019; Wang et al., 2018). Anthropogenic disturbances like land-use change and nutrient pollution result in further alterations to coastal carbon cycles (Bauer et al., 2013). Agricultural runoff and wastewater effluent that enter the coastal ocean bring excess nutrients

like nitrogen and phosphorus with them, with subsequent eutrophication resulting in hypoxic and acidic conditions (Paerl et al., 2018; Wallace et al., 2014).

1.2 Seawater Carbonate Chemistry

The seawater inorganic carbonate system acts as a key control on overall seawater acid-base chemistry. Four parameters are used to characterize the seawater carbonate system: dissolved inorganic carbon (DIC), total alkalinity (TA), pH, and the seawater partial pressure of CO_2 (pCO_2) (Dickson et al., 2007). By measuring any two carbonate system parameters alongside salinity and temperature, derivation of the other two parameters and saturation state of calcium carbonate (Ω) is possible (Dickson, 2010). DIC is inclusive of aqueous CO_2 ($CO_2(aq)$), carbonic acid (H_2CO_3), bicarbonate (HCO_3^-), and carbonate ions (CO_3^{2-}), providing the sum of total inorganic carbon acid-base species in the water column (Zeebe and Wolf-Gladrow, 2001). Speciation of carbon dioxide is controlled by a series of acid-base equilibrium equations (Zeebe and Wolf-Gladrow, 2001).

Transfer of CO_2 across the air-water interface is controlled by the solubility equilibrium between concentrations of carbon dioxide gas [CO_2(g)] in the air and aqueous carbon dioxide [CO_2(aq)] in the water (Equation 1) (Dickson, 2010). Physical water properties, including salinity and temperature, alter the solubility of CO_2 in water, wherein CO_2 is more soluble in colder, fresher water (Zeebe and Wolf-Gladrow, 2001).

$$CO_2(g) \leftrightarrow CO_2(aq) \qquad \text{Equation 1}$$

Once dissolved in seawater, CO_2(aq) can undergo a series of acid-base dissociation reactions such that chemical equilibria is maintained across concentrations of three main inorganic forms of carbon dioxide: CO_2, bicarbonate (HCO_3^-), and carbonate ions (CO_3^{2-}). First, hydration of CO_2(aq) produces carbonic acid (H_2CO_3) (Zeebe and Wolf-Gladrow, 2001). Because concentrations of H_2CO_3 are very small compared to [CO_2(aq)] at typical seawater pH levels, the two are often combined and referred to together as CO_2 (as used in Equation 2) (Dickson, 2010; Zeebe and Wolf-Gladrow, 2001).

$$CO_2 + H_2O \rightleftharpoons HCO_3^- + H^+ \qquad \text{Equation 2}$$

The addition of CO_2 to seawater with a typical pH of about 8 favors a forward reaction of Equation 2, resulting in increased $[HCO_3^-]$ and hydrogen ion concentrations ($[H^+]$). The increased availability of H^+ ions promotes the reverse reaction of Equation 3, reducing $[CO_3^{2-}]$ and increasing $[HCO_3^-]$.

$$HCO_3^- \rightleftharpoons CO_3^{2-} + H^+ \qquad \text{Equation 3}$$

Ultimately, increased concentrations of H^+ ions result in lower pH, where $pH = -\log_{10}[H^+]$, and more acidic conditions (Equation 4).

$$pH = -log_{10}\,[H^+] \qquad \text{Equation 4}$$

Inorganic carbon species participate in other important reactions occurring in the ocean. One such reaction is the formation of calcium carbonate solids ($CaCO_3$), which is produced by the bonding of CO_3^{2-} and calcium ions (Ca^{2+}). In the marine environment, calcifying organisms use mineral forms of $CaCO_3$ to build skeletons and shells. However, under heightened seawater CO_2 conditions, H^+ ions act to lower carbonate ion concentrations (Equation 3), resulting in lower saturations of calcium carbonate (Dickson, 2010). The saturation state (Ω) reflects $CaCO_3$ solubility where K_{sp} is the equilibrium coefficient specific for each of the various carbonate mineral forms, including amorphous calcium carbonate, aragonite, and calcite (Dickson, 2010).

$$\Omega = \frac{[CO_3^{2-}]\,[Ca^{2+}]}{K_{sp}} \qquad \text{Equation 5}$$

If $\Omega > 1$, calcium carbonate is supersaturated in the water column for that mineral form and precipitation of solid $CaCO_3$ is favorable. When $\Omega < 1$, dissolution of calcium carbonate is thermodynamically favorable. A Ω value of 1 represents a thermodynamic threshold, but biological thresholds at which organisms experience detrimental effects to growth and development often occur at Ω values above 1. Because different species and life stages utilize specific mineral forms of calcium carbonate, saturation state is expressed in terms of those mineral forms (i.e., aragonite saturation state, ΩAr; calcite saturation state, ΩCa).

As the sum of proton donors subtracted from the sum of proton acceptors, total alkalinity reflects the acid neutralizing capacity of a solution (Middleburg et al., 2020). Dickson (1981) defined alkalinity in terms of titration, where total alkalinity is equal to the moles of hydrogen ions required to match the moles of excess proton acceptors. In seawater, it is dictated primarily by the concentrations of carbonate and borate acid-base species (Equation 6), but also can include minor contributions from other acid-base systems (Equation 7) (Dickson, 1981; Middleburg et al., 2020).

$$TA = [HCO_3^-] + 2[CO_3^{2-}] + [B(OH)_4^-] + [OH^-] - [H^+] \quad \text{Equation 6}$$

$$TA = [HCO_3^-] + 2[CO_3^{2-}] + [B(OH)_4^-] + [OH^-] + [HPO_4^{2-}] + 2[PO_4^{3-}] + [H_3SiO_4^-] + [NH^3] + [HS^-] + 2[S^{2-}] - [H^+] - [HF] - [HSO_4^-] - [H_3PO_4] \quad \text{Equation 7}$$

In addition to inorganic acid-base systems, organic alkalinity has been observed as an important component of total alkalinity, especially in the nearshore marine environment (Song et al., 2020). Organic alkalinity comprises a diverse group of proton accepting dissolved organic compounds, which can be either terrestrial or marine in origin (Hu, 2020; Ko et al., 2016). Substantial contributions of organic alkalinity to TA have been observed in estuaries and waters adjacent to salt marshes (Cai et al., 1998; Song et al., 2020).

When TA and DIC are added or removed from seawater, the process is accompanied by resultant changes in pH and pCO_2 where the system's initial conditions influence the direction and magnitude of change (often depicted in Deffeyes diagrams, see Middleburg et al. (2020)). Well buffered seawater, with a high ratio of TA:DIC, is less sensitive to carbonate system perturbations, resulting in lower overall change to pH and pCO_2 in response to alterations in DIC and TA (Soetaert et al., 2007). Below, I will explore the influence of several processes that exert control on oceanic DIC and TA fluctuations: 1) lateral exchange of DIC and TA between distinct coastal ecosystems and 2) biogeochemical processes that produce and consume DIC and TA, with a focus on salt marsh and seagrass ecosystems.

1.2.1 Lateral Transport

Lateral flux of inorganic carbon and alkalinity between neighboring coastal ecosystems is driven by rivers, hydraulic gradients, currents, and tides (Najjar et al., 2018). Freshwater flowing from terrestrial to marine environments can enter the coastal ocean via riverine or groundwater inputs (Santos et al., 2012). Freshwater inputs can impact the carbonate system by decreasing salinity or by adding inorganic carbon and rock-weathering products into the coastal ocean. If groundwater is high in alkalinity relative to DIC, large inputs to the coastal ocean would increase the buffering capacity of the coastal carbonate system. Alternatively, low alkalinity freshwater inputs can exacerbate coastal acidification (Rheuban et al., 2019). Elsewhere in the nearshore coastal zone, tidal exchange and currents promote transfer of water between various ecosystems with distinct chemical signatures (Wang et al., 2016).

1.3 Biogeochemical Influences

Biogeochemical processes like aerobic and anaerobic respiration, primary production, redox processes, and dissolution/precipitation of $CaCO_3$, all directly impact DIC and TA concentrations in the water column (Soetaert et al., 2007; Yin et al., 2024). Ecosystem metabolism can exert control on local seawater carbonate chemistry, with net effects dependent on the balance between heterotrophy and autotrophy (Lowe et al., 2019). Photosynthetic uptake of CO_2 by autotrophs results in a reduction of DIC and an increase pH whereas respiration results in an increase in DIC and subsequent decrease in pH (Soetaert et al., 2007). Biocalcification produces in a net decrease in TA and DIC in a 2:1 ratio (Zeebe and Wolf-Gladrow, 2001). Other biogeochemical processes like nitrification, denitrification, sulfate reduction, and more, produce variable effects on DIC and TA (Soetaert et al., 2007). As net ecosystem metabolism fluctuates in accordance with diel cycles, nutrient and light availability, and seasonal patterns, so too does its effect on the seawater carbonate system (Lowe et al., 2019; Ricart et al., 2021a).

"Carbonate weather" describes the changes to the seawater carbonate system that occur on time scales relevant to marine organisms (Waldbusser and Salisbury, 2014). For species vulnerable to acidification, the magnitude, frequency, and duration of high pCO_2, low pH events all dictate their ultimate biological response. While long-term climatic changes like globally declining surface ocean pH are a constant press on marine ecosystems, carbonate weather

comprises more frequent pulse events that widely vary the range of local carbonate conditions (Waldbusser and Salisbury, 2014). Large shifts in seawater carbonate chemistry can occur over tidal cycles or diurnal and seasonal patterns of net community production (Cyronak et al., 2018; Wang et al., 2016). Tidal cycles can facilitate inorganic carbon, alkalinity, and nutrient transport between nearshore ecosystems, altering the coastal carbonate system (Santos et al., 2019; Cai et al. 2003). Additionally, tidal stages can dilute or concentrate locally generated biogeochemical signals (Cyronak et al., 2018). For example, benthic respiration that adds DIC to the water column would be exacerbated by a low tide but abated by a high tide because the excess DIC and increase in hydrogen ions would become more dilute under increased water height (Cyronak et al., 2018).

1.3.1 Intertidal Salt Marshes

Relative to their small spatial extent, intertidal salt marshes are important contributors to nearshore coastal carbon cycles (Najjar et al., 2018). As biological hotspots hosting a multitude of primary producers, heterotrophs, and decomposers, salt marsh systems facilitate the production and consumption of DIC and TA (Wang and Cai, 2004; Wang et al., 2016). Both organic and dissolved inorganic forms of marsh-derived carbon and alkalinity can follow several pathways of lateral exchange, resulting in delivery of high DIC and or TA water to adjacent coastal waters. Although extensive research has been done on the subject of marsh carbon pathways, uncertainties remain regarding the quantity and direction of marsh organic and inorganic carbon (Najjar et al., 2018; Wang et al., 2018). Due to complex biogeochemical controls and high spatiotemporal heterogeneity, salt marsh seawater inorganic carbonate chemistry dynamics require further characterization (Wang et al., 2016; Wang et al., 2018; Wallace et al., 2021). Salt marshes are also some of the most vulnerable ecosystems in the world, experiencing sharp declines in extent due to human activities and climate change. In the past 100 years alone, U.S. salt marshes have experienced areal losses of 50-80%, with the Gulf Coast experiencing the highest rates of marsh degradation (Deegan et al., 2012; Russi et al., 2013). As sea level rise, erosion, and changing climate conditions continue to alter the integrity of salt marshes, the quantity and pathways of marsh carbon transport will likely change as well (Ganju et al., 2019; Schiebel et al., 2019).

Organic and inorganic forms of alkalinity and carbon are generated through numerous biogeochemical pathways in salt marshes (Eldridge and Cifuentes, 2000). Despite high rates of primary productivity, temperate salt marsh systems are typically characterized as net heterotrophic (Cai et al., 2003; Wallace et al., 2021). Decomposers and other heterotrophs thrive in salt marshes, producing DIC through aerobic and anaerobic remineralization of organic carbon, where some of the organic carbon may be the result of net import from other adjacent ecosystems (Valiela et al., 1985). Anaerobic respiration occurring in salt marsh sediments also acts as a particularly large source of alkalinity, with denitrification and sulfate reduction nearing or reaching parity in DIC and TA production (in TA:DIC ratios of 0.8 and 1.0, respectively) (Martínez-Espinosa et al., 2021; Krumins et al., 2013).

Direct photosynthetic uptake of aqueous CO_2 in salt marsh vegetation is constrained by tidal cycles, photosynthetically available radiation which is controlled by turbidity and diel cycles, and seasonal marsh vegetation growing patterns (Huang et al., 2022; Mao et al., 2023). During tidal inundation, the submerged salt marsh vegetation switches from utilizing atmospheric CO_2 to taking up aqueous forms of inorganic carbon, thereby directly altering the seawater carbonate system (Mao et al., 2023; Song et al., 2023). A recent study quantified the photosynthetic CO_2 uptake in an inundated salt marsh, finding that salt marsh photosynthesis dampened net vertical and lateral CO_2 exchange, reducing air-sea CO_2 efflux by a mean of 31% and export flux by a mean of 11% (Song et al., 2023).

In addition to interacting with inorganic carbon systems, primary producers, such as marsh vegetation, phytoplankton, and algae, can also act as sources of particulate organic carbon (POC) and dissolved organic carbon (DOC) in the marsh while decomposers are the main source of DIC. POC exports from the marsh can be comprised of fragments of marsh vegetation, sediment, or living biomass (i.e., phytoplankton) (Dame et al., 1991). DOC consists of particles of marsh organic carbon small enough to dissolve in seawater, or fit through a filter with a 0.22 - 0.7 μm mesh size. Organic carbon produced in the marsh is initially highly labile and is therefore easily broken down chemically or digested by other organisms (del Giorgio and Davis, 2003). The salt marsh itself facilitates the transformation of some POC into DOC, through the physical breakdown of particles by wave action (Jordan et al., 1983). Photochemical degradation can also initiate the release of DOC from suspended marsh POC; this method of transformation accounts

for the production of 10-22% of marsh-derived DOC in coastal waters (Schiebel et al., 2015). Labile marsh DOC can further decompose into dissolved inorganic carbon (DIC), often with the help of microbial decomposers (Eldridge and Cifuentes, 2000). Microbial mineralization chemically decomposes DOC, producing DIC as a respiratory product (Weston et al., 2011).

Spatial gradients of marsh organic carbon in coastal waters show clear evidence of lateral exchange between marshes and coastal ecosystems (Ganju et al., 2019; Wang and Cai, 2004). In the early 1960s, the outwelling hypothesis emerged as the leading explanation of marsh lateral transport (Odum, 1968). According to this hypothesis, organic matter is exported from the highly productive marsh to coastal waters, fueling offshore secondary production (Odum, 1980). In recent years, this treatment of salt marsh lateral transport has proved too simplistic (Odum, 1980; Wang and Cai, 2004). Extreme spatiotemporal heterogeneity in marsh geomorphology and biogeochemistry means that marshes can act as either net importers or exporters of carbon (Wang and Cai, 2004). Furthermore, lateral exchange between marshes and adjacent waters transports not only organic carbon, but also inorganic carbon and alkalinity (Wang and Cai, 2004). Local marsh characteristics dictate whether a marsh is a net importer or exporter of carbon and also impact the type and quantity of carbon transported (Odum, 1980; Ganju et al., 2019).

Lateral carbon transfer between marshes and the coastal ocean can occur in two main ways: tide water exchange and pore water drainage. The majority of respiration in marsh-estuarine complexes occurs during high tide in flooded marshes (Cai et al., 1999, Canuel et al., 2016). After respiration peaks during high tide, an ebb tide carries the respiratory products and older, refractory sediment carbon to adjacent waters, resulting in an export of inorganic carbon (Cai et al., 1999; Fagherazzi et al., 2013). Conversely, flooding tides can bring carbon inputs to the marsh (Canuel et al., 2016). While tidal exchange is a major component of marsh lateral carbon transfer, it remains poorly constrained due to the high spatial heterogeneity of the marsh and temporal variability of fluxes (Najjar et al., 2018).

Pore water drainage is a mechanism of marsh export through which water seeps through marsh sediment to eventually join adjacent tidal creeks (Guimond and Tamborski, 2021; Santos et al., 2019). As water flushes through sediments, it carries with it carbon respiratory products

and particulate forms of carbon produced in the marsh (Santos et al., 2019). Pore water drainage is driven by tidal pumping, which is the result of shifting hydraulic gradients between the salt marsh and nearby tidal creeks (Wilson and Gardner, 2006; Krask et al., 2022). Ebb and low tides produce hydraulic gradients that result in enhanced pore water drainage of water rich in marsh-derived DIC and TA into adjacent tidal creeks (Wilson and Gardner, 2006; Krask et al., 2022; Wang et al., 2016). When seawater overtops the marsh platform at high tide, pores are recharged with water. The magnitude of exchange is relative tidal amplitude and elevation of marsh platforms (Guimond and Tamborski, 2021). Pore water drainage is enhanced by increased sediment permeability and macropore structures, which, for example, can be facilitated by invertebrate burrowing (Guimond and Tamborski, 2021; Schiebel et al., 2019; Kostka et al., 2002). While both DIC and DOC are exported in large quantities from marshes through pore water drainage, DIC represents a larger proportion of exported carbon products (Cai et al., 2003; Bouillon et al., 2007; Tamborski et al., 2021).

1.3.2 Seagrass Meadows

Seagrasses are marine angiosperms found in nearshore coastal environments worldwide (McKenzie et al., 2020). Seagrasses are able to alter the surrounding environment in numerous ways, by creating densely vegetated meadows, attenuating wave action and slowing current velocity, and trapping sediments and organic material (Bos et al., 2007; Hansen and Reidenbach, 2013; Zhu et al., 2021). These modifications result in numerous ecosystem services including protection from shoreline erosion, improved water quality, organic carbon storage, and provisioning of sheltered habitat for marine species (Zhu et al., 2022; Waycott at al., 2009; Pacella et al., 2018). As autotrophs, seagrasses also alter their surrounding chemical environment through photosynthetic uptake of aqueous CO_2 (Hendriks et al., 2014; Ricart et al., 2021). Their role in local seawater carbonate chemistry has sparked interest in the potential for seagrass meadows to act locally as catalysts of CO_2 drawdown and moderators of ocean acidification (Ollivier et al., 2022; Nielsen et al., 2018). When compared to unvegetated systems, *Zostera marina* meadows exhibited heightened pH 65% of the time with a mean increase in pH of 0.07 ± 0.008 SE (Ricart et al., 2021a). Mitigation of ocean acidification in the nearshore marine environment is of particular importance due to the presence of vulnerable marine calcifying species. Because of this, field and laboratory studies have focused on the efficacy of seagrass

meadows to act as refugia from increasingly acidic conditions elsewhere (Saderne et al., 2015; Ricart et al., 2021b). However, significant uncertainties remain regarding regional and local spatial heterogeneity, variability in short-term and seasonal timescales, and key drivers of seagrass meadow seawater carbonate chemistry (Koweek et al., 2018).

Local net ecosystem metabolism is a key determinator of whether or not a seagrass meadow demonstrates higher pH relative to nearby unvegetated systems (Lowe et al., 2019). For this reason, factors that augment photosynthesis, thereby increasing uptake of carbon dioxide, can lead to a local increase in pH. Alternatively, increases in respiration within a seagrass meadow reduce local pH. Previous work done in seagrass meadows found positive correlations between pH and daylength, light availability, leaf area index, and shoot density, all of which are indicators of seagrass metabolism (Hendriks et al., 2014). Upwelling events that bring nutrient and carbon-rich waters into seagrass meadows can also accelerate seagrass growth and utilization of carbon (Strong et al., 2014; Ricart et al., 2021a). Tight coupling of metabolic processes in seagrass meadows result in close correspondence of pCO_2 and dissolved oxygen (O_2) in seagrass meadows (Berg et al., 2019). This often extends to pH, with positive correlations observed between pH and O_2 (Lowe et al., 2019). Increases in seagrass biomass not only result in greater pH elevation, but also in a larger diel range (Ricart et al., 2021b). Temporal variation in seagrass metabolism yields both diel and seasonal variations in seagrass meadow pH. In temperate meadows, maximum seagrass meadow pH has been observed coinciding with primary productivity annual highs occurring in the spring and summer (Ricart et al., 2021a).

While biogeochemical processes are important drivers of seagrass meadow pH patterns, hydrodynamics also play an important role in the longevity of locally generated seawater carbonate chemistry signals. Lateral transport of DIC and TA between seagrass meadows and adjacent systems through currents, tides, and wind-driven waves can disperse biogeochemical signals produced within the seagrass meadow (Lowe et al., 2019; Ricart et al., 2021a). However, dense vegetation in seagrass meadows begets higher water residence times, often lessening potential rates of lateral exchange (James et al., 2020). Diffusive boundary layers (DBLs) in seagrass meadows work to slow near bottom velocities and increase the residence time of water in the ecosystem (James et al., 2020). DBLs form as water comes into contact with seagrass shoots, creating zones where turbulent fluxes are reduced, and molecular diffusion becomes a

more dominant transport term. In densely vegetated environments, like most seagrass meadows, the DBLs of individual shoots overlap, resulting in a DBL that is inclusive of the entire meadow (James et al., 2020). This increases water residence time within seagrass meadows, resulting in larger diel pH swings (James et al., 2020). When water residence time in the seagrass meadow is low, seawater with heightened pH is flushed out of the seagrass meadow (Cyronak et al., 2018; James et al., 2020). In cases like this, seagrass meadows can heighten the pH of surrounding unvegetated areas at the expense of slightly lowering their own local pH (Cyronak et al., 2018; James et al., 2020). For example, in modeled, mesocosm, and field experiments, seagrass meadows and macroalgae have been shown to increase calcification in corals downstream of the meadow (Liu et al., 2020; Unsworth et al., 2012; Manzello et al., 2012).

Tidal cycles are another aspect of hydrodynamics that can impact local pH (Cyronak et al., 2018; James et al., 2020). Higher water at high tide can lead to dilution of local metabolic signals from both photosynthesis and respiration (Cyronak et al., 2018). Alternatively, low tides can concentrate local metabolic signals (Cyronak et al., 2018). Existing diel fluctuations in pH due to shifts in net ecosystem metabolism can be exacerbated or modulated by concurrence with high and low tides. Positive and negative trends in ΔpH over multiple days, seen in both vegetated and unvegetated sites, often correspond with shifting tidal amplitudes (Ricart et al., 2021).

Seagrass meadows exhibit high pH variability on short time scales (diel and tidal), manifesting in several variations of diel patterns in seagrass meadow pH relative to unvegetated sites (ΔpH = seagrass meadow pH – unvegetated site pH) (Ricart et al., 2021a). Across six years of pH observations collected by Ricart and colleagues (2021a), the most commonly observed diel pH pattern in a *Zostera marina* meadow reflected a positive ΔpH in which the seagrass meadow had a consistently higher pH than nearby unvegetated areas (Ricart et al., 2021a). In another common pattern, positive ΔpH was observed during daylight hours but by the end of the night minimal pH difference was observed between vegetated and unvegetated sites (Ricart et al., 2021a). The least commonly observed scenarios were those in which seagrass meadow pH dipped below unvegetated site pH (Ricart et al., 2021a). Seasonally mediated heightened pH events in seagrass meadows can result in long periods of relief from ocean acidification, in which

pH can remain continuously elevated for longer than a full 24-hour cycle (Ricart et al., 2021a). Relative to unvegetated sites, events with a positive anomaly in pH within seagrass meadows lasted longer and had greater magnitudes than events with a negative anomaly in pH in seagrass meadows relative to adjacent unvegetated sites (Ricart et al., 2021a). In a site off the coast of California, positive pH elevations above 0.1 pH units lasted up to 21 days (Ricart et al., 2021a).

While seagrasses have shown the potential to locally induce a net elevation of pH, some findings suggest that seagrass meadows can amplify acidity under certain conditions (Cyronak et al., 2018; Ricart et al., 2021a). Despite exhibiting heightened pH during daylight hours, seawater pH in seagrass meadows was often lower than open ocean values at night in studies conducted in Bermuda and Mission Bay, CA (Cyronak et al., 2018). High residence time within seagrass meadows and daily pH minima (nighttime or near sunrise) coinciding with low tides can result in lower pH relative to nearby unvegetated sites (Cyronak et al., 2018; James et al., 2020). The frequency of negative ΔpH occurrences arise from the hydrodynamic setting of a seagrass meadow and temporal shifts in net ecosystem metabolism.

1.4 Summary

As a result of physical and biogeochemical forcings, nearshore coastal seawater inorganic carbon chemistry exhibits heterogeneity across local and regional spatial scales and short to long term time scales. Physicochemical processes, like lateral and air-sea gas exchange, exert control over fluxes and geographic distributions of water column CO_2, TA, and DIC. Diverse biogeochemical activity in nearshore coastal marine systems can alter DIC, TA, pH, and pCO_2 and impart substantial spatiotemporal variability to coastal inorganic carbon cycles. Temporal variations in net ecosystem metabolism occurring on tidal, diel, and seasonal cycles modulate the magnitude of biological effects. Intertidal salt marshes and seagrasses exemplify two biogeochemical extremes in which salt marshes often acidify adjacent waters and seagrasses are expected to partially counter acidification and elevate local pH. Despite playing important roles in critical climate issues, the drivers of nearshore coastal inorganic carbon cycles remain poorly constrained. This dissertation seeks to further characterize drivers and spatiotemporal heterogeneity of seawater carbonate chemistry in interconnected nearshore coastal marine

systems. Chapters 3 and 4 include data collected in the Virginia Coast Reserve, a dynamic coastal setting which comprises shallow coastal bays, salt marshes, restored seagrass meadows, and lagoons.

1.5 Outline of Chapters

Chapter 1 (this chapter) serves as a review of foundational concepts and relevant literature in the field of seawater inorganic carbonate chemistry in nearshore marine systems. Current understanding of seawater carbonate chemistry dynamics in intertidal salt marshes and temperate seagrass meadows is discussed.

Chapter 2 synthesizes metadata from surveys and publicly available sources to produce an inventory of the methodology, data quality, spatial distribution, and frequency of seawater carbonate system sampling in the U.S. Mid-Atlantic from 1984 to 2023 spanning from tidal rivers and estuaries to the continental shelf and slope. A summary of regional data gaps with respect to highly variable and vulnerable ecosystems is presented based on spatial analysis.

Chapter 3 explores local drivers as well as spatial and seasonal trends in seawater carbonate chemistry at the landscape scale in the Virginia Coast Reserve. Effects of conservative mixing, the biogeochemical influence of tidal salt marshes, and air-sea gas exchange are quantified and discussed.

Chapter 4 evaluates spatiotemporal pH patterns across a shallow bay in the Virginia Coast Reserve. pH variability in a seagrass meadow and a nearby marsh-influenced unvegetated site is assessed on diel and tidal time scales during peak seagrass growing season.

1.6 References

Berg, P., Delgard, M. L., Polsenaere, P., McGlathery, K. J., Doney, S. C., and Berger, A. C. (2019). Dynamics of benthic metabolism, O2, and pCO2 in a temperate seagrass meadow. Limnology and Oceanography, 64(6), 2586-2604.

Bos, A. R., Bouma, T. J., de Kort, G. L., and van Katwijk, M. M. (2007). Ecosystem engineering by annual intertidal seagrass beds: sediment accretion and modification. *Estuarine, Coastal and Shelf Science*, *74*(1-2), 344-348.

Bouillon, S., Middelburg, J. J., Dehairs, F., Borges, A. V., Abril, G., Flindt, M. R., ... and Kristensen, E. (2007). Importance of intertidal sediment processes and porewater exchange on the water column biogeochemistry in a pristine mangrove creek (Ras Dege, Tanzania).

Cai, W. J., Wang, Y. C. , and Hodson, R. E. (1998). Acid-base properties of dissolved organic matter in the estuarine waters of Georgia, USA. *Geochimica et Cosmochimica Acta*, 62(3), 473–483. 10.1016/s0016-7037(97)00363-3

Cai, W. J., Pomeroy, L. R., Moran, M. A., and Wang, Y. (1999). Oxygen and carbon dioxide mass balance for the estuarine-intertidal marsh complex of five rivers in the southeastern US. *Limnology and Oceanography*, *44*(3), 639-649.

Cai, W. J., Wang, Y., Krest, J., and Moore, W. S. (2003). The geochemistry of dissolved inorganic carbon in a surficial groundwater aquifer in North Inlet, South Carolina, and the carbon fluxes to the coastal ocean. *Geochimica et Cosmochimica Acta*, *67*(4), 631-639.

Cai, W. J., Wang, Z. A., and Wang, Y. (2003). The role of marsh-dominated heterotrophic continental margins in transport of CO2 between the atmosphere, the land-sea interface and the ocean. *Geophysical Research Letters*, *30*(16).

Canuel, E. A., and Hardison, A. K. (2016). Sources, ages, and alteration of organic matter in estuaries. *Annual Review of Marine Science*, *8*, 409-434.

Chu, S. N., Wang, Z. A., Gonneea, M. E., Kroeger, K. D., and Ganju, N. K. (2018). Deciphering the dynamics of inorganic carbon export from intertidal salt marshes using high-frequency measurements. *Marine Chemistry*, *206*, 7-18.

Cyronak, T., Andersson, A. J., D'Angelo, S., Bresnahan, P., Davidson, C., Griffin, A., ... and White, M. (2018). Short-term spatial and temporal carbonate chemistry variability in two contrasting seagrass meadows: implications for pH buffering capacities. *Estuaries and Coasts*, *41*(5), 1282-1296.

Dame, R. F., Spurrier, J. D., Williams, T. M., Kjerfve, B., Zingmark, R. G., Wolaver, T. G., ... and Vernberg, F. J. (1991). Annual material processing by a salt marsh-estuarine basin in South Carolina, USA. *Marine Ecology Progress Series*, 153-166.

Deegan, L. A., Johnson, D. S., Warren, R. S., Peterson, B. J., Fleeger, J. W., Fagherazzi, S., and Wollheim, W. M. (2012). Coastal eutrophication as a driver of salt marsh loss. *Nature*, *490*(7420), 388-392.

del Giorgio, P. A., Davis, J., Findlay, S. E. G., and Sinsabaugh, R. L. (2003). Aquatic ecosystems: interactivity of dissolved organic matter. *Elsevier Science (USA)*, 400-424.

Dickson, A. G. (1981). An exact definition of total alkalinity and a procedure for the estimation of alkalinity and total inorganic carbon from titration data. *Deep Sea Research Part A. Oceanographic Research Papers*, *28*(6), 609-623.

Dickson, A. G., Sabine, C. L., and Christian, J. R. (2007). *Guide to best practices for ocean CO2 measurements*. North Pacific Marine Science Organization.

Dickson, A. G. (2010). The carbon dioxide system in seawater: equilibrium chemistry and measurements. *Guide to best practices for ocean acidification research and data reporting*, *1*, 17-40.

Doney, S. C., Fabry, V. J., Feely, R. A., and Kleypas, J. A. (2009). Ocean acidification: the other CO2 problem. *Annual review of marine science*, *1*, 169-192.

Eldridge, P. M., and Cifuentes, L. A. (2002). A stable isotope model approach to estimating the contribution of organic matter from marshes to estuaries. In *Concepts and controversies in tidal marsh ecology* (pp. 495-513). Springer, Dordrecht.

Fagherazzi, S., Wiberg, P. L., Temmerman, S., Struyf, E., Zhao, Y., and Raymond, P. A. (2013). Fluxes of water, sediments, and biogeochemical compounds in salt marshes. *Ecological Processes*, *2*(1), 3.

Ganju, N. K., Defne, Z., Elsey-Quirk, T., and Moriarty, J. M. (2019). Role of tidal wetland stability in lateral fluxes of particulate organic matter and carbon. *Journal of Geophysical Research: Biogeosciences*, *124*(5), 1265-1277.

Gattuso, J. P., Magnan, A., Billé, R., Cheung, W. W., Howes, E. L., Joos, F., ... and Turley, C. (2015). Contrasting futures for ocean and society from different anthropogenic CO2 emissions scenarios. *Science*, *349*(6243), aac4722.

Guimond, J., and Tamborski, J. (2021). Salt marsh hydrogeology: A review. *Water*, *13*(4), 543.

Groner, M. L., Burge, C. A., Cox, R., Rivlin, N. D., Turner, M., Van Alstyne, K. L., ... and Friedman, C. S. (2018). Oysters and eelgrass: potential partners in a high pCO2 ocean. *Ecology*, *99*(8), 1802-1814.

Hendriks, I. E., Olsen, Y. S., Ramajo, L., Basso, L., Steckbauer, A., Moore, T. S., ... and Duarte, C. M. (2014). Photosynthetic activity buffers ocean acidification in seagrass meadows. *Biogeosciences*, *11*(2), 333-346.

Hu, X. (2020). Effect of organic alkalinity on seawater buffer capacity: A numerical exploration. *Aquatic Geochemistry*. 10.1007/s10498-020-09375-x

Huang, Y., Zhou, C., Du, M., Wu, P., Yuan, L., and Tang, J. (2022). Tidal influence on the relationship between solar-induced chlorophyll fluorescence and canopy photosynthesis in a coastal salt marsh. *Remote Sensing of Environment, 270*, 112865.

James, R. K., van Katwijk, M. M., van Tussenbroek, B. I., van Der Heide, T., Dijkstra, H. A., van Westen, R. M., ... and Bouma, T. J. (2020). Water motion and vegetation control the pH dynamics in seagrass-dominated bays. *Limnology and Oceanography*, *65*(2), 349-362.

Jewett, L., and Romanou, A. (2017). Ocean acidification and other ocean changes. *Climate science special report: fourth national climate assessment*, *1*, 364-392.

Jordan, T. E., Correll, D. L., and Whigham, D. F. (1983). Nutrient flux in the Rhode River: tidal exchange of nutrients by brackish marshes. *Estuarine, Coastal and Shelf Science*, *17*(6), 651-667.

Khatiwala, S., Tanhua, T., Mikaloff Fletcher, S., Gerber, M., Doney, S. C., Graven, H. D., ... and Sabine, C. L. (2013). Global ocean storage of anthropogenic carbon. *Biogeosciences*, *10*(4), 2169-2191.

Kirwan, M. L., and Blum, L. K. (2011). Enhanced decomposition offsets enhanced productivity and soil carbon accumulation in coastal wetlands responding to climate change. *Biogeosciences*, *8*(4), 987.

Kirwan, M. L., and Mudd, S. M. (2012). Response of salt-marsh carbon accumulation to climate change. *Nature*, *489*(7417), 550-553.

Ko, Y. H. , Lee, K. , Eom, K. H. , and Han, I. (2016). Organic alkalinity produced by phytoplankton and its effect on the computation of ocean carbon parameters. *Limnology and Oceanography*, 61, 1462–1471. 10.1002/lno.10309

Kostka, J. E., Gribsholt, B., Petrie, E., Dalton, D., Skelton, H., and Kristensen, E. (2002). The rates and pathways of carbon oxidation in bioturbated saltmarsh sediments. *Limnology and Oceanography*, *47*(1), 230-240.

Koweek, D. A., Zimmerman, R. C., Hewett, K. M., Gaylord, B., Giddings, S. N., Nickols, K. J., ... and Caldeira, K. (2018). Expected limits on the ocean acidification buffering potential of a temperate seagrass meadow. *Ecological Applications*, *28*(7), 1694-1714.

Krask, J. L., Buck, T. L., Dunn, R. P., and Smith, E. M. (2022). Increasing tidal inundation corresponds to rising porewater nutrient concentrations in a southeastern US salt marsh. *Plos one*, *17*(11), e0278215.

Krumins, V., Gehlen, M., Arndt, S., Van Cappellen, P., and Regnier, P. (2013). Dissolved inorganic carbon and alkalinity fluxes from coastal marine sediments: model estimates for different shelf environments and sensitivity to global change. *Biogeosciences*, *10*(1), 371-398.

Le Quéré, C., Andrew, R. M., Friedlingstein, P., Sitch, S., Hauck, J., Pongratz, J., ... and Zheng, B. (2018). Global carbon budget 2018. *Earth System Science Data*, *10*(4), 2141-2194.

Liu, P. J., Ang, S. J., Mayfield, A. B., and Lin, H. J. (2020). Influence of the seagrass Thalassia hemprichii on coral reef mesocosms exposed to ocean acidification and experimentally elevated temperatures. Science of the Total Environment, 700, 134464.

Lowe, A. T., Bos, J., and Ruesink, J. (2019). Ecosystem metabolism drives pH variability and modulates long-term ocean acidification in the Northeast Pacific coastal ocean. *Scientific Reports*, *9*(1), 1-11.

Mao, L., Mishra, D. R., Hawman, P. A., Narron, C. R., O'Connell, J. L., and Cotten, D. L. (2023). Photosynthetic Performance of Tidally Flooded Spartina alterniflora Salt Marshes. *Journal of Geophysical Research: Biogeosciences*, *128*(3), e2022JG007161.

Manzello, D. P., Enochs, I. C., Melo, N., Gledhill, D. K., and Johns, E. M. (2012). Ocean acidification refugia of the Florida Reef Tract. *PloS one*, *7*(7), e41715.

Martínez-Espinosa, C., Sauvage, S., Al Bitar, A., Green, P. A., Vörösmarty, C. J., and Sánchez-Pérez, J. M. (2021). Denitrification in wetlands: A review towards a quantification at global scale. *Science of the total environment*, *754*, 142398.

McKenzie, L. J., Nordlund, L. M., Jones, B. L., Cullen-Unsworth, L. C., Roelfsema, C., and Unsworth, R. K. (2020). The global distribution of seagrass meadows. *Environmental Research Letters*, *15*(7), 074041.

Middelburg, J. J., Soetaert, K., and Hagens, M. (2020). Ocean alkalinity, buffering and biogeochemical processes. *Reviews of Geophysics*, *58*(3), e2019RG000681.

Najjar, R. G., Herrmann, M., Alexander, R., Boyer, E. W., Burdige, D. J., Butman, D., ... and Feagin, R. A. (2018). Carbon budget of tidal wetlands, estuaries, and shelf waters of eastern North America. *Global Biogeochemical Cycles*, *32*(3), 389-416.

Nielsen, K. J., Stachowicz, J. J., Carter, H., Boyer, K., Bracken, M., Chan, F., ... and Wheeler, S. (2018). Emerging understanding of seagrass and kelp as an ocean acidification management tool in California.

Odum, E. P. (1968). A research challenge: evaluating the productivity of coastal and estuarine water. In *Proceedings of the second sea grant conference* (pp. 63-64). University of Rhode Island.

Odum, E. P. (1980). The status of three ecosystem-level hypotheses regarding salt marsh estuaries: tidal subsidy, outwelling, and detritus-based food chains. In *Estuarine perspectives* (pp. 485-495). Academic Press.

Ollivier, Q. R., Maher, D. T., Pitfield, C., and Macreadie, P. I. (2022). Net drawdown of greenhouse gases (CO2, CH4 and N2O) by a temperate australian seagrass meadow. *Estuaries and Coasts*, *45*(7), 2026-2039.

Oreska, M. P., Wilkinson, G. M., McGlathery, K. J., Bost, M., and McKee, B. A. (2018). Non-seagrass carbon contributions to seagrass sediment blue carbon. *Limnology and Oceanography*, *63*(S1), S3-S18.

Pacella, S. R., Brown, C. A., Waldbusser, G. G., Labiosa, R. G., and Hales, B. (2018). Seagrass habitat metabolism increases short-term extremes and long-term offset of CO2 under future ocean acidification. *Proceedings of the National Academy of Sciences*, *115*(15), 3870-3875.

Paerl, H. W., Otten, T. G., and Kudela, R. (2018). Mitigating the expansion of harmful algal blooms across the freshwater-to-marine continuum.

Rheuban, J. E., Doney, S. C., McCorkle, D. C., and Jakuba, R. W. (2019). Quantifying the effects of nutrient enrichment and freshwater mixing on coastal ocean acidification. *Journal of Geophysical Research: Oceans*, *124*(12), 9085-9100.

Ricart, A. M., Ward, M., Hill, T. M., Sanford, E., Kroeker, K. J., Takeshita, Y., ... and Gaylord, B. (2021). Coast-wide evidence of low pH amelioration by seagrass ecosystems. *Global Change Biology*.

Ricart, A. M., Gaylord, B., Hill, T. M., Sigwart, J. D., Shukla, P., Ward, M., ... and Sanford, E. (2021). Seagrass-driven changes in carbonate chemistry enhance oyster shell growth. *Oecologia*, *196*(2), 565-576.

Russi D., ten Brink P., Farmer A., Badura T., Coates D., Förster J., Kumar R. and Davidson N. (2013). The Economics of Ecosystems and Biodiversity for Water and Wetlands. *IEEP, London and Brussels*; Ramsar Secretariat, Gland.

Saderne, V., Fietzek, P., Aßmann, S., Körtzinger, A., and Hiebenthal, C. (2015). Seagrass beds as ocean acidification refuges for mussels? High resolution measurements of pCO 2 and O 2 in a Zostera marina and Mytilus edulis mosaic habitat. *Biogeosciences Discussions*, *12*(14), 11423-11461.

Santos, I. R., Maher, D. T., Larkin, R., Webb, J. R., and Sanders, C. J. (2019). Carbon outwelling and outgassing vs. burial in an estuarine tidal creek surrounded by mangrove and saltmarsh wetlands. Limnology and Oceanography, 64(3), 996-1013.

Schiebel, H.N., Wang X, Chen RF, Peri F. (2015). Photochemical release of dissolved organic matter from resuspended salt marsh sediments. Estuaries and Coasts 38(5):1692–1705

Schiebel, H. N., Peri, F., and Chen, R. F. (2019). Dissolved Organic Matter Export from Surface Sediments of a New England Salt Marsh. *Wetlands*, 1-13.

Soetaert, K., Hofmann, A. F., Middelburg, J. J., Meysman, F. J., and Greenwood, J. (2007). Reprint of "The effect of biogeochemical processes on pH". *Marine Chemistry*, *106*(1-2), 380-401.

Song, S., Wang, Z. A., Gonneea, M. E., Kroeger, K. D., Chu, S. N., Li, D., and Liang, H. (2020). An important biogeochemical link between organic and inorganic carbon cycling: Effects of organic alkalinity on carbonate chemistry in coastal waters influenced by intertidal salt marshes. *Geochimica et Cosmochimica Acta*, *275*, 123-139.

Strong, A. L., Kroeker, K. J., Teneva, L. T., Mease, L. A., and Kelly, R. P. (2014). Ocean acidification 2.0: Managing our changing coastal ocean chemistry. Bioscience, 64(7), 581-592

Tamborski, J. J., Eagle, M., Kurylyk, B. L., Kroeger, K. D., Wang, Z. A., Henderson, P., and Charette, M. A. (2021). Pore water exchange-driven inorganic carbon export from intertidal salt marshes. *Limnology and Oceanography*, *66*(5), 1774-1792.

Temmerman S, Moonen P, Schoelynck J, Govers G, Bouma TJ. (2012). Impact of vegetation die-off on spatial flow patterns over a tidal marsh. *Geophys Res Lett*, 39: L03406.

Unsworth, Richard KF, Catherine J. Collier, Gideon M. Henderson, and Len J. McKenzie. "Tropical seagrass meadows modify seawater carbon chemistry: implications for coral reefs impacted by ocean acidification." *Environmental Research Letters* 7, no. 2 (2012): 024026.

Valiela, I., Teal, J. M., Allen, S. D., Van Etten, R., Goehringer, D., and Volkmann, S. (1985). Decomposition in salt marsh ecosystems: the phases and major factors affecting disappearance of above-ground organic matter. *Journal of experimental marine biology and ecology*, *89*(1), 29-54.

Waldbusser, G. G., and Salisbury, J. E. (2014). Ocean acidification in the coastal zone from an organism's perspective: multiple system parameters, frequency domains, and habitats. *Annual review of marine science*, *6*, 221-247.

Wallace, R. B., Peterson, B. J., and Gobler, C. J. (2021). Ecosystem metabolism modulates the dynamics of hypoxia and acidification across temperate coastal habitat types. *Frontiers in Marine Science*, *8*, 611781.

Wang, Z. A., and Cai, W. J. (2004). Carbon dioxide degassing and inorganic carbon export from a marsh-dominated estuary (the Duplin River): A marsh CO2 pump. *Limnology and Oceanography*, *49*(2), 341-354.

Wang, Z. A., Kroeger, K. D., Ganju, N. K., Gonneea, M. E., and Chu, S. N. (2016). Intertidal salt marshes as an important source of inorganic carbon to the coastal ocean. *Limnology and Oceanography*, *61*(5), 1916-1931.

Wang, S. R., Di Iorio, D., Cai, W. J., and Hopkinson, C. S. (2018). Inorganic carbon and oxygen dynamics in a marsh-dominated estuary. *Limnology and Oceanography*, *63*(1), 47-71.

Wanninkhof, R. (2014). Relationship between wind speed and gas exchange over the ocean revisited. *Limnology and Oceanography: Methods*, *12*(6), 351-362.

Waycott, M., Duarte, C. M., Carruthers, T. J., Orth, R. J., Dennison, W. C., Olyarnik, S., ... and Williams, S. L. (2009). Accelerating loss of seagrasses across the globe threatens coastal ecosystems. *Proceedings of the national academy of sciences*, *106*(30), 12377-12381.

Weston, N. B., Vile, M. A., Neubauer, S. C., and Velinsky, D. J. (2011). Accelerated microbial organic matter mineralization following salt-water intrusion into tidal freshwater marsh soils. *Biogeochemistry*, *102*(1-3), 135-151.

Wilson AM, Gardner LR. Tidally driven groundwater flow and solute exchange in a marsh: Numerical simulations. *Water Resources Research*. 2006; 42: W01405.

Zeebe, R. E., and Wolf-Gladrow, D. (2001). *CO2 in seawater: equilibrium, kinetics, isotopes* (Vol. 65). Gulf Professional Publishing.

Zhu, Q., Wiberg, P. L., and Reidenbach, M. A. (2021). Quantifying seasonal seagrass effects on flow and sediment dynamics in a back-barrier bay. *Journal of Geophysical Research: Oceans*, *126*(2), e2020JC016547.

Zhu, Q., Wiberg, P. L., and McGlathery, K. J. (2022). Seasonal growth and senescence of seagrass alters sediment accumulation rates and carbon burial in a coastal lagoon. *Limnology and Oceanography*, *67*(9), 1931-1942.

Chapter 2: MACAN Coastal and Ocean Acidification Monitoring Inventory Analysis

2.1 Abstract

Ocean acidification is causing long-term change in surface ocean pH globally, but the severity and effects of acidification vary widely at regional and local levels. Monitoring of seawater carbonate system parameters, pH, pCO_2, dissolved inorganic carbon, and total alkalinity, can provide crucial information regarding the local status of acidification. In this chapter, the locations and methods of carbonate system sampling and monitoring efforts conducted between 1984 and 2023 in the U.S. Mid-Atlantic were combined into a publicly available inventory (available on the MARCO Ocean Data Portal) and then analyzed in the context of regional monitoring priorities. This work was done in collaboration with the Mid-Atlantic Coastal Acidification Network (MACAN) to assess the spatiotemporal distribution of sampling efforts in the coastal waters of New York, New Jersey, Delaware, Maryland, and Virginia, as well as the eastern adjacent coastal and open ocean. We summarize sampling methodologies, data quality (GOA-ON), temporal frequency of sampling, and spatial distribution of sites with respect to measurement depth, salinity, eutrophication, and ecosystems of interest. While the majority of sites in the inventory were sampled once via underway cruise, 3,340 sites across the Mid-Atlantic study region engaged in repeat monitoring efforts. High quality measurements were common in sampling efforts conducted between 2019 and 2023, but 60% of sites measured one carbonate system parameter at climate or weather quality while only 8% of sites measured two. Sampling was conducted across diverse estuarine and marine systems, but the inventory was lacking in sites that collect bottom and depth profile measurements, conduct biological co-monitoring, and collect high frequency, continuous data. Overall, gaps in the current distribution of seawater carbonate system sampling highlight areas of interest for future Mid-Atlantic monitoring that could be addressed through regional coordination efforts.

2.2 Introduction

Since the onset of the Industrial Revolution, the ocean has absorbed 30-40% of the carbon dioxide associated with anthropogenic emissions, resulting in ocean acidification: an increase in oceanic pCO_2 coinciding with a decrease in pH and calcium carbonate saturation state

(Doney et al., 2009; Sabine et al., 2004). Along coastlines, localized environmental conditions like riverine freshwater inputs, eutrophication, upwelling, biogeochemical cycles, and seasonality, can further alter carbonate system patterns driving acidification (Cai et al., 2021; Feely et al., 2010; Wallace et al., 2014). This leads to significant variability in the magnitude and impact of acidification at the regional, coastal level (Gledhill et al., 2015; IPCC, 2021).

The Mid-Atlantic Region comprises five coastal states including New York, New Jersey, Delaware, Maryland, and Virginia, and is longitudinally bound by the extended continental shelf. The region is highly industrialized and populated, with over 34 million people residing in Mid-Atlantic coastal counties (NOEP, 2021). Several large, eutrophic estuaries are present in the region, including the Chesapeake Bay, the Delaware estuary, the Hudson estuary, and the Long Island Sound (Bricker et al., 2007). Summer upwelling and numerous freshwater inputs can act to further exacerbate acidification along the Mid-Atlantic Coast (Glenn et al., 2004). In the U.S. Mid-Atlantic, the coastal waters of the northernmost states of the region are projected cross sublethal acidification thresholds for bivalve larvae between 2071-2099 under RPC 8.5 CO2 emissions (van Hooidonk et al., 2014).

Monitoring coastal and ocean acidification (COA) at the regional level can help to resolve local spatiotemporal carbonate system variability while honing in on regionally important ecosystem, species, and socioeconomic impacts (Goldsmith et al., 2019; Saba et al., 2019). Organizations like the Mid-Atlantic Coastal Acidification Network (MACAN) serve as organizational bodies for regional efforts to monitor and address COA impacts. MACAN, which is co-coordinated by the Mid-Atlantic Regional Council on the Ocean (MARCO) and the Mid-Atlantic Regional Association Coastal Ocean Observing System (MARACOOS), serves as a facilitator for regional COA information sharing and response planning among an interdisciplinary network of scientists, policy-makers, resource managers, and industry partners. This chapter provides an analysis of current Mid-Atlantic carbonate system sampling and monitoring efforts based on the 2023 MACAN COA Inventory (LaRoche et al., 2023). The analysis and corresponding dataset are in support of MACAN's goals to aid in the development of a robust COA monitoring network driven by regional priorities.

Crucial to our understanding of the extent and impact of acidification is high quality acidification monitoring conducted at a sufficient spatiotemporal resolution (Newton et al., 2015). COA can be assessed by measuring four carbonate system parameters: pH, pCO_2, Dissolved Inorganic Carbon (DIC), and Total Alkalinity (TA) (Zeebe and Wolf-Gladrow, 2001). By measuring any two of these parameters in conjunction with salinity and temperature, the other two can be estimated, from empirical thermodynamic relationships, along with saturation state (Ω), which indicates whether conditions are favorable for calcium carbonate dissolution or precipitation (Lewis and Wallace, 1998). A variety of methods can be used to measure seawater inorganic carbon parameters, but commonly used tactics include discrete bottle sampling and continuous autonomous sensors (either stationary or on a moving platform like a glider or research vessel). To date, there are no viable remote sensing measurement approaches.

Previous studies of the Mid-Atlantic system indicate a need for high quality carbonate system data in diverse ecosystems from estuaries to shelf environments, across a full depth profile, in conjunction with biological studies, and with consideration of other coastal acidification drivers like eutrophication and riverine inputs (Goldsmith et al., 2019; Kinkade et al., 2020; Saba et al., 2019). Higher spatial and temporal frequency of monitoring would also benefit efforts to resolve variability in regional models (Goldsmith et al., 2019; Kinkade et al., 2020). Additionally, anticipated COA effects to calcifying organisms highlight the need to improve regional understanding of COA impacts on local aquaculture and coastal communities (Ekstrom et al., 2015; Kinkade et al., 2020). In this report, the MACAN inventory data will be assessed in the context of Mid-Atlantic regional monitoring priorities. We are, however, unable to assess direct completion of Mid-Atlantic objectives and action items with the inventory data alone.

2.3 Methods

2.3.1 General Methods and Study Area

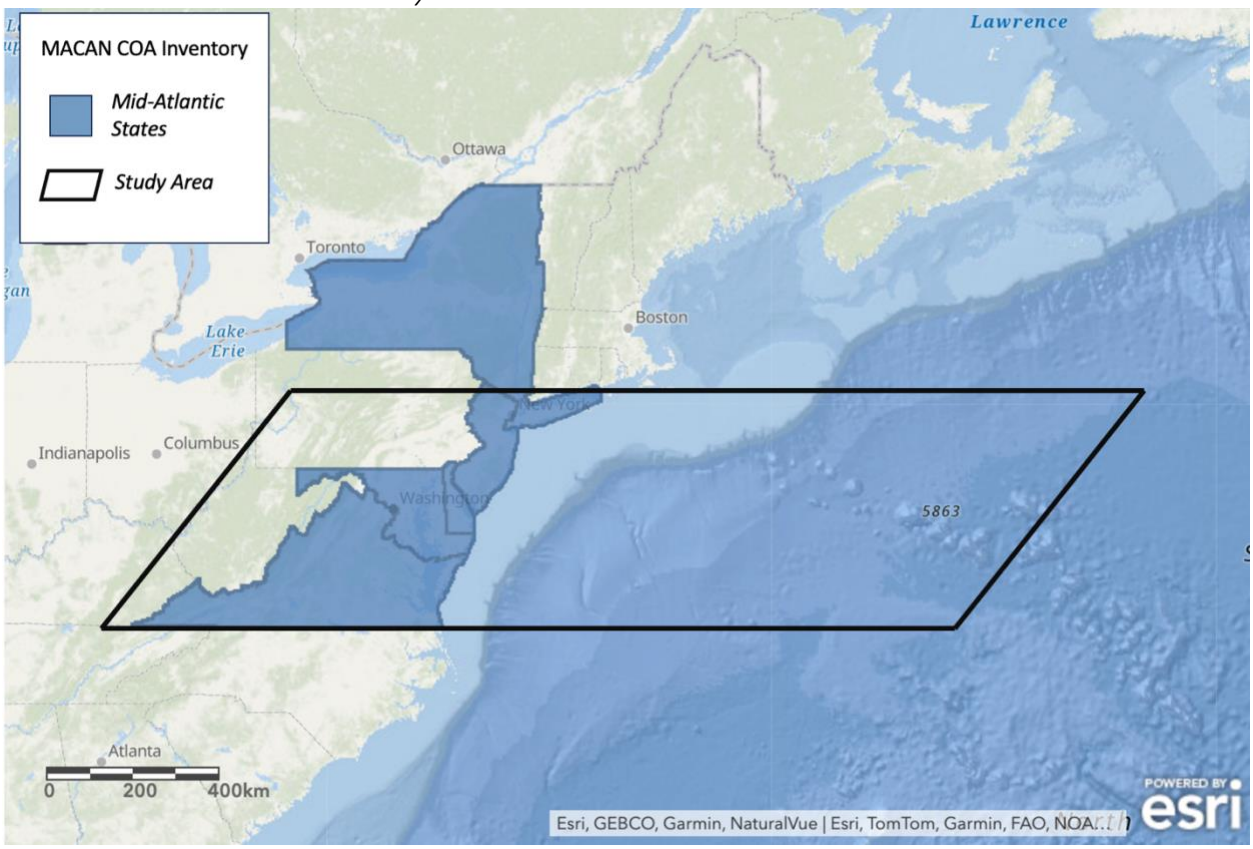

Figure 1: Map of study area, with the five Mid-Atlantic states, New York, New Jersey, Delaware, Maryland, and Virginia, highlighted in blue.

Descriptive statistics and spatial analyses were conducted on 2023 COA inventories (LaRoche et al., 2023; Saba et al., 2019). Each unique sampling location counts as one site, with glider tracks being the exception; each glider deployment is assessed as one site due to the high volume of locations sampled during each glider deployment. While underway cruise data also exhibits high spatial frequency of sampling, data are assessed at the spatial frequency reported by source agencies to maintain metadata, such as collection date, unique to a single site.

For the purposes of this analysis, inventory data were clipped to assess sites within the coastal Mid-Atlantic region extending out to the U.S. Extended Continental Shelf (ECS) boundary (United States Department of State, 2023). The ArcGIS Pro tool Clip was used to exclude sites beyond the boundaries of Mid-Atlantic states and the ECS boundary (United States Department of State, 2023). Regional priorities indicate a need for monitoring of carbonate system parameters across a range of salinities, including riverine freshwater endmembers, whose

outflow can contribute to acidification in receiving waters. For this reason, riverine sites are included in the inventory analysis up to the Atlantic Seaboard Fall Line which is marked by the geologic boundary between the Piedmont and the Atlantic coastal plain. The Mid-Atlantic coastal states included in this analysis are New York, New Jersey, Delaware, Maryland, and Virginia (Figure 1). Although the northern edge of the study area exhibits some overlap with the coastal waters of adjacent states, we limit our discussion of state-specific coastal sampling to the five states served by MACAN. Coastal waters of adjacent northeast and southeast states are under the jurisdiction of the Northeast Coastal Acidification Network (NECAN) and the Southeast Ocean and Coastal Acidification Network (SOCAN). While beyond the scope of this chapter, further coordination and analysis of acidification monitoring efforts in boundary zones between Eastern U.S. Atlantic coastal regions is important for seamless integration of COA monitoring at the coast-wide and national level.

2.3.2 Data Quality categorization

In support of global ocean acidification observing goals, the Global Ocean Acidification Observing Network (GOA-ON) has defined two levels of carbonate system measurement quality: "Climate" and "Weather" (Newton et al., 2015). Climate quality data necessitates a relative standard uncertainty of 1% for carbonate ion concentrations and is suitable for observing long term trends in ocean carbon chemistry (Newton et al., 2015). This is achieved through a standard uncertainty of 0.003 for pH measurements, 2 µmol/kg in TA and DIC measurements, and a relative standard uncertainty of 0.5% for pCO_2 measurements (Newton et al., 2015) (Table 1). Weather quality data, which is more appropriate for assessing spatial variability and short-term variation in carbonate system trends, requires a relative standard uncertainty of 10% for carbonate ion concentrations (Newton et al., 2015). Therefore, weather quality pH, TA, DIC, and pCO_2 measurements meet the following standards: 0.02 standard uncertainty for pH, 10 µmol/kg standard uncertainty for TA and DIC, and 2.5% relative standard uncertainty for pCO_2. All data which have uncertainty greater than the parameter-specific thresholds defined for weather quality are of undefined quality (Newton et al., 2015).

To evaluate the data quality of carbonate system sampling across the Mid-Atlantic, sites that reported sufficiently detailed methods were classified as climate quality, weather quality, and undefined quality. Sites that did not report sufficient methods to determine data quality are

referred to as “unreported” data quality. Throughout this chapter, sample collection achieving climate or weather quality will be referred to as “high quality data”. Other factors influence the uncertainty of measured and calculated seawater carbonate system parameters and the overall quality of sites. In this work we employ a simplified treatment of data quality to enable large-scale characterization of data quality across many sites and collection types.

Table 1: Definitions of Climate, Weather, and Undefined Quality uncertainties for pH, pCO2, TA, and DIC (After Newton et al., 2015)

Quality Category	**pH standard uncertainty**	**pCO_2 relative standard uncertainty**	**TA standard uncertainty**	**DIC standard uncertainty**
Climate Quality	0.003	0.5%	2 µmol/kg	2 µmol/kg
Weather Quality	0.02	2.5%	10 µmol/kg	10 µmol/kg
Undefined Quality	>0.02	>2.5%	>10 µmol/kg	>10 µmol/kg

2.3.3 Spatial analysis of sites

Coastal Wetlands: Extent and type of coastal wetlands were produced by NOAA’s Office for Coastal Management and acquired for this analysis from the MARCO Mid-Atlantic Ocean Data Portal (NOAA Office for Coastal Management, 2023). The ESRI tool Summarize Nearby was used to quantify the number of sampling sites located within 0.5 kilometers of coastal wetlands.

Seagrass: Seagrass shapefiles produced by NOAA’s Office for Coastal Management were intersected with the COA monitoring inventory data using ESRI’s ArcGIS Pro in order to determine the number of carbonate system sampling and monitoring sites within seagrass beds (NOAA Office for Coastal Management, 2022). This analysis was repeated with high-quality sites and high-quality sites measuring two or more parameters. Results were evaluated at the Mid-Atlantic regional and state level.

Deep-sea Corals: A dataset modeling the distribution of deep-sea coral habitat for the order Alcyonacea was accessed through the MARCO Mid-Atlantic Ocean Data Portal for analysis

(Kinlan et al., 2013). These data were produced for the Mid-Atlantic by the National Centers for Coastal Ocean Science in collaboration with scientists at the NOAA/NMFS Northeast Fisheries Science Center. Sites within predicted coral habitat were quantified with the ArcGIS Pro Intersect tool. Results were further filtered by collection depth, to determine the number of sites sampling within range of deep-sea coral habitat.

Shellfish Beds: Shapefiles of shellfish beds located in state waters were acquired from the NRDC. The NRDC collated shellfish bed data from numerous state agencies, and therefore the data do not necessarily have uniform methodology or sampling time periods. In this analysis, shellfish data were clipped to the Mid-Atlantic study area and so we include data from the following agencies: Delaware Division of Fish and Wildlife, New Jersey Department of Environmental Protection: Division of Fish and Wildlife, and Virginia Department of Environmental Quality. Similar shellfish shapefiles were not available for Maryland or New York, so they were excluded from the analysis. A buffer of one kilometer was produced around the shellfish beds to assess nearby sampling. Sites were then intersected with the buffered shellfish layer to determine the number of sampling or monitoring sites within one kilometer of a shellfish bed.

Estuary Eutrophication Score: Estuary eutrophication scores developed by Bricker and colleagues (2007) were used as a proxy for an estuary's potential to exhibit exacerbated coastal acidification due to eutrophic conditions. Scores were on a scale of 1-5, with 1 being Low Eutrophication and 5 being High Eutrophication (Bricker et al., 2007). The number of carbonate system sampling or monitoring sites present within each eutrophication category was determined by using the Intersect tool in ArcGIS Pro. This analysis was repeated with high quality sites and high-quality sites measuring two or more parameters. Results were evaluated at the Mid-Atlantic regional and state level. Shapefiles were prepared by NRDC.

2.4 Results

2.4.1 Overview of carbonate system sampling in the Mid-Atlantic

There are 46,639 seawater carbonate system sampling sites within the Mid-Atlantic study area that operated anytime between 1984 and 2023 (Figure 2). The majority of sites in the inventory were active in the last ten years, with 31.2% of sites active between 2013-2018 and

38.3% of sites active between 2019-2023. The remaining 30.5% of sites were active before 2013. Underway shipboard measurements account for the majority of monitoring locations, with 92.8% of sites being sampled from research ships. Discrete and continuous sampling methods comprise 6.4% and <1% of all sampling sites, respectively. 43,299 sites were classified as one-time carbonate system sampling sites; few research cruises report repeat sampling efforts. The remaining 3,340 sites have engaged in repeat carbonate system sampling efforts.

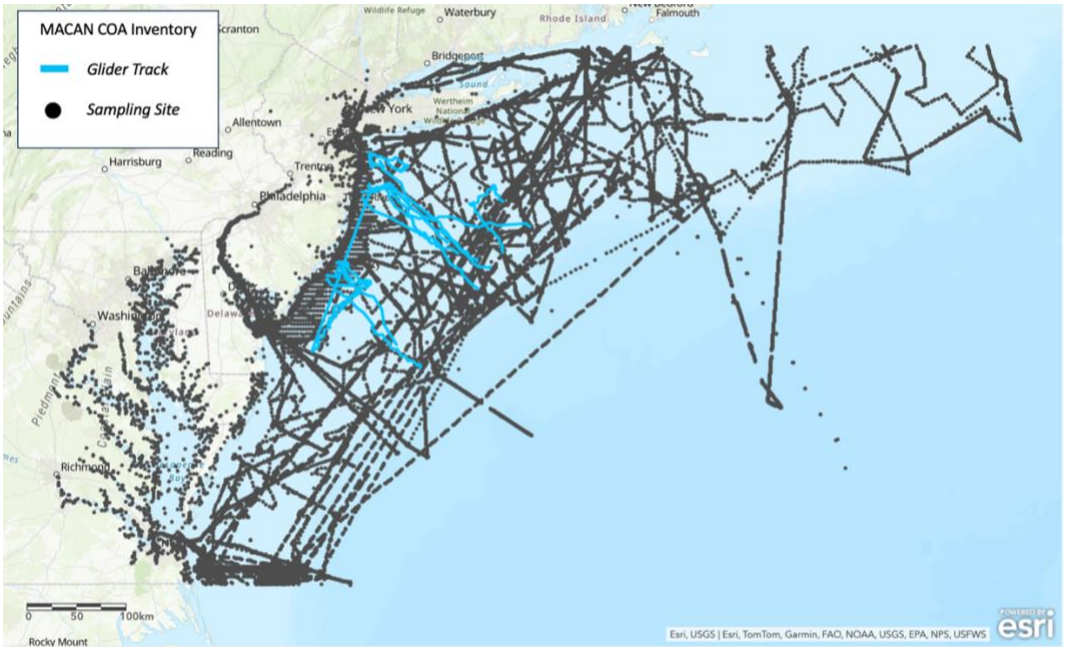

Figure 2: All seawater carbonate system sampling sites (black dots) and glider tracks (light blue lines) within the study area.

Table 2: Summary of sites sampling pH, pCO_2, TA, and DIC in the Mid-Atlantic region. Information on participating sectors and number of sites reporting methods is included for each parameter.

Parameter	Number of Sites		Participating Sectors
	Total Sites	*Sites Reporting Methods*	*Listed Most to Least*
pH	19,507 + 13 glider tracks	2,785	State, Federal, Research/ Academic Institution, NGO, local gov
pCO_2	41,334	13,390	Research/ Academic Institution, Federal Agency
TA	6,705	6,705	Research/ Academic Institution, NGO, State Gov
DIC	2,357	2,357	Research/ Academic Institution, Federal Agency
Any	46,639	-	State Agency, Federal Agency, Research/Academic Institution, NGO, local government

2.4.2 Data Quality

All sampling methodologies reported for pCO_2, DIC, and TA met either climate quality or weather quality criteria (Appendix 1). While nearly all sites measuring DIC and TA report methodologies, only 32.4% of sites measuring pCO_2 report methods. Of the 2,785 pH sampling sites for which methods were reported, 254 are of climate quality and 187 are of weather quality (Appendix 1). 10,933 sites, 23.4% of total sites, measure one carbonate system parameter to a high quality, while 5,801, or 12.4% of sites, measure two or more parameters at a high quality. The majority of sites measuring two or more carbonate system parameters at a high quality are single sampled sites; only 340 are repeat monitoring sites. Categorization of data quality was completed only for sites where methods were reported. Therefore, a large component of sites measuring pH and pCO_2 were not included in this analysis. Sites active before 2013 had the largest fraction of unreported methods/quality (Figure 3).

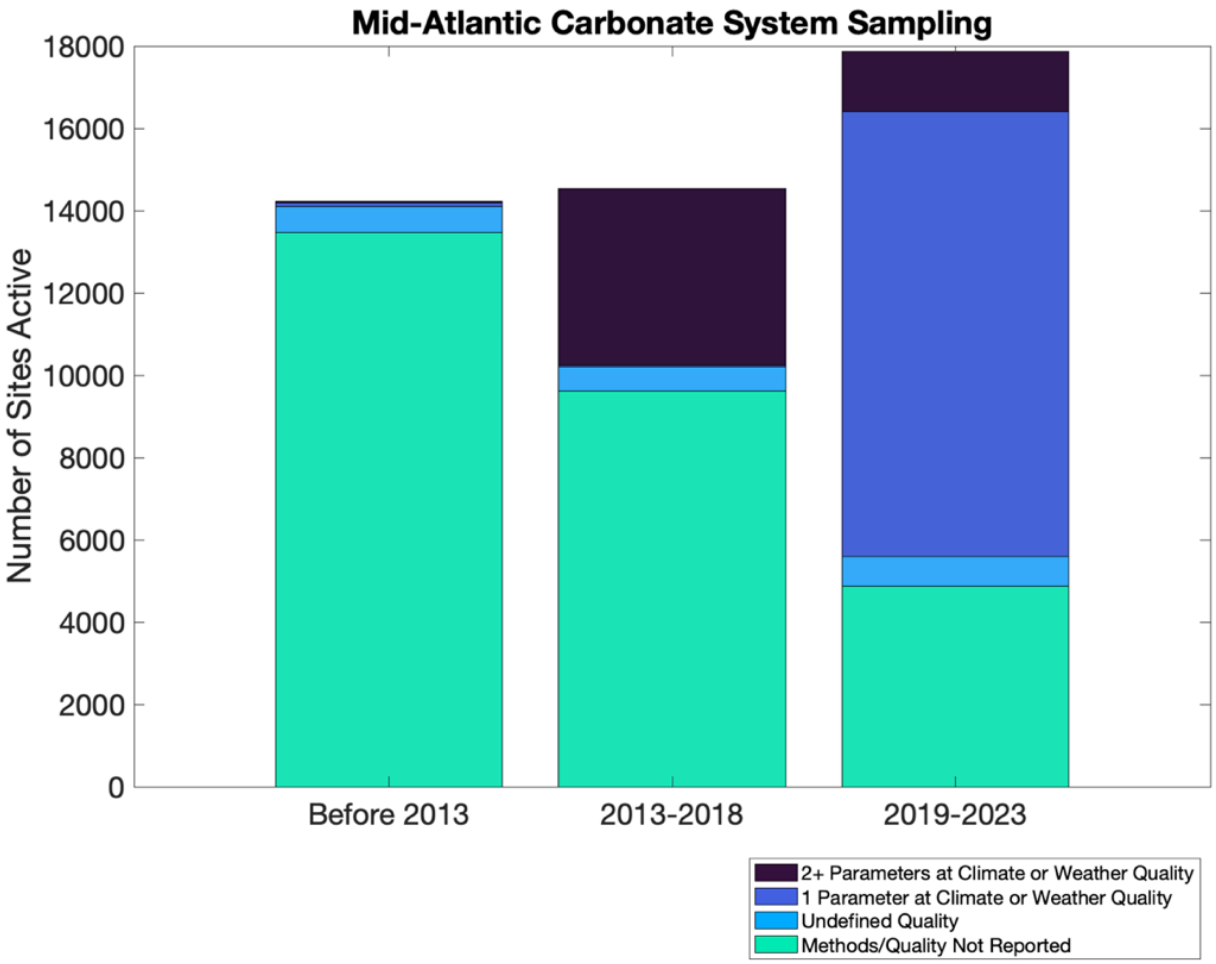

Figure 3: The number of seawater carbonate system sampling sites in the Mid-Atlantic study area active before 2013 (anytime between 1984-2013), between 2013-2018, and between 2019-2023. Different colors in each time period refer to different levels of data quality.

2.4.3 Summary of pCO_2, pH, TA, and DIC Sampling Efforts

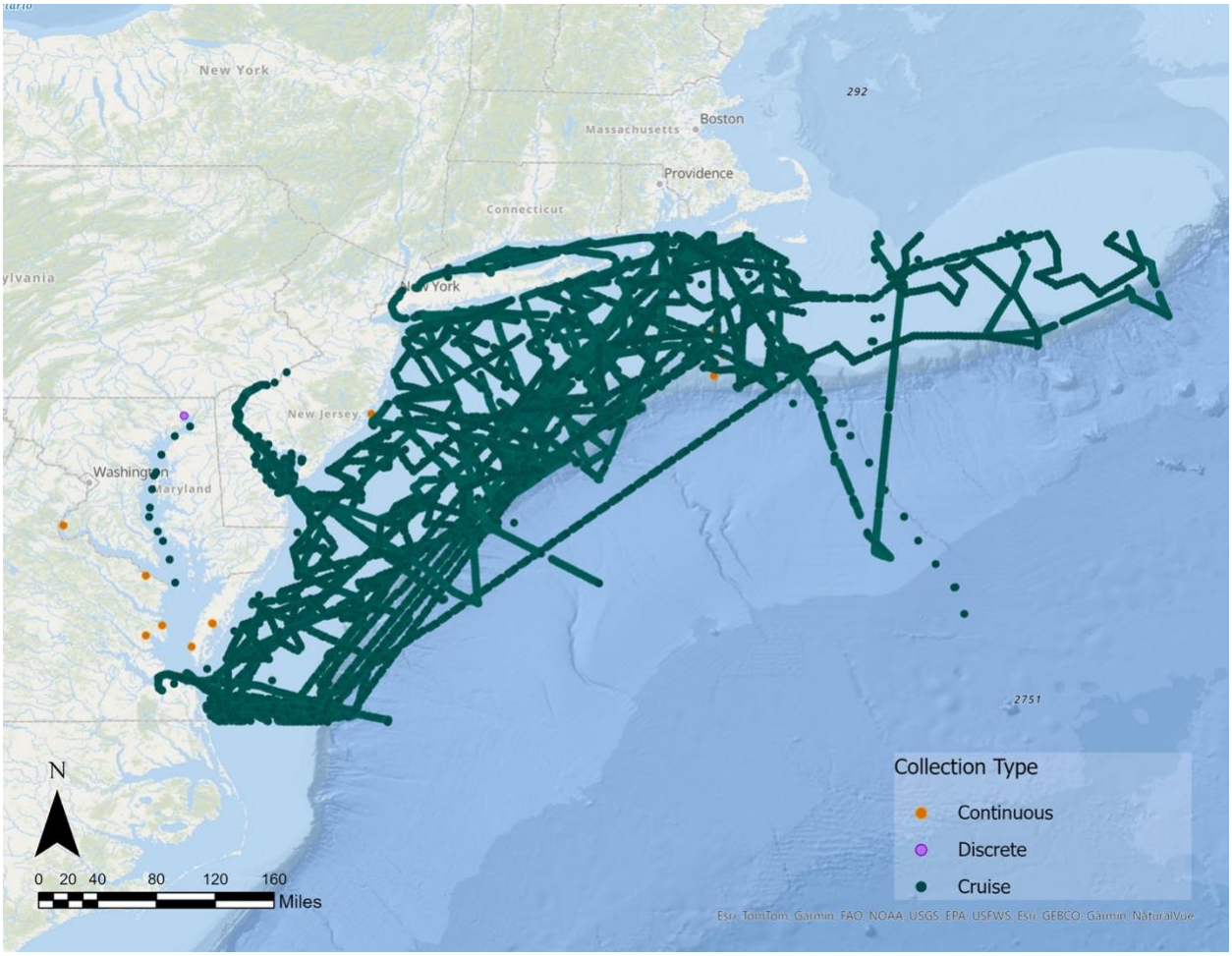

Figure 4: Map of Mid-Atlantic pCO_2 sampling sites, colored by collection method: continuous, discrete, or underway cruise.

pCO_2 is the most commonly measured carbonate system parameter at sites in the Mid-Atlantic, with 41,334 sites measuring pCO_2 in the inventory, representing 88.6% of all monitoring sites (Figure 4). The vast majority of pCO_2 measurements are collected by ship underway sampling. Only 14 sites collect pCO_2 data via continuous or discrete methods at a stationary site. pCO_2 sampling is most frequently carried out by academic and research institutions, as well as federal agencies.

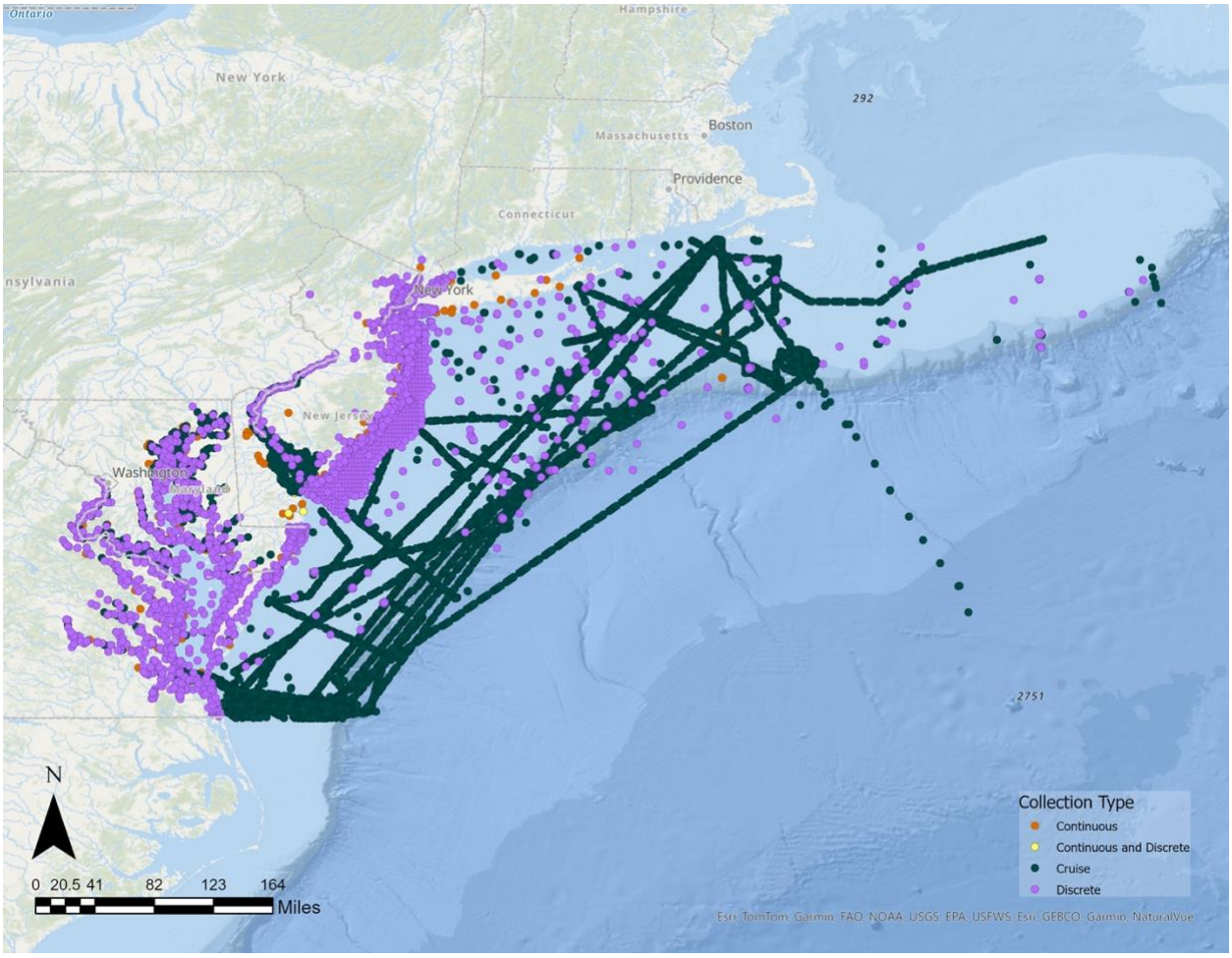

Figure 5: Map of Mid-Atlantic pH sampling sites, colored by collection method: continuous, continuous and discrete, discrete, or cruise.

pH was measured at 19,507 sites and across 13 glider deployments. Together, cruise sampling and discrete sampling account for nearly all pH monitoring sites, comprising 80% and 18% of sites sampling pH, respectively (Figure 5). When compared to other carbonate system parameters, pH has the greatest variability in methodology with 15 unique methods represented in the inventory. Among discrete sites that detail methodology, handheld probes are the most common sensors in use with employment at nearly 2,000 sites. A variety of handheld probes are used to measure pH in the Mid-Atlantic, including YSI Water Quality Meters, Oakton Handheld Meters with pH Probes, Eureka Manta2 Water Probes, and more (Figure 7). Spectrophotometry was used at 426 discrete sites. Less than 2% of all pH monitoring sites used continuous methods to measure pH (Figure 6). YSI EXO multiparameter sondes were the most common sensor reported in the inventory for continuous monitoring of pH. Other continuous sensors in use

across the region include the Honeywell Durafet III, the Sunburst SAMI-pH, and the Seabird SeaFET™. Of the methods discussed, the Sunburst SAMI-pH continuous sensor and spectrophotometry discrete sampling were the only ones that produced climate quality data. Weather quality data can be obtained with potentiometry, the Honeywell Durafet III, and the Oakton handheld pH probe. Many sectors participate in pH monitoring, with state and federal agencies accounting for the majority of sampling. Other sectors participating in pH monitoring include academic or research institutions, NGOs, and local governments. It is important to note that pH monitoring is often conducted for the purpose of understanding water quality, rather than ocean acidification dynamics.

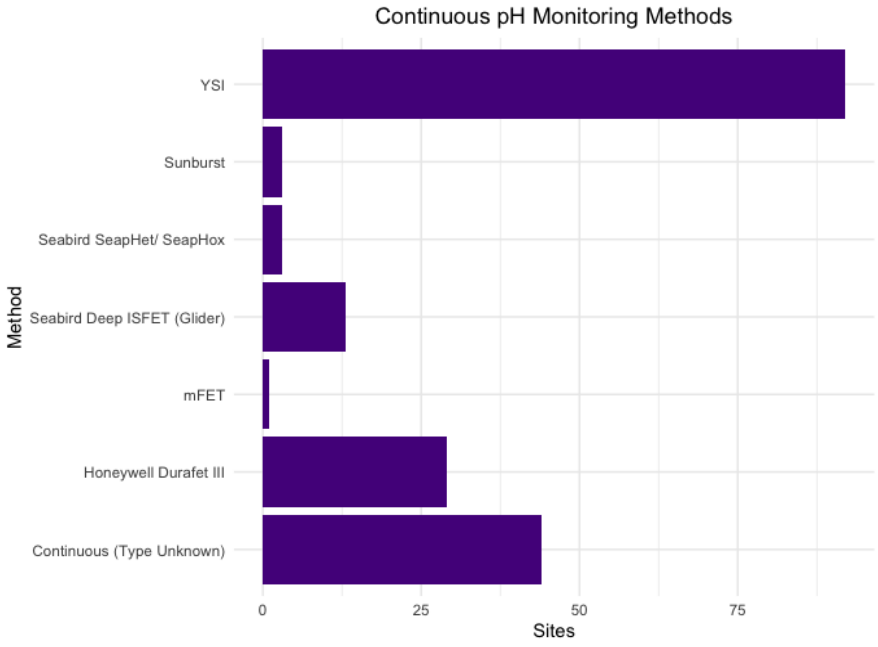

Figure 6: Continuous methods used at pH sampling sites across the Mid-Atlantic inventory.

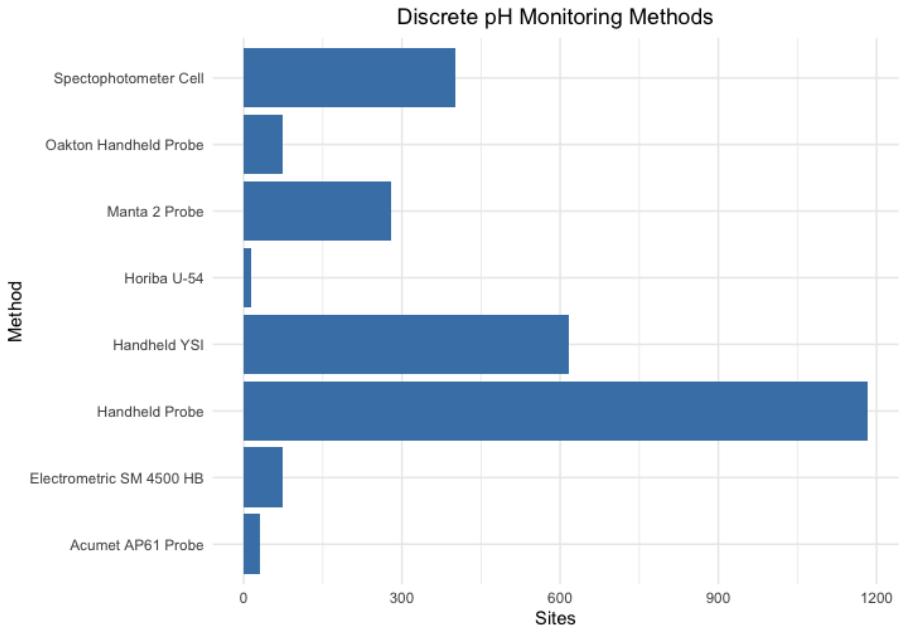

Figure 7: Discrete methods used across pH sampling sites in the Mid-Atlantic inventory.

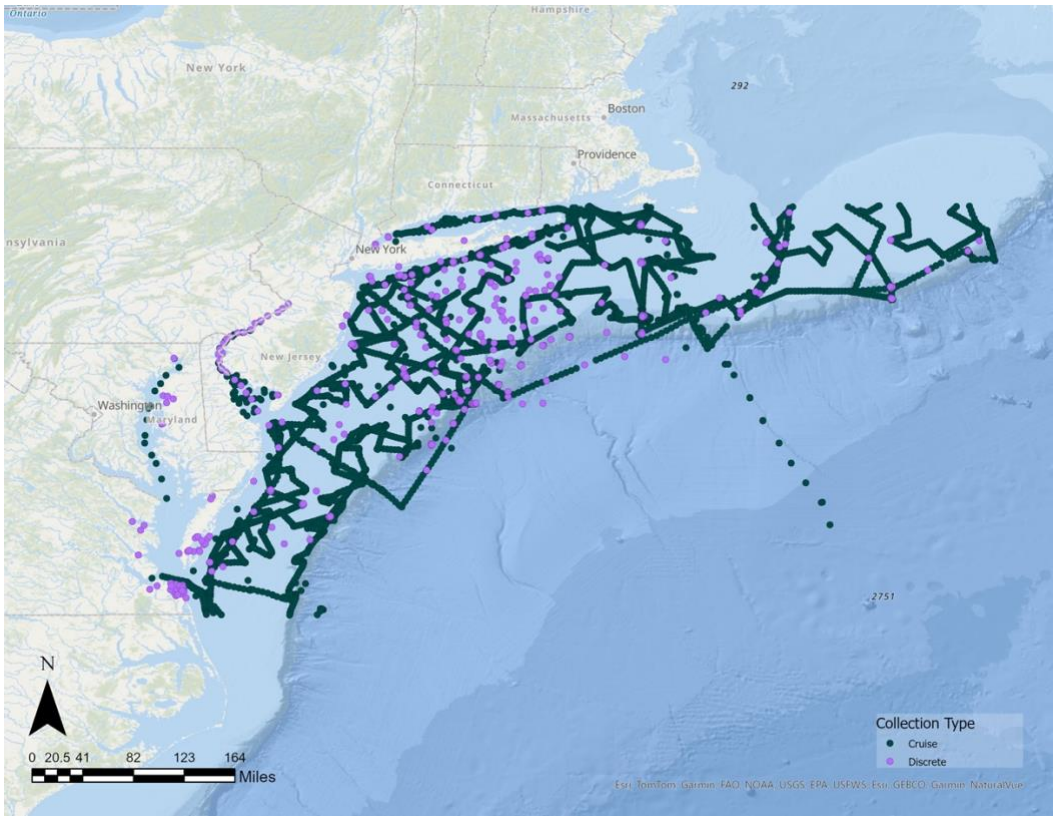

Figure 8: Map of Mid-Atlantic TA sampling sites, colored by collection method: discrete or underway cruise.

Total Alkalinity (TA) is measured at 6,705 sites in the Mid-Atlantic, with over 90% of sites collecting TA samples via underway cruise (Figure 8). At the remaining 589 sites, TA is collected and measured with discrete methods. Academic or research institutions are most likely to measure TA, but some sampling has been done by NGOs or State Government organizations.

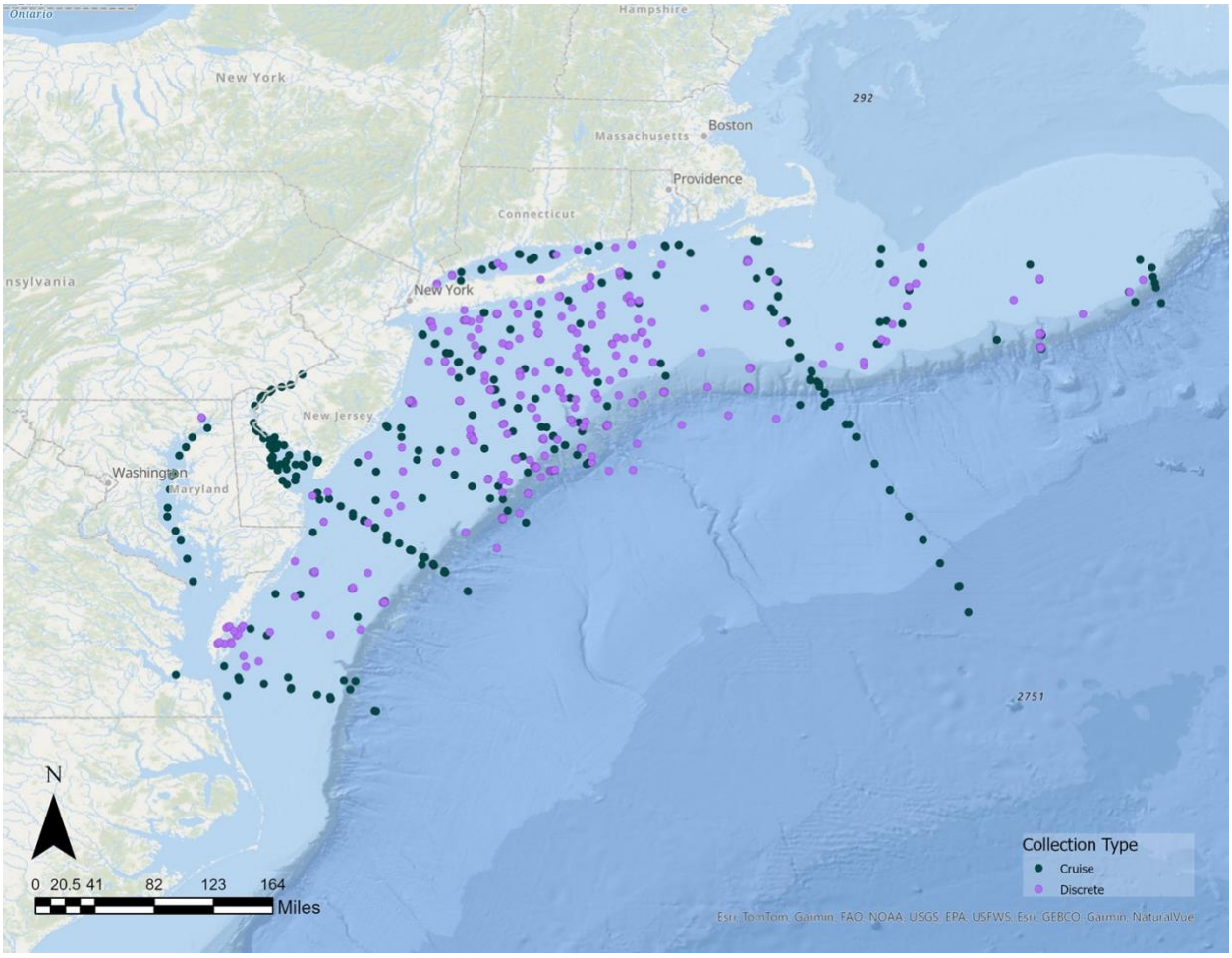

Figure 9: Map of Mid-Atlantic DIC sampling sites, colored by collection method: discrete, or cruise.

DIC is measured at the fewest number of sites in the Mid-Atlantic, with a total of 2,357 locations (Figure 9). Much like the other carbonate system parameters, the majority of DIC sampling occurred during a cruise. Discrete sampling methods make up the remaining 19% of sites where DIC was collected. Sectors that participate in DIC monitoring include academic and research institutions and federal agencies.

2.4.4. Spatial Distribution of COA Monitoring

2.4.4a Offshore vs. Coastal sampling

The majority of pH measurements were offshore, beyond Coastal Zone Management Act Boundary (CZMA), which is defined as three nautical miles from shore. 32% of sites in the study area were located nearshore within the CZMA Boundary. When considering the spatial distribution of high-quality sites, the discrepancy between the number of offshore and coastal sites grows. Only 14% of sites that measure at least two climate or weather quality parameters are located within the coastal zone. The majority of coastal monitoring sites collected data via underway cruise sampling. In addition to cruises, there are 362 continuous monitoring sites and a little over 2,500 discrete monitoring sites.

Table 3: Distribution of carbonate system sampling between coastal and offshore sites across the entire inventory time period, from 2013-2023, and from 2019-2023.

Sampling time period	**Offshore**	**Total Coastal**	**New York**	**New Jersey**	**Delaware**	**Maryland**	**Virginia**
All sites (1984-2023)	31,684	14,955	1,736	4,352	5,844	1,512	1,494
Sites Active 2013-2023	18,613	13,792	1,712	4,036	5,830	1,168	1,046
Sites Active 2019-2013	14,712	3,153	1,406	492	24	331	900

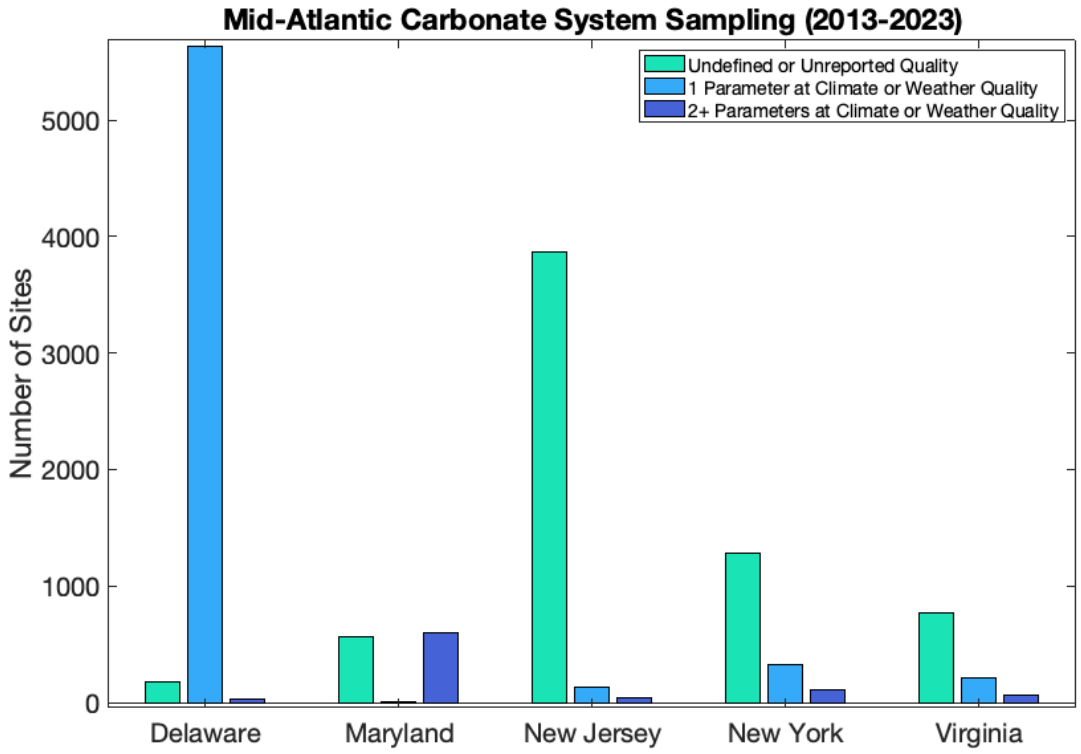

Figure 10: Number of sites in each Mid-Atlantic state active between 2013-2023. Colors correspond to three levels of data quality: undefined or unreported, one parameter measured to climate or weather quality, or two or more parameters at climate or weather quality.

2.4.4b Collection Depth

For the 17,358 sites that report collection depth, the majority of carbonate system sampling occurred at surface level. When considering collection depth patterns of each carbonate system parameter individually, surface sampling alone is most common for all parameters except for DIC, for which 89% of sites collect samples in profile (n = 533). Proportionally, TA and pCO_2 were infrequently collected in profile, with over 90% of samples for both parameters collected at the surface. Through a combination of profiling glider deployments and bottom-moored sensors, pH sampling occurs across the greatest variety of collection depths. In addition to the profiling glider deployments, 1,537 pH sampling sites collect samples at multiple depths.

Table 4: Number of sites collecting samples at various depths, including bottom, surface, profile, and surface and bottom, for each carbonate system parameter.

Carbonate System Parameter	**Collection Depth**				
	Bottom	*Surface*	*Profile*	*Surface and Bottom*	*Number of sites reporting collection depth*
pH	34	1,560	676 + 13 glider tracks	861	3,144
pCO_2	0	13,352	37	3	13,392
TA	0	4,375	476	0	4,851
DIC	0	57	476	0	533
Any	**34**	**15,657**	**806**	**861**	**17,358**

2.4.4c Estuarine Sampling

Estuaries and coastal bays in the Mid-Atlantic encompass a diverse array of coastal habitats, including salt marshes, seagrass meadows, and oyster reefs. These productive ecosystems support high biodiversity (Basset et al., 2013; Sharpe et al., 2009). Commercial fisheries in the Mid-Atlantic rely on estuaries, with 83-97% of total catch by value attributed to estuarine landings (Lellis-Dibble et al., 2008). Several estuarine species of economic importance, including Eastern Oysters, are expected to be negatively impacted by projected end-of-century OA conditions in the Mid-Atlantic (Waldbusser et al., 2011).

Estuaries exhibit naturally variable carbonate chemistry due to acidic freshwater inputs, steep spatial gradients in physical parameters, and varied influence from biological processes (Feely et al., 2010; Salisbury et al., 2008). Eutrophication, driven by excessive nutrient loading from anthropogenic sources, can amplify acidification through biogeochemical pathways (Cai et al., 2011; Wallace et al., 2014). The presence of vulnerable species and reliant economies and communities necessitates an understanding of the variability and drivers of acidification in Mid-Atlantic coastal ecosystems (Ekstrom et al., 2015). Here, we assess the spatial distribution of

carbonate system sampling across salinity gradients, levels of eutrophication, and proximity to coastal ecosystems of interest.

2.4.4d Salinity Gradient: Chesapeake Bay

Estuaries exhibit physical and chemical gradients that impart influence on pH, DIC, TA, and pCO_2. Carbonate system sampling across a gradient of mean surface salinity was assessed in the Chesapeake Bay estuary. Salinity in the Chesapeake Bay and surrounding tributaries ranges from freshwater (< 0.5 ppt) to polyhaline (18-30 ppt). In the Chesapeake Bay, carbonate system sampling is conducted across a full range of salinities, with the most sites occurring at low salinities (0-1 ppt) and mid-salinities (10-15 ppt). The middle to upper Chesapeake Bay is predominantly characterized by mesohaline (5-18 ppt) conditions. With 1,314 sites, the majority of carbonate system sampling is occurring within the mesohaline areas of the Chesapeake Bay. While carbonate system sampling is active across a wide range of salinities, most sampling efforts are of undefined or unreported quality. Sites that sample at least one parameter to climate or weather quality are present across all salinity categories, with clusters of increased sampling at mid-salinities (10-15 ppt) and high salinities (24-25 ppt).

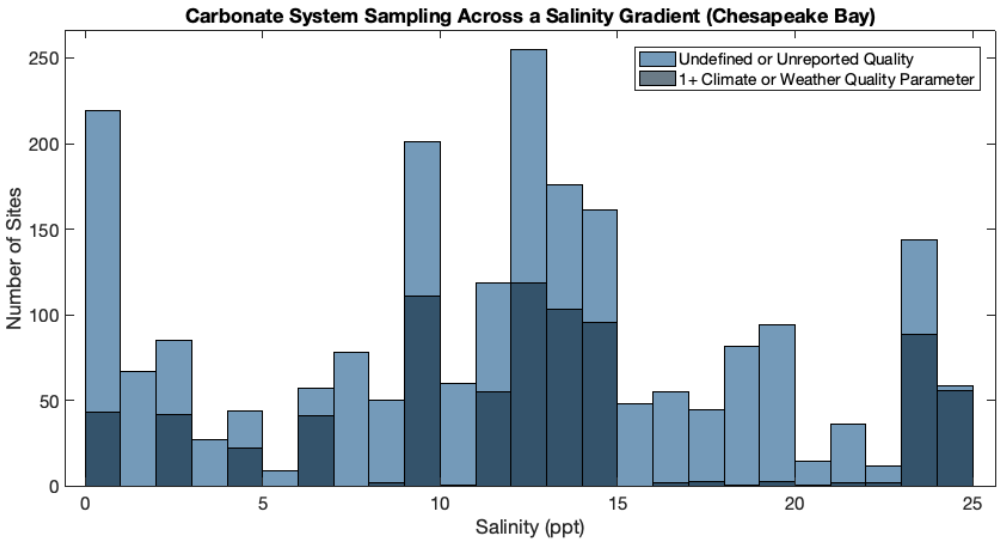

Figure 11: Chesapeake Bay seawater carbonate system sampling across a salinity gradient. Colors represent quality level of measurements.

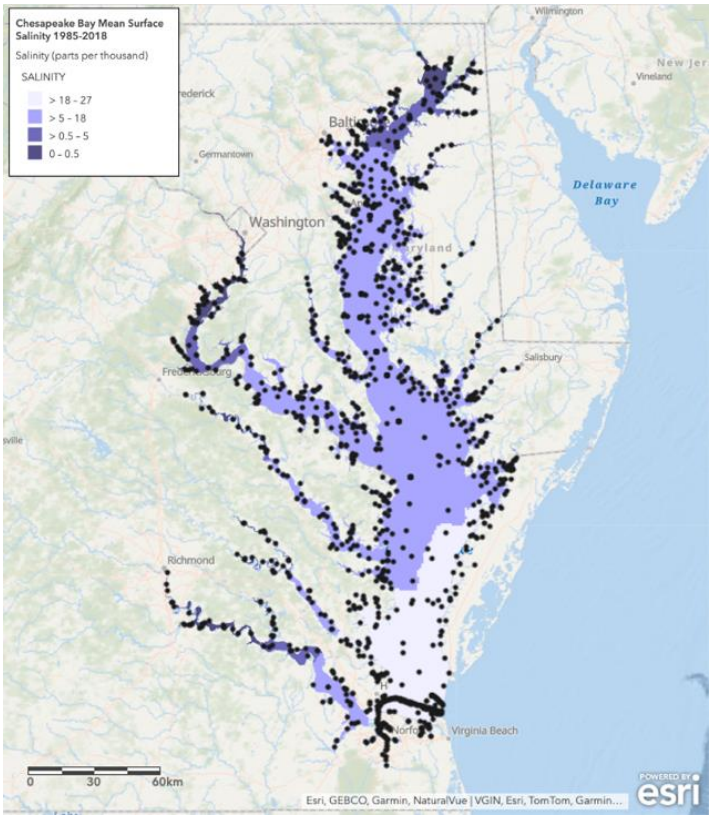

Figure 12: Chesapeake Bay seawater carbonate system sampling across a salinity gradient. Salinity ranges include freshwater (0-0.5 ppt), oligohaline (0.5-5 ppt), mesohaline (5-18 ppt), to polyhaline (18-30 ppt).

2.4.4e Eutrophication

Prominent Mid-Atlantic estuaries and coastal bays exhibit moderate to high levels of eutrophication, with the highest regional eutrophication scores seen in the Long Island Sound, the coastal bays of southern New Jersey, and the Chesapeake Bay (Bricker et al., 2007). Approximately half of the 2,588 sites in highly eutrophic estuaries measure one or more carbonate system parameters at climate or weather quality. Moderately high eutrophication areas, seen in the Chesapeake Bay and the south shore of Long Island, contain 450 sampling sites, ~98% of which had undefined or unknown quality. Regions of high and moderately-high eutrophication displayed similar densities of sampling sites, with an average of 2.2 and 1.7 sites per square kilometer, respectively.

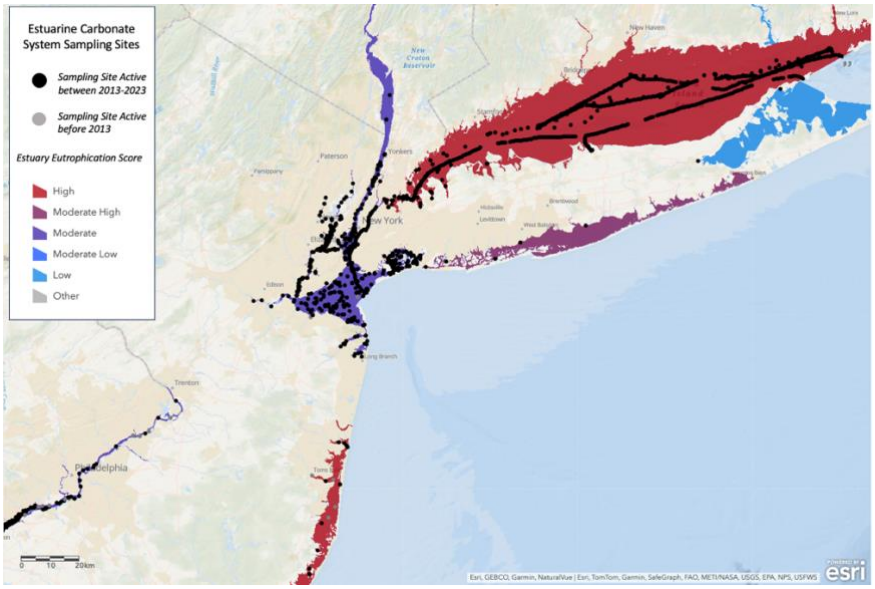

Figure 13: Carbonate system sampling sites located within estuaries or coastal bays, taking a closer look at the northern Mid-Atlantic region. Sites active anytime between 2013-2023 in black and sites active prior to 2013 in gray.

Despite accounting for 80% of the estuarine area in the Mid-Atlantic, moderate-high to highly eutrophic regions have a lower density of carbonate system measurements than estuaries with lower eutrophication scores (Figure 13; Figure 14). Moderately eutrophic areas, including the Delaware Bay, Raritan Bay, and New York Bay, have over 10,000 unique sampling sites with a mean sampling density of 28 sites per square kilometer. The majority of the sampling sites in the moderately eutrophic region were collected by underway cruise and are not repeat sampling efforts. Despite high sampling density among moderately eutrophic sites, fewer than 100 sites measure carbonate system parameters to a high quality. This discrepancy likely reflects the large proportion of historic cruise sampling that did not report methods, yielding inconclusive quality levels.

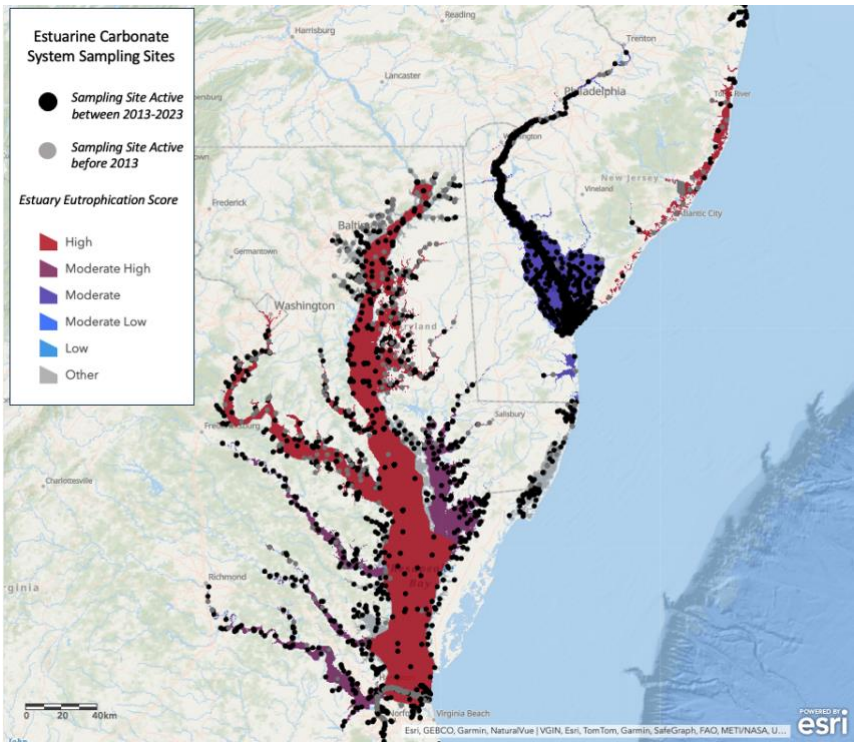

Figure 14: Carbonate system sampling sites located within estuaries or coastal bays, taking a closer look at the southern Mid-Atlantic states. Sites active anytime between 2013-2023 in black and sites active prior to 2013 in gray.

Table 5: Number of carbonate system sampling sites located in Mid-Atlantic estuaries exhibiting high, moderate high, and moderate eutrophication scores. Density of sampling and number of high quality sites are reported.

Eutrophication Score	**Area (km^2)**	**Total Number of Monitoring Sites**	**Mean Density (Sites per km^2)**	**Sites measuring 1 parameter at Climate or Weather Quality**	**Sites measuring 2+ parameters at Climate or Weather Quality**
High	1,182	2,588	2.2	629	726
Moderate High	269	450	1.7	3	5
Moderate	363	10,010	28	49	48

2.4.4f Proximity to Marine and Estuarine Intertidal Habitats

Biological processes exert influence on estuarine and marine carbon cycles, leading to variable effects on the extent of acidification (Johnson et al., 2013). Estuaries host biological hotspots like salt marshes and seagrass meadows that have opposing effects on carbonate chemistry. Salt marshes, which are prevalent across Mid-Atlantic estuaries, are exporters of DIC and can exacerbate acidification in nearby coastal waters (Baumann et al., 2015; Wang et al., 2016). Alternatively, seagrass meadows have been shown to increase pH locally, lessening the effects of acidification (Hendriks et al., 2014; Ricart et al., 2021). In other ecosystems, biological effects on carbonate chemistry can differ based on the specific biological processes at work. For example, aerobic and anaerobic respiration, primary production, and nitrification, all produce or consume DIC and TA in variable quantities.

In the coastal zone, 9,014 carbonate system sampling sites are located within 0.5 km of estuarine intertidal habitats and 297 sites located within 0.5 km of marine intertidal habitats. Of estuarine intertidal sites, 65% are adjacent to emergent marsh sites and ~1% are located near aquatic beds, comprising seagrass and macroalgal habitats. Using a different data source estimating Mid-Atlantic seagrass area, there are 63 sites located within seagrass meadows. Regionally, emergent marsh area greatly exceeds the area of submerged aquatic vegetation. The remaining estuarine intertidal sites were located near a variety of coastal habitats, including unconsolidated shore (comprising mudflats, sandy bottoms, etc.), coastal forests, scrub-shrub, and rocky shore. There are 2,144 carbonate system sampling sites located within 1 km of shellfish survey sites, 133 of which are measuring two or more parameters at a high quality.

2.4.4g Spatial Distribution of Deep Sea Corals

While sparsely studied, deep-sea corals are an important marine resource in the Mid-Atlantic that are prevalent in submarine canyons just beyond the continental shelf break (Packer et al., 2007; Shank et al., 2020). Deep-sea corals provide essential habitat to fish and other invertebrates. Their slow growth rates make these organisms particularly vulnerable to any changes in environmental conditions, including ocean acidification (Turley et al., 2007). Under current ocean acidification rates in the North Atlantic, the depth of the aragonite saturation horizon is expected to rise in the water column, such that deep-sea corals will be exposed to

water that is undersaturated with respect to aragonite by 2050 (Perez et al., 2018). While there is still limited information about how Mid-Atlantic deep-sea corals may respond to acidification, some evidence suggests that they could experience decreases in net calcification or, in extreme cases, dissolution of existing coral structure. In a study off the coast of California, living deep-sea corals were found to be robust to acidification effects when experiencing aragonite undersaturation (Hennige, et al., 2020). However, dead coral skeletons, which typically form the underlying foundation of living coral structures, became more porous under acidified conditions (Hennige, et al., 2020). Crumbling dead coral structures endangered structural integrity at the ecosystem scale (Hennige, et al., 2020).

Here, we assess distribution of carbonate system sampling efforts that coincide with modelled deep-sea coral habitat for the Mid-Atlantic shelf (Kinlan et al., 2013). In total, there were 6,219 sites where seawater carbonate chemistry sampling occurred within the spatial footprint of the deep-sea coral habitat. Of those, the majority were surface samples, with only 99 sites collecting samples in profile. In this case, surface samples did not adequately represent the conditions experienced in the habitat of interest, as the deep-sea corals are found on the seafloor, at depths between 700 and 1850 meters.

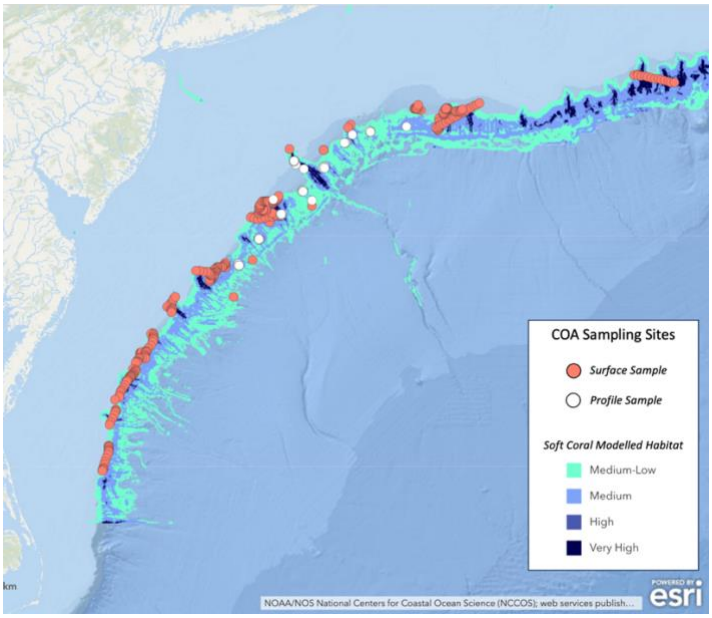

Figure 14: COA sampling sites measuring 2+ carbonate system parameters at a high quality that overlap with modelled deep-sea coral habitat. White circles represent samples that were collected in profile.

2.5 Summary

The current state of Mid-Atlantic seawater carbonate system monitoring are summarized with respect to a subset of Mid-Atlantic acidification research priorities as discussed in regional studies and the NOAA Ocean, Coastal, and Great Lakes Acidification Research Plan: 2020-2029 (Goldsmith et al., 2019; Kinkade et al., 2020; Saba et al., 2019). Below, we highlight data quality, spatial distribution of sampling across diverse ecosystems, and sampling with respect to known drivers of coastal acidification.

Data Quality of Carbonate System Sampling

A key priority identified for the region is for carbonate system data to be of a quality befitting the intended use of the data (Kinkade et al., 2020). Climate and weather quality data are appropriate for assessing long-term COA changes and short-term or spatial COA patterns, respectively (Newton et al., 2015). In Mid-Atlantic carbonate system sampling efforts between 2019 and 2023, 60% of sites measured one carbonate system parameter at climate or weather

quality, while 8% of sites measured two parameters to a high quality. While there is a large proportion of sites reporting high quality data, increasing the number of seawater carbonate system parameters being measured to two or more would allow for complete characterization of the carbonate system. The majority of sites measuring two or more carbonate system parameters at a high quality were sampled only once, while only 340 sites in the MACAN inventory are repeat monitoring sites. Many sites in the MACAN inventory, especially those active prior to 2013, do not have sufficient metadata to assess methods or data quality. Explicit reporting of data quality, methodology, and QA/QC for past, present, and future COA monitoring sites will allow for improved opportunities for data sharing and comparison across the Mid-Atlantic region.

Sampling Across Diverse Ecosystems

COA monitoring across a diverse array of ecosystems and depths can resolve spatial heterogeneity in regional carbonate system conditions, and is therefore a Mid-Atlantic monitoring priority (Goldsmith et al., 2019; Kinkade et al., 2020; Saba et al., 2019). According to analysis of the MACAN inventory, Mid-Atlantic carbonate system sampling sites are located across varied ecosystems from estuaries to the continental shelf, with high quality sites located in proximity to seagrass meadows, emergent wetlands, deep-sea coral habitat, and shellfish beds. Bottom and profiled depth measurements are infrequent, representing only 10% of reported measurement depths. In particular, the coastal zone has few high-quality, bottom measurements. Benthic and profiling samples were most likely to be collected during cruises, offshore, and at sites that did not engage in repeat monitoring. Additionally, few high frequency, continuous measurements are being collected in benthic sites. In the coastal zone, there are a total of 34 continuous pH sensors of undefined quality moored at depth. Offshore glider deployments in recent years have substantially increased the amount of high frequency carbonate system measurements occurring across a range of depths.

Sampling with Respect to Coastal Acidification Drivers

Another regional priority is to assess acidification with respect to drivers of coastal acidification, including eutrophication and freshwater inputs (Goldsmith et al., 2019; Kinkade et al., 2020; Saba et al., 2019). In sections 1.4.4c and 1.4.4d, we discuss the number of sites in the

MACAN inventory located in eutrophic estuaries and across a salinity gradient in the Chesapeake Bay, respectively. Despite accounting for 80% of the estuarine area in the Mid-Atlantic, moderate-high to highly eutrophic regions have a lower density of carbonate system measurements than estuaries with lower eutrophication scores. In the Chesapeake Bay, carbonate system sampling is well distributed across low-to-high salinities.

2.6 Appendix 1: Data Quality

Table 1: pH methods reported in the Mid-Atlantic with associated accuracy, precision, and quality category.

pH Measurement Method	**Accuracy**	**Precision**	**Quality**
YSI EXO2	± 0.1 pH units within ±10˚C of calibration temp; ±0.2 pH units for entire temp range	± 0.01 pH units	Undefined
Sunburst SAMI-pH	± 0.003 pH units	± 0.001 pH units	Climate
Seabird Seaphox V2	± 0.05 pH units (factory calibration)	± 0.004 pH units	Undefined
Honeywell Durafet®-based pH Sensor	± 0.01-0.03 pH units	± 0.005 pH units	Weather
Spectrophotometric pH (m-Cresol Purple dye)	± 0.01 pH units	± 0.0004 units	Weather
Oakton handheld pH probe	± 0.01 pH units	± 0.01	Weather

Manta 2 probe	± 0.1 pH units within 10 Cº of calibration; ± 0.2 otherwise	± 0.01	Undefined
Horiba U-54	± 0.1 pH units	± 0.05pH	Undefined
YSI handheld	± 0.2 pH units	± 0.01	Undefined
Potentiometry	± 0.02 pH units	No Data	Weather

Table 2: TA methods reported in the Mid-Atlantic with associated accuracy, precision, and quality category.

TA Measurement Method	**Accuracy**	**Precision**	**Quality**
Apollo-Scitech	0.1% or better		Climate
Contros HydroFIA TA	± 5 µmol kg-1	± 2 µmol kg-1	Weather
Metrohm 765	± 0.2%		Weather

Table 4: pCO_2 methods reported in the Mid-Atlantic with associated accuracy, precision, and quality category.

pCO_2 Measurement Method	**Accuracy**	**Quality**
LI-7000 Infrared Analyzer	Accuracy: 1%.	Weather

LI-6262 Infrared Analyzer	± 1 ppm at 350 ppm (<3 ppm maximum). ± 2 ppm at 1000 ppm (<6 ppm maximum).	Climate
Pro Oceanus Pro CV	± 0.5%	Climate

2.7 Appendix 2: Supplemental Data Tables

Table 1: Total number of sampling sites and high-quality sampling sites located within or nearby ecosystems of interest.

Ecosystem Type		Total Number of Sampling Sites	Number of High-Quality Sampling Sites measuring 2+ parameters
Seagrass		63	0
Deep-Sea Soft Corals		6,219	600
Estuarine Intertidal (sites within 0.5 km)	Emergent Marsh	5,814	-
	Unconsolidated Shore	2,717	-
	Aquatic Bed (Macroalgal or submerged aquatic veg)	85	-
	Other (scrub-shrub, rocky shore, etc.)	398	-
Marine Intertidal (sites within 0.5 km)	Unconsolidated Shore	279	-
	Rocky Shore	18	-
Within 1km of Shellfish Survey Site		2,144	133

Table 2: Number of sampling sites in the Chesapeake Bay located across four salinity classes.

Salinity Range	Number of Sampling Sites (Chesapeake Bay)

Polyhaline (18-30 ppt)	433
Mesohaline (5-18 ppt)	1,314
Oligohaline (0.5-5 ppt)	293
Freshwater (< 0.5)	149

2.8 References

Basset, A., Elliott, M., West, R. J., and Wilson, J. G. (2013). Estuarine and lagoon biodiversity and their natural goods and services. *Estuarine, Coastal and Shelf Science*, *132*, 1-4.

Baumann, H., Wallace, R. B., Tagliaferri, T., and Gobler, C. J. (2015). Large natural pH, CO_2 and O_2 fluctuations in a temperate tidal salt marsh on diel, seasonal, and interannual time scales. *Estuaries and Coasts*, *38*, 220-231.

Bricker, S. B., Longstaff, B., Dennison, W., Jones, A., Boicourt, K., Wicks, C., and Woerner, J. (2008). Effects of nutrient enrichment in the nation's estuaries: a decade of change. *Harmful Algae*, *8*(1), 21-32.

Cai, W. J., Feely, R. A., Testa, J. M., Li, M., Evans, W., Alin, S. R., ... and Bednaršek, N. (2021). Natural and anthropogenic drivers of acidification in large estuaries. *Annual Review of Marine Science*, *13*, 23-55.

Cai, W. J., Hu, X., Huang, W. J., Murrell, M. C., Lehrter, J. C., Lohrenz, S. E., ... and Gong, G. C. (2011). Acidification of subsurface coastal waters enhanced by eutrophication. *Nature geoscience*, *4*(11), 766-770.

Doney, S. C., Fabry, V. J., Feely, R. A., and Kleypas, J. A. (2009). Ocean acidification: the other CO2 problem. *Annual review of marine science*, *1*, 169-192.

Ekstrom, J. A., Suatoni, L., Cooley, S. R., Pendleton, L. H., Waldbusser, G. G., Cinner, J. E., ... and Portela, R. (2015). Vulnerability and adaptation of US shellfisheries to ocean acidification. *Nature climate change*, *5*(3), 207-214.

Feely, R. A., Alin, S. R., Newton, J., Sabine, C. L., Warner, M., Devol, A., ... and Maloy, C. (2010). The combined effects of ocean acidification, mixing, and respiration on pH and

carbonate saturation in an urbanized estuary. *Estuarine, Coastal and Shelf Science*, *88*(4), 442-449.

Feely, R. A., Sabine, C. L., Lee, K., Berelson, W., Kleypas, J., Fabry, V. J., and Millero, F. J. (2004). Impact of anthropogenic CO2 on the CaCO3 system in the oceans. *Science*, *305*(5682), 362-366.

Gledhill, Dwight K., Meredith M. White, Joseph Salisbury, Helmuth Thomas, Ivy Mlsna, Matthew Liebman, Bill Mook et al. "Ocean and coastal acidification off New England and Nova Scotia." *Oceanography* 28, no. 2 (2015): 182-197.

Glenn, S., Arnone, R., Bergmann, T., Bissett, W. P., Crowley, M., Cullen, J., ... and Schofield, O. (2004). Biogeochemical impact of summertime coastal upwelling on the New Jersey Shelf. *Journal of Geophysical Research: Oceans*, *109*(C12).

Goldsmith, K. A., Lau, S., Poach, M. E., Sakowicz, G. P., Trice, T. M., Ono, C. R., ... and Saba, G. K. (2019). Scientific considerations for acidification monitoring in the US Mid-Atlantic Region. *Estuarine, Coastal and Shelf Science*, *225*, 106189.

Hendriks, I. E., Olsen, Y. S., Ramajo, L., Basso, L., Steckbauer, A., Moore, T. S., ... and Duarte, C. M. (2014). Photosynthetic activity buffers ocean acidification in seagrass meadows. *Biogeosciences*, *11*(2), 333-346

Hennige, S. J., Wolfram, U., Wickes, L., Murray, F., Roberts, J. M., Kamenos, N. A., ... and Etnoyer, P. J. (2020). Crumbling reefs and cold-water coral habitat loss in a future ocean: evidence of "Coralporosis" as an indicator of habitat integrity. *Frontiers in Marine Science*, *7*, 668.

Johnson, Z. I., Wheeler, B. J., Blinebry, S. K., Carlson, C. M., Ward, C. S., and Hunt, D. E. (2013). Dramatic variability of the carbonate system at a temperate coastal ocean site (Beaufort, North Carolina, USA) is regulated by physical and biogeochemical processes on multiple timescales. *PLoS One*, *8*(12), e85117.

Kinlan, B., M. Poti, D. Dorfman, C. Caldow, A. Drohan, D. Packer, and M. Nizinski. 2016. Model output for deep-sea coral habitat suitability in the U.S. North and Mid-Atlantic from 2013 (NCEI Accession 0145923). NOAA National Centers for Environmental Information. Dataset.

Kinkade, C., Meseck, S. L., Chambers, R. C., Gledhill, D. K., Hyde, K. J., Melrose, C., Phelan, B., Poach, M. E., and Turner, E. (2020). Mid-Atlantic Bight Region Acidification Research. Chapter 9 in *NOAA Ocean, Coastal, and Great Lakes Acidification Research Plan: 2020–2029.* E.B. Jewett, E.B. Osborne, K.M. Arzayus, K. Osgood, B.J. DeAngelo, and J.M. Mintz, eds, National Oceanic and Atmospheric Administration, US Department of Commerce.

LaRoche, Carly; Wakefield, Kirstin; Reimer, Janet J. (2023). "Coastal and Ocean Acidification Monitoring Inventory for the Mid-Atlantic", https://doi.org/10.18130/V3/RWBODF, University of Virginia Dataverse, V1.

Lellis-Dibble, K. A., McGlynn, K. E., and Bigford, T. E. (2008). Estuarine fish and shellfish species in US commercial and recreational fisheries: economic value as an incentive to protect and restore estuarine habitat. (NOAA Technical Memorandum NMFS-F/SPO-90). U.S. Department of Commerce, National Oceanic and Atmospheric Administration, National Marine Fisheries Service.

Lewis, E. R., and Wallace, D. W. R. (1998). *Program developed for CO2 system calculations* (No. cdiac: CDIAC-105). Environmental System Science Data Infrastructure for a Virtual Ecosystem (ESS-DIVE)(United States).

National Ocean Economics Program (NOEP). (2021). *Coastal Population and Housing*. https://www.oceaneconomics.org/NOEP/Demographics/PHsearch.aspx

Newton, J. A., Feely, R. A., Jewett, E. B., Williamson, P., and Mathis, J. (2015). Global ocean acidification observing network: requirements and governance plan.

Packer, D. B., Boelke, D., Guida, V., and McGee, L. A. (2007). State of deep coral ecosystems in the Northeastern US region: Maine to Cape Hatteras. In: SE Lumsden, Hourigan TF, Bruckner AW and Dorr G (eds.) The State of Deep Coral Ecosystems of the United States. NOAA Technical Memorandum CRCP-3. Silver Spring MD, 195-232 pp.

Perez, F. F., Fontela, M., García-Ibáñez, M. I., Mercier, H., Velo, A., Lherminier, P., ... and Padin, X. A. (2018). Meridional overturning circulation conveys fast acidification to the deep Atlantic Ocean. *Nature*, *554*(7693), 515-518.

Ricart, A. M., Ward, M., Hill, T. M., Sanford, E., Kroeker, K. J., Takeshita, Y., ... and Gaylord, B. (2021). Coast-wide evidence of low pH amelioration by seagrass ecosystems. *Global change biology*, *27*(11), 2580-2591.

Saba, G. K., Goldsmith, K. A., Cooley, S. R., Grosse, D., Meseck, S. L., Miller, A. W., ... and Zimmerman, R. (2019). Recommended priorities for research on ecological impacts of ocean and coastal acidification in the US Mid-Atlantic. *Estuarine, Coastal and Shelf Science*, *225*, 106188.

Sabine, C. L., Feely, R. A., Gruber, N., Key, R. M., Lee, K., Bullister, J. L., ... and Rios, A. F. (2004). The oceanic sink for anthropogenic CO2. *science*, *305*(5682), 367-371.

Salisbury, J., Green, M., Hunt, C. W. and Campbell, J. Coastal acidification by rivers: a threat to shellfish? *EOS Trans. Am. Geophys. Union* **89**, 513–528 (2008).

Shank, T. M., Heyl, T. P. (2020). Deep-water coral and fish of U.S. mid-Atlantic canyons: Implications for management and conservation. Mid-Atlantic Regional Ocean Council.

Sharpe, P. J., and Baldwin, A. H. (2009). Patterns of wetland plant species richness across estuarine gradients of Chesapeake Bay. *Wetlands*, *29*, 225-235.

Turley, C. M., Roberts, J. M., and Guinotte, J. M. (2007). Corals in deep-water: will the unseen hand of ocean acidification destroy cold-water ecosystems?. *Coral reefs*, *26*, 445-448.

United States Department of State. (2023). *GIS Data of U.S. ECS Outer Limits: Atlantic* [Data: shapefile]. https://www.state.gov/downloads-us-ecs-project/

van Hooidonk, R. J., Maynard, J. A., Manzello, D. and Planes, S. Opposite latitudinal gradients in projected ocean acidification and bleaching impacts on coral reefs. *Glob. Change Biol.* 103–112, (2014).

Waldbusser, G. G., Voigt, E. P., Bergschneider, H., Green, M. A., and Newell, R. I. (2011). Biocalcification in the eastern oyster (Crassostrea virginica) in relation to long-term trends in Chesapeake Bay pH. *Estuaries and coasts*, *34*, 221-231.

Wallace, R. B., Baumann, H., Grear, J. S., Aller, R. C., and Gobler, C. J. (2014). Coastal ocean acidification: The other eutrophication problem. *Estuarine, Coastal and Shelf Science*, *148*, 1-13.

Wang, Z. A., Kroeger, K. D., Ganju, N. K., Gonneea, M. E., and Chu, S. N. (2016). Intertidal salt marshes as an important source of inorganic carbon to the coastal ocean. *Limnology and Oceanography*, *61*(5), 1916-1931.

Zeebe, R. E., and Wolf-Gladrow, D. (2001). *CO2 in seawater: equilibrium, kinetics, isotopes* (Vol. 65). Gulf Professional Publishing.

Chapter 3: Characterizing Variability and Drivers of Seawater Carbonate Chemistry in the Virginia Coast Reserve

3.1 Abstract

Given the high variability of seawater carbonate chemistry in nearshore marine systems, quantification of spatiotemporal trends and drivers of variability can help us better understand the role of estuaries, coastal bays, and tidal wetlands in important coastal climate issues. In this chapter, we assess spatial and seasonal trends in seawater carbonate chemistry across 13 sites in the marsh-fringed coastal bays of the Virginia Coast Reserve. We also assess contributions of physical, thermodynamic, and biogeochemical drivers of variability across four sampling efforts (March, July, and October 2022 and April 2023). Conservative mixing was a key driver of TA and DIC concentrations across all seasons, with deviations most evident among marsh adjacent samples in July. High temperatures and increased summertime biological activity disproportionately impacted seawater carbonate system dynamics in marsh adjacent sites when

compared to lagoonal-inlet sites, resulting in high July DIC and pCO_2 in sites located near marshes. Thermal and biogeochemical drivers experience site-specific seasonal change in July that result in heightened divergence of seawater carbonate chemistry at marsh adjacent sites and lagoonal-inlet sites.

3.2 Introduction

Varied biogeochemical and physical forcings across the nearshore coastal marine environment, spanning estuaries, tidal wetlands, and shallow bays, produce a landscape of heterogenous seawater inorganic carbonate chemistry (Cai et al., 2011; Wallace et al., 2014). These highly productive systems present a patchwork of biogeochemical processes that locally modify concentrations of dissolved inorganic carbon (DIC) and total alkalinity (TA) in distinct, process-dependent ratios (Doney et al., 2007; Herrmann et al., 2014; Soetaert et al., 2007). Hydrodynamic regimes dictating the flow of coastal waters, including tidal cycles and currents, facilitate lateral exchange between nearshore marine systems resulting in the mixing of seawater with unique inorganic carbonate chemistry signatures (James et al., 2020; Paulsen et al., 2018). In estuaries, mixing of fresh and saline endmembers produce gradients in physical seawater properties and seawater carbonate chemistry, in which the composition and quantity of freshwater inputs can introduce variable effects on receiving waters (Cai et al., 2021).

Comprising DIC, TA, pCO_2, and pH, the inorganic seawater carbonate system in the nearshore marine environment is an essential component of the global carbon cycle, and its characterization enhances understanding of critical climate issues like carbon burial, degassing, and seawater acid-base chemistry (Cai et al., 2011; Najjar et al., 2018; Prentice et al., 2020; Wallace et al., 2014). However, a background of extreme spatiotemporal heterogeneity in the nearshore seawater carbonate system paired with anthropogenic perturbations means that seawater carbonate chemistry dynamics in the nearshore marine environment remain poorly constrained (Najjar et al., 2018). Many coastal and estuarine areas already undergo large seasonal swings in seawater carbonate chemistry, often experiencing more change in pH over a year than the open ocean is expected to undergo over the next century (Boulais et al., 2017). For example, pH annual ranges of <7.0 to 8.2 have been observed in estuaries along the East Coast of the United States (Boulais et al., 2017). Long term trends in ocean acidification paired with

ongoing nutrient pollution may intensify seasonal carbonate system variability of coastal ecosystems (Feely et al., 2010). A regional carbon budget constructed for the East Coast of North America highlights several priority research areas in which our understanding of the coastal carbon cycle is currently lacking, including effects of net ecosystem production, coastal gas exchange, lateral exchange between tidal wetlands and shelf waters, and an overall need for increased carbonate system observations in highly variable coastal ecosystems (Najjar et al., 2018).

Encompassing an array of dynamic coastal ecosystems, the Virginia Coast Reserve (VCR) provides an ideal backdrop to study the variability of carbonate system dynamics at the landscape scale. The VCR is situated on the southern end of the Delmarva Peninsula and is the site of a Long Term Ecological Research project (LTER). Stretching 110 kilometers along the Atlantic Coast, the VCR research region comprises barrier islands, lagoons, upland coastal forests, saltmarshes, and seagrass meadows. VCR salt marshes facilitate long term carbon storage, but are experiencing rapid migration and areal losses due to high rates of sea level rise present along the US Mid-Atlantic coast (Miller et al., 2013; Smith and Kirwan, 2021). At an individual ecosystem level, changes in areal extent threaten the stability of coastal carbon stocks (Kirwan and Megonigal, 2013; Smith and Kirwan, 2021; Smith et al. 2024). However, recent work demonstrates relative carbon stability over time in the VCR study region at the landscape scale, with carbon losses from some ecosystems compensated for by carbon gains in nearby ecosystems (Smith et al. 2024). Understanding mechanisms and directionality of DIC lateral exchange in the VCR across various systems can further inform carbon connectivity at the landscape scale.

In Chapter 3, I employ a variety of methods to assess patterns, determine drivers, and understand the implications of spatial and seasonal variability in the seawater inorganic carbonate system in the coastal lagoons of the Virginia Coast Reserve. This research aims to contribute to the body of seawater carbonate system observations in highly variable, coastal systems toward a better understanding of the processes driving acidification, coastal gas exchange, and lateral carbon transfer between ecosystems. In this chapter, a two-endmember linear mixing model between groundwater and ocean inlet endmembers is utilized to determine

the effects of conservative mixing on observed DIC and TA concentrations. Estimates of air-sea CO_2 gas exchange and thermal drivers of pCO_2 are also included among the analyses. Relationships between carbonate system parameters and biogeochemical nutrient signals are assessed to explore biological drivers of TA and DIC. With a lack of substantial riverine inputs, and therefore limited delivery of nutrient pollution, the VCR also provides a unique setting to assess the thermodynamic and biological drivers of nearshore marine systems alone, without the added variability of riverine delivery of excess nutrients.

Thermodynamic and Physical Drivers

Currents and tidal flushing represent dominant forms of flow in the VCR and can dictate lateral movement of DIC and TA. To understand the effects of mixing between two parcels of water with different initial DIC and TA conditions, two-endmember mixing models are often used to assess the contribution of conservative mixing on DIC and TA concentrations (Cai et al., 2010; Reimer et al., 2023). In the open ocean, TA concentrations are primarily controlled by physical processes so it is considered a semi-conservative tracer that varies linearly with salinity (Millero et al., 1998). However, in estuaries and lagoons, the assumption that TA is a semi-conservative tracer is not always valid (Wang et al., 2016). Heightened biogeochemical activity in the nearshore coastal zone can substantially alter TA concentrations through uptake and release of alkalinity (Yin et al., 2024). This is especially true of salt marshes, where high rates of anaerobic respiration produce significant amounts of organic and inorganic alkalinity (Wang et al., 2016). Additionally, regionally accepted TA-S relationships may not hold true at the local, nearshore level, where local variations in freshwater TA inputs may diverge from the regional freshwater endmember TA (Cai et al., 2010).

The local TA-S relationship is of particular interest in the VCR, where groundwater and rainfall comprise the majority of freshwater inputs, as opposed to riverine inputs which act as important contributors elsewhere in the U.S. Mid-Atlantic (Cai et al., 2010). Groundwater on Virginia's Eastern Shore is contained by four aquifers: the surficial Columbia aquifer, Upper Yorktown-Eastover aquifer, Middle Yorktown-Eastover aquifer, and Lower Yorktown-Eastover aquifer (Accomack-Northampton Planning District Commission and the Eastern Shore of Virginia Groundwater Committee [ANPDC and ESVGC], 2013). Of the four, the surficial

Columbia aquifer is the main source of groundwater discharge to the Eastern Shore's lagoonal systems and tidal creeks (ANPDC and ESVGC, 2013). A compilation of USGS groundwater analyses across the four aquifers reports that salinity, bicarbonate alkalinity, and pH increase with depth, with the Columbia aquifer containing the freshest, most acidic water (ANPDC and ESVGC, 2013).

In addition to lateral exchange between systems, air-sea CO_2 gas exchange represents another pathway for inorganic carbonate chemistry change in nearshore coastal systems. Numerous physical factors impact the gas transfer velocity of CO_2 across the air-sea interface, including currents, wind speeds, waves and white capping, bubbles, surfactants, and other processes that disrupt the boundary layer between the ocean and the atmosphere (Wanninkhof et al., 2014). As direct measurement of the gas transfer velocity is impractical with the exception of targeted and intensive field experiments, wind speed parametrizations are commonly used to estimate gas transfer velocity in the ocean (Nightingale et al., 2000; Wanninkhof et al., 2014). However, these parameterizations have limitations at low wind speeds and in coastal nearshore environments, as few were derived in fetch-limited, shallow systems (Granville, 2024; Ollivier et al., 2022). Recent work has assessed the efficacy of various wind speed gas transfer velocity relationships in a back-barrier vegetated shallow lagoon in the VCR (Granville, 2024); here, we derive CO_2 flux with respect to one of the best fitting parameterizations identified by Granville (2024).

pCO_2 concentrations and gas exchange of CO_2 between the atmosphere and the ocean are moderated by physical and chemical drivers that influence CO_2 solubility and the gas transfer velocity. CO_2 is more soluble in colder water, with seasonal and spatial variations in sea surface temperature contributing to global patterns in ocean CO_2 in-gassing and out-gassing (Roobaert et al., 2019). As climate change continues to increase sea surface temperatures, the geographic distribution of oceanic CO_2 sinks and sources will be altered (Heinze et al., 2015). At an average depth of 1.2 meters, the VCR lagoons may experience variable thermal heating dependent on depth, water residence time, and frequency of tidal flushing bringing cooler coastal ocean water (Safak et al., 2015). VCR shallow tidal creek sites closer the mainland typically exhibit higher temperatures than deeper sites located near ocean inlets (Brahmey et al., 2024). The VCR is also

experiencing marine heat waves of increased frequency and greater duration (Wiberg, 2024), which in turn would reduce CO_2 solubility during pulse events.

3.2.1 Biogeochemical Drivers

Biological activity is an important driver of nearshore carbonate chemistry, with photosynthesis, aerobic respiration, and anaerobic respiration all contributing to DIC and TA dynamics. Anthropogenically enhanced delivery of nitrogen to the coastal ocean can stimulate biogeochemical activity, and therefore plays an important role in mediating the coastal biological carbon pump (Fennel et al., 2008). Primary production consumes CO_2, thereby decreasing DIC, while respiration produces CO_2, thereby increasing DIC (Emerson and Hedges, 2008). Primary production and aerobic respiration have variable effects on TA depending on the form of nitrogen utilized during biomass production: consumption of ammonium leads to a TA decrease while consumption of nitrate leads to a TA increase (Doney et al., 2007). Anaerobic respiration, including denitrification, sulfate reduction, manganese reduction, and iron reduction, can generate both TA and DIC in anaerobic sediments in unique TA:DIC ratios depending on specific process. TA:DIC ratios for common marine biogeochemical processes are presented in Table 1 (Yin et al., 2024). When corroborated with nutrient data, the stoichiometric relationship of observed TA:DIC can shed light on biological contributions to the carbonate system (Yin et al., 2024).

Coastal sediments are often sites of enhanced biogeochemical cycling as a result of heightened microbial activity that consume, produce, and transform carbon and nitrogen (Fennel et al., 2006; Koch et al., 1992; Murphy et al., 2020). In shallow coastal systems like the VCR, benthic release of alkalinity produced by anaerobic denitrification in sediments acts as a key contributor to TA (Brenner et al., 2016; Fennel et al., 2008). Sediment denitrification rates are known to increase under warming temperatures, with optimal conditions exceeding 35ºC in estuarine sites (Tan et al., 2020). This would predict seasonally mediated sediment efflux of TA and DIC, with amplification from marine heatwave events and long-term warming (Tan et al., 2020). Much like the overlying water column, sediments in the VCR also experience heatwaves that are closely coupled with heatwaves occurring in the overlying water column (Tassone,

2023). In shallow estuarine sites, benthic photosynthesis enhances coupled sediment nitrification and denitrification (An and Joye, 2001).

Salt marshes are a hotbed of primary productivity, aerobic respiration, and anaerobic respiration, manifesting in a complex internal carbon cycle that interacts with adjacent tidal creeks and lagoonal systems through tidal and pore-water exchange (Santos et al., 2019; Cai et al., 2003). As marshes support diverse biological activity generating both TA and DIC, they present a "paradox of acidification and alkalinization" (Wang et al., 2016). Photosynthesis occurring in salt marshes serves to decrease DIC, but the carbonate system effects from aerobic and anaerobic respiration outweigh those from primary productivity (Wang et al., 2016). In particular, denitrification is favored in the underlying anoxic sediments of marshes (Martínez-Espinosa et al., 2021). While wetlands are excellent facilitators of organic carbon storage, Eastern US salt marshes only store 20 ± 7% of carbon produced within the marsh, while the remaining 80 ± 7% is exported via lateral transport to estuaries and shelf waters (Najjar et al., 2018). Current global salt marsh carbon budgets suggest that carbon export from marshes is dominated by inorganic carbon forms, including CO_2 outgassing and DIC export (Reithmaier et al., 2023). DIC accounts for 90% of lateral carbon export from the marsh-estuarine complex, greatly overshadowing particulate and dissolved organic carbon exports (Santos et al., 2019).

Two prominent calcifying species present in the Virginia Coast Reserve are the Eastern Oyster, *Crassostrea virginica*, and the Hard Clam or Northern Quahog, *Mercenaria mercenaria*. For both species, larval exposure to low ΩAr and high pCO_2 can lead to detrimental effects, including higher metabolic expenditure, reduced growth and survival rates, and shell deformities (Gobler and Talmage, 2014; Miller et al., 2020). Annual pH lows in estuaries often occur in the spring, coinciding with *C. virginica* reproductive seasons. Severely acidic springtime conditions (pH < 7.1) have been linked to lower reproductive success (Boulais et al., 2017). Understanding spatial and seasonal patterns in ΩAr, pH, and pCO_2, can aid in identification of acidification events and hotspots.

This chapter aims to quantify seasonal and geographic variability across a temperate lagoonal system, while estimating contributions of biogeochemical, thermodynamic, and

physical drivers. Potential implications of observed seawater carbonate chemistry for air-sea gas exchange and marine organisms will also be discussed.

Table 1: Stoichiometry of selected metabolic processes and the resulting impact on TA and DIC, presented as molar ratios. Positive ΔTA and ΔDIC values indicate that the process produces TA or DIC, while negative values indicate that the process consumes TA or DIC. Table adapted from Yin et al., (2024).

Process	Formula	ΔTA: ΔDIC
Primary Production (nitrate)	$106CO_2 + 16HNO_3 + H_3PO_4 + 122H_2O \rightarrow (CH_2O)_{106}(NH_3)_{16}(H_3PO_4) + 138O_2$	17 : -106
Primary Production (ammonium)	$106CO_2 + 16NH_3 + H_3PO_4 + 106H_2O \rightarrow (CH_2O)_{106}(NH_3)_{16}(H_3PO_4) + 106O_2$	-15 : -106
Aerobic remineralization (nitrate)	$(CH_2O)_{106}(NO_3)_{16}(H_3PO_4) + 106O_2 \rightarrow 106CO_2 + 16NH_3 + H_3PO_4 + 106H_2O$	15 : 106
Aerobic remineralization (ammonium)	$(CH_2O)_{106}(NH_3)_{16}(H_3PO_4) + 138O_2 \rightarrow 106CO2 + 16HNO_3 + H_3PO_4 + 122H_2O$	-17 : 106
Nitrification	$NH_4^+ + 2O_2 \rightarrow HNO_3 + H_2O + H^+$	-2 : 0
Denitrification	$5(CH_2O)_{106}(NH_3)_{16}(H_3PO_4) + 424HNO_3 \rightarrow 530CO_2 + 212\ N_2 + 742H_2O + 5H_3PO_4 + 80NH_3$	499 : 530
Calcification	$Ca^{2+} + CO_3^2 \leftrightarrow CaCO_3$	-2 : -1
Carbonate Dissolution	$CaCO_3 \leftrightarrow Ca^{2+}2+ + CO_3^2$	2 : 1

3.3 Methods

3.3.1 Study Sites and Discrete Sampling

Quarterly water quality sampling surveys have been an integral part of the long-term monitoring conducted at the VCR- LTER. VCR-LTER water quality sampling is conducted quarterly during an outgoing tide at 13 sites that include a wide array of habitats, including marsh-lined tidal creeks, mudflats, seagrass meadows, and inlets (Figure 1; Table 2). Discrete

seawater carbonate system samples were collected across four water quality surveys, including March 2022, July 2022, October 2022, and April 2023 with field and laboratory protocols in accordance with best practices (Dickson et al., 2007). DIC water samples were collected in triplicate at each site in 12 ml borosilicate exetainers, immediately poisoned with a mercuric chloride solution, and stored between 2-4 ºC until laboratory analysis. TA samples were collected in duplicate at each site in 250 ml Nalgene bottles, poisoned with a mercuric chloride solution in the field, and similarly stored between 2-4 ºC until laboratory analysis. Discrete measurements of temperature, salinity, and dissolved oxygen (DO) were collected with a handheld YSI and additional water samples were collected in triplicate to later assess nitrate + nitrite, NH_4, PO_4, total dissolved nitrogen (TDN), and chlorophyll-a (McGlathery and Christian, 2024). Water samples collected for evaluation of nutrients were filtered and frozen for later analysis. In addition to samples collected during water quality surveys, groundwater samples were collected from the surficial Columbia Aquifer in September of 2023 from a well located in an upland forest plot in the Brownsville Preserve. A submersible pump flushed the volume of the well three times before a peristaltic pump was used to collect water samples.

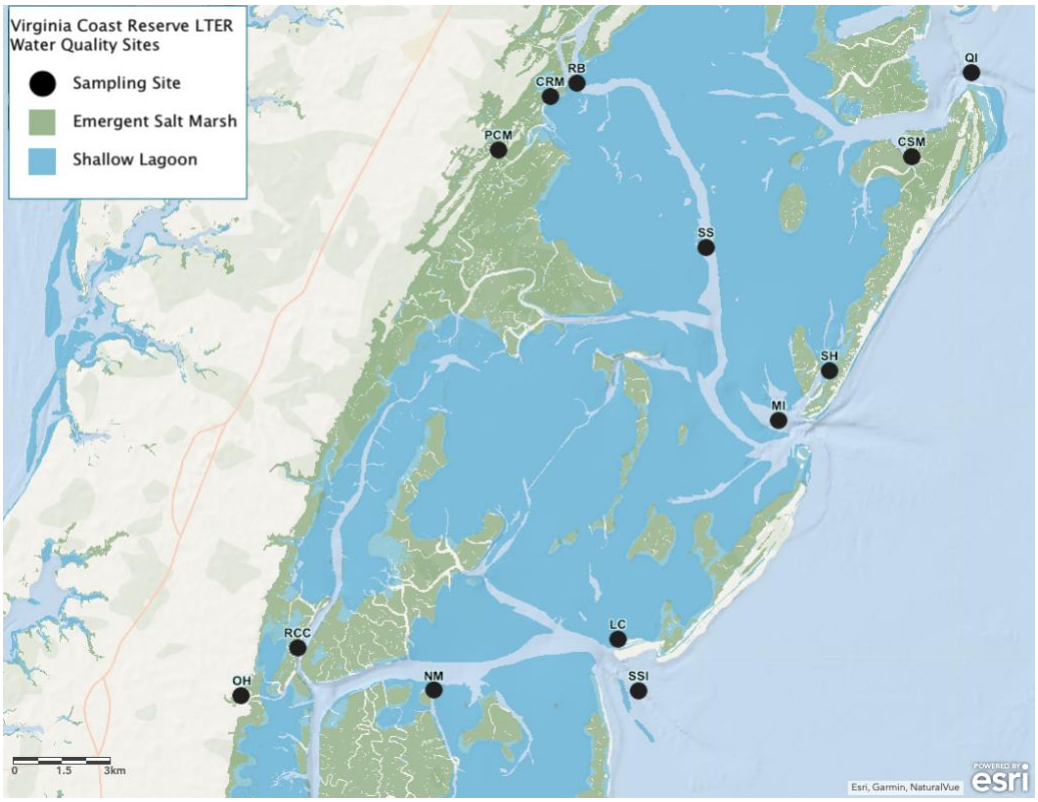

Figure 1: Map of the VCR-LTER seasonal water quality sampling sites, with emergent salt marsh in green and shallow lagoons in darker blue.

Groundwater and water quality water samples were assessed for DIC concentrations using a laser-based Apollo SciTech AS-C3 DIC analyzer connected with a Licor LI-7000 CO_2/H_2O analyzer (Neubauer and Anderson, 2003). Each vial was measured in triplicate. Every day of sample processing, a standard curve was produced with Certified Reference Material and potential instrument drift was assessed by running Certified Reference Material every 10-15 samples. Open-cell potentiometric titration was performed to determine the total alkalinity of water samples. Certified titrant (0.1 M HCl acid in 0.6 M NaCl; A. Dickson laboratory) and an automatic titrator, the Metrohm 855 Robotic Titro, were used to titrate two replicates per bottle sample. To ensure accuracy, titrations were performed on Certified Reference Material on each day of sample processing. A correction was applied to poisoned samples to amend any acidification effects due to the addition of mercuric chloride.

Table 2: Names, abbreviations, coordinates, and site descriptions for long-term water quality sampling sites located in the VCR.

Site Name	**Latitude**	**Longitude**	**Site Description**	**Site Type**
Redbank Creek Mouth (**CRM**)	37.460	-75.816	Mainland Creek	Marsh Adjacent
Cattleshed Creek Mouth (**CSM**)	37.443	-75.689	Barrier Creek	Marsh Adjacent
Little Cobb Island (LC)	37.305	-75.792	Back-barrier	Lagoonal-Inlet
Machipongo Inlet (**MI**)	37.368	-75.736	Ocean Inlet	Lagoonal-Inlet
New Marsh (**NM**)	37.291	-75.857	Lagoon Shoal	Lagoonal-Inlet
Oyster Harbor (**OH**)	37.289	-75.924	Harbor	Marsh Adjacent
Phillips Creek Marsh (PCM)	37.445	-75.834	Mainland Creek	Marsh Adjacent
Quinby Inlet (**QI**)	37.467	-75.668	Ocean Inlet	Lagoonal-Inlet
Ramshorn Channel Creek (**RCC**)	37.303	-75.905	Lagoon Shoal	Marsh Adjacent
Red Bank (**RB**)	37.464	-75.807	Mainland Creek	Marsh Adjacent
South Hog (**SH**)	37.382	-75.718	Barrier Creek	Lagoonal-Inlet
Shoal Site (**SS**)	37.417	-75.761	Lagoon Shoal	Lagoonal-Inlet
Sand Shoal Inlet (**SSI**)	37.290	-75.785	Ocean Inlet	Lagoonal-Inlet

Coastal wetlands spatial data produced by NOAA's Office for Coastal Management were utilized to determine ecosystem makeup surrounding each of the 13 water quality sites (NOAA's Office for Coastal Management, 2023). The Buffer tool in ArcGIS Online was used to encircle a

representative area around each water quality site with a radius of 500 meters. Wetland data located within each site's representative area were then summarized by area and National Wetland Inventory (NWI) Class using the ArcGIS Online Summarize Within tool. The distance between each site and the nearest marsh and nearest inlet was measured using the Find Nearest ArcGIS Online tool. Based on NWI classifications, proximity to emergent salt marsh, and proximity to ocean inlets, sites were sorted into two classifications: marsh adjacent sites and lagoonal-inlet sites.

pCO_2, pH, and ΩAr were estimated with *in situ* temperature, salinity, DIC, and TA data with the MATLAB package CO2SYS v3.1.1 using Millero's (2010) K1 and K2 dissociation constants for carbonic acid and bicarbonate, Dickson's (1998) KSO4 dissociation constant, and the KF dissociation constant from Perez and Fraga (1987) (Lewis and Wallace, 1998; Orr et al. 2018; Sharp et al., 2023; Van Heuven et al., 2011). CO2SYS v3.1.1 error subroutine was used to calculate uncertainty of estimated parameters pH, pCO_2, and Ω. Apparent oxygen utilization (AOU) was computed by finding the difference between DO concentrations at saturation and observed DO (Equation 1; Redfield at el., 1963).

$$AOU = [O_2^{Sat}(\theta, S)] - [O_2]$$

Equation 1

3.3.2 Decomposition of pCO_2 Variability

In order to determine how seasonal shifts in water temperature impact annual pCO_2 variability at each site, computed pCO_2 was decomposed to highlight the thermal drivers of variability. Using the pCO_2 temperature dependence coefficient ($\partial ln(pCO_2)/\partial T = 0.0423$ 1/deg. C) from Takahashi et al. (2002), we calculated a temperature-normalized pCO_2 ($pCO_{2(T_{mean})}$; Equation 2) using site-specific mean annual temperature as was previously estimated by Brahmey et al. (2024), in which composite harmonic fits for annual temperature cycles were produced for each of the 13 sites based on 20-30 years of quarterly temperature data.

$$pCO_{2(T_{mean})} = pCO_{2(observed)} \times e^{0.0423 \times (T_{mean} - T_{observed})}$$

Equation 2

Thermal drivers of pCO_2 variability were estimated by subtracting $pCO_{2(T_{mean})}$ from the observed pCO_2 at each site ($\Delta pCO_{2(thermal)}$) (Reimer et al., 2023; Xue et al., 2016).

$$\Delta pCO_{2(thermal)} = pCO_{2(observed)} - pCO_{2(T_{mean})}$$

Equation 3

The seasonal variations in $pCO_{2(Tmean)}$ also provide information on the non-thermal drivers.

3.3.3 Air-Sea CO_2 Gas Exchange Estimations

CO_2 air-sea gas exchange was estimated across study sites, where resultant positive fluxes reflect a release of CO_2 into the atmosphere and negative fluxes represent oceanic CO_2 uptake (Wanninkhof, 2014).

$$F = k\, K_0 (pCO_{2w} - pCO_{2a})$$

Equation 4

The solubility coefficient, K_0, was calculated with water temperature and salinity as inputs and has an estimated error of ± 0.2 % (Weiss, 1974). We used the gas transfer velocity k_{600} from the wind speed parameterization proposed by Nightingale and colleagues (2000), and then converted results to *k* with Schmidt numbers based on *in situ* temperature and salinity data (Wanninkhof et al., 2014). The Nightingale et al. (2000) wind speed parameterization was selected to best account for the fetch-limited, shallow coastal environment. It has been independently confirmed as a good fit for directly measured gas transfer velocities in the Virginia Coast Reserve (Granville, 2024). The gas transfer velocity equation has an error of ± 20 % (Nightingale et al., 2000).

$$k = (\, 0.333 U_{10} + 0.222\, U_{10}^2 \,) \ast (Sc./600)^{-0.5}$$

Equation 5

The k value from Equation 5 for VCR was derived with respect to surface wind speed measured on site using a handheld Kestral anemometer. Monthly averages for 2022 of discrete atmospheric CO_2 collected at the Tudor Hill, Bermuda observing location were sourced from the NOAA GML Carbon Cycle Cooperative Global Air Sampling Network (Lan et al., 2023). Atmospheric xCO_2 was converted to pCO_2 (Equation 6). Vapor pressure of water was computed with vapress, based on equations from Dickson's (2007) best practices, using inputs of mean

seasonal local salinity and temperature (Orr, 2014). Local pressure data was obtained from a Hog Island, Phillips Creek Marsh, and Oyster, VA dataset (Porter et al., 2023).

$$pCO_{2a} = xCO_2\left(P - P_{vap}\right)$$

Equation 6

3.3.4 Statistical Analyses

Statistical tests were conducted on discrete water quality carbonate system data (DIC, pCO_2, pH, TA, ΩAr) grouped by site type and by sampling month to assess spatial and seasonal carbonate system trends. First, to determine whether to use a parametric or non-parametric method, Shapiro-Wilkes tests were conducted to assess normality of each treatment group. Visual inspection of Q-Q plots and histograms further confirmed normality assessments. For groups that were strongly non-normal, a non-parametric test was performed in place of a parametric test. Across all statistical tests, a significance level of $\alpha = 0.05$ was defined for resulting p-values of statistical analyses.

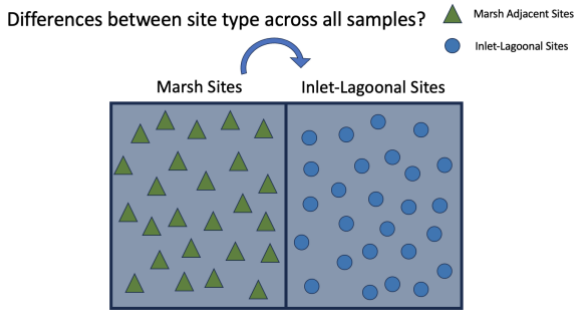

Figure 2: A Student's t-test or a Mann Whitney U test was performed between all marsh adjacent samples and all lagoonal-inlet samples to assess differences in DIC, TA, pCO_2, pH, and ΩAr between site types. Similar statistical tests were also applied to data subsets broken down by sampling month.

Student's t-tests were performed to assess similarity of carbonate system parameter means between all marsh adjacent site data and all lagoonal-inlet site data (Figure 2). Site type differences were then evaluated by sampling month by conducting a Student's t-test between March marsh adjacent data and March lagoonal-inlet data, April marsh adjacent data and April lagoonal-inlet data, and so on. The assumptions of a Student's t-test were met for the majority of paired groups; groups exhibited normality or approximate normality. As a Student's t-test is

robust to some non-normality and does not assume equal variance, it serves as a good fit for the site type data. For non-normal data, a Mann Whitney U test (MWU) was used to assess the hypothesis that the marsh adjacent data and lagoonal-inlet have similar medians.

An Analysis of Variance, or an ANOVA, was conducted to examine the differences in carbonate system parameters between samples collected in March, April, July, and October. For groups that were not normally or approximately normally distributed, a Kruskal-Wallis test (KW) was performed to evaluate the equality of means on rank between seasonal groups.

After assessing statistical trends between seasons using data from all site types, an ANOVA was conducted with only lagoonal-inlet data, comparing between groups of samples collected in March, April, July, and October. The analysis was then repeated with marsh adjacent data. Descriptive statistics, including means, standard deviation, and variance (Equation 7) were also performed and reported for each group. Finally, Levene's test was performed to assess homogeneity of variance among all treatment groups.

$$\sigma^2 = \frac{\sum(x_i - \overline{x})^2}{n - 1}$$

Equation 7

Root Mean Square Error (RMSE) was used to assess linear regression model fits of DIC-S and TA-S relationships (Equation 8).

$$RMSE = \sqrt{\frac{\sum_{i=1}^{N}(Predicted_i - Actual_i)^2}{N}}$$

Equation 8

Mean bias error (MBE) was also calculated to assess bias in linear regression model fits, where negative MBE indicates a negative bias in the model and positive MBE indicates a positive bias in the model (Equation 9).

$$Mean\ Bias\ Error\ (MBE) = \frac{\sum_{i=1}^{N}(Predicted_i - Actual_i)}{N}$$

Equation 9

3.4 Results and Discussion

3.4.1 Site Type Characterization

Emergent salt marsh, intertidal mudflat, and marine subtidal were the three most prominent habitat types within a 500 m radius of each water quality site (Figure 3). Two other habitat types with smaller extents were present within sites' representative areas; submerged aquatic vegetation made up 5.8% of the representative area surrounding LC and scrub-shrub vegetation represented less than 2% of area surrounding OH and PCM. Six sites, CRM, CSM, OH, PCM, RB, and RCC, were classified as marsh adjacent due to proximity to salt marsh and high proportions of salt marsh within the surrounding environment. These sites typically were closer to the mainland and have high residence times (Safak et al., 2015). Seven sites were classified as lagoonal-inlet sites, including LC, MI, NM, QI, SH, SS, and SSI. Lagoonal-inlet sites have little to no salt marsh habitat within 0.5 km of the site, with marine subtidal and intertidal mudflats dominating the sites' immediate surroundings.

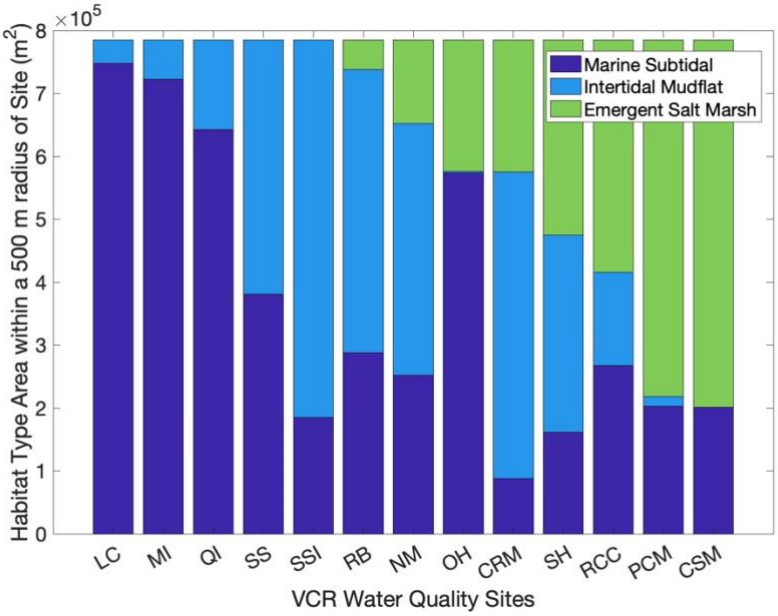

Figure 3: Proportion of area surrounding each water quality site that can be classified as marine subtidal, intertidal mudflat, or emergent salt marsh.

3.4.2 Conservative Mixing of DIC and TA

Total alkalinity and salinity data collected during quarterly VCR water quality surveys between March 2022 and April 2023 were used alongside groundwater endmembers to establish a localized Alkalinity-Salinity relationship (Figure 4). Due to a lack of substantial riverine freshwater inputs, the surficial aquifer constitutes the major freshwater endmember in the VCR. With a salinity near zero, the groundwater endmember has a TA concentration of 200.9 ± 18.4 µmol/ kg and a DIC concentration of 1335.4 ± 19.3 µmol/ kg. TA concentrations are in approximate agreement with nearby USGS carbonate alkalinity samples of the surficial aquifer (ANPDC and ESVGC, 2013).

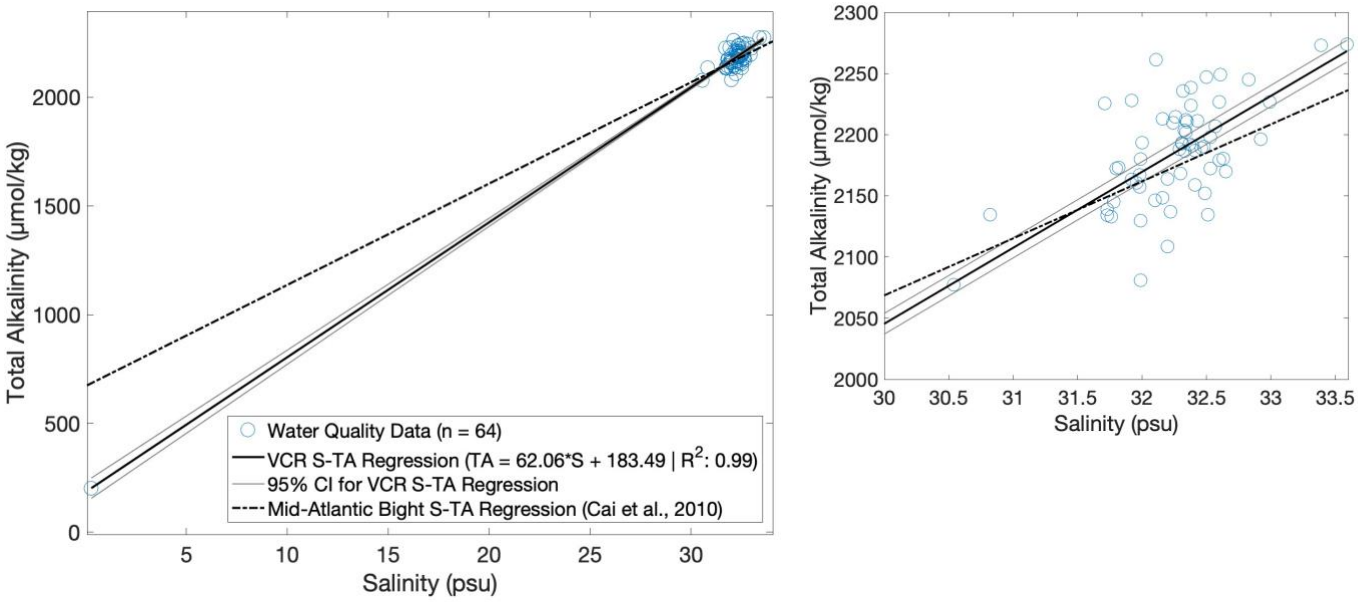

Figure 4: A linear regression including a local groundwater sample and VCR water quality survey samples show that alkalinity has a strong positive relationship with salinity in the VCR. The VCR S-TA regression varies slightly from a Mid-Atlantic regional S-TA model, Cai et al. (2010) (left). A high salinity subsection of plot shows the overlap between the VCR S-TA regression and the Cai et al. (2010) Mid-Atlantic Bight regression (right).

The VCR TA-S regression line shows the greatest deviation from the Mid-Atlantic Bight (MAB) Cai et al. (2010) TA-S regression model at low salinities owing to different intercepts, with the gap between the two models closing at salinities between 30 and 35 psu. In the absence

of data estimating TA and DIC contributions from rainfall and overland freshwater runoff, we assume the freshwater endmember in the VCR to be groundwater. This assumption may account for the difference between freshwater endmembers between the VCR TA-S regression and the Cai et al. (2010) TA-S regression. In future, additional sampling and estimations of groundwater and rainwater could help further constrain freshwater endmember characteristics in the VCR.

Despite the differences between the freshwater endmember characteristics, the regional TA-S regression model (Cai et al., 2010) is able to predict VCR alkalinity at high salinities. For discrete samples with salinities above 30 psu, the VCR TA-S model performed only slightly better than the regional model, with root mean square errors (RMSE) of 40.93 µmol/kg and 42.77 µmol/kg, respectively. Freshwater contributions in the VCR are minimal, as is demonstrated by the consistently high salinities across the tidal creeks and lagoons, so the Cai et al. (2010) regression is acceptable to use in most VCR scenarios.

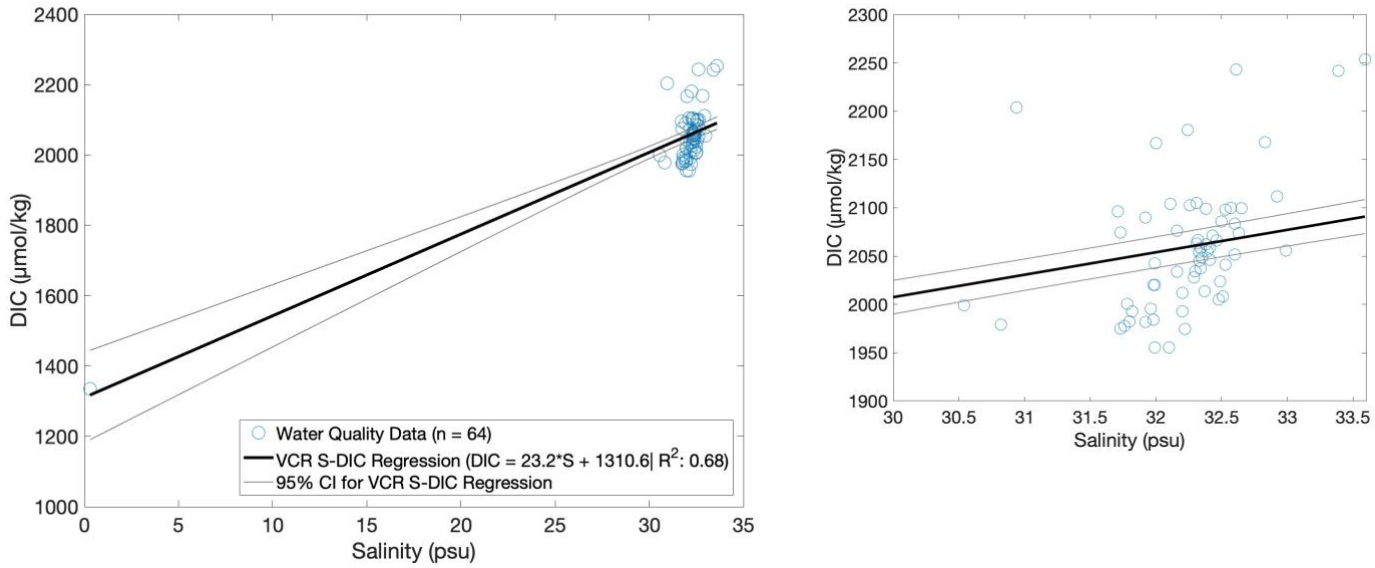

Figure 5: A linear regression of DIC on salinity including a local groundwater sample and VCR water quality survey samples show that DIC has a positive relationship with salinity in the VCR, with the regression line reflecting the conservative mixing line for DIC (left). The high salinity subsection of plot shows that sample DIC deviates both positively and negatively from the conservative mixing line (right).

A DIC-S linear regression model was also estimated using data collected across the 13 VCR water quality sites between March 2022 and April 2023 (Figure 5). Overall, the conservative mixing linear regression model for TA-S approximated observed TA values (R^2 = 0.99) better than the DIC-S model approximated observed DIC values (R^2 = 0.68). This finding reflects the semi-conservative nature of TA. To further investigate contributions of conservative mixing to observed DIC and TA across VCR sampling sites, we then assessed deviations from the seasonal predicted conservative mixing line.

To account for seasonal variability in conservative mixing, conservative mixing TA-S and DIC-S relationships were then estimated for each sampling month using the three inlet sites (MI, SSI, QI) as the ocean endmember and groundwater samples as the freshwater endmember. TA-S and DIC-S predicted conservative mixing line equations vary little from month to month, but do have variable confidence intervals (Table 3; Table 4). Linear regressions exhibited positive mean bias error in April, July, and October and negative mean bias error in March (Table 3). March and October had the largest bias, with MBEs of -46.92 and 39.92 µmol/kg, respectively (Table 3).

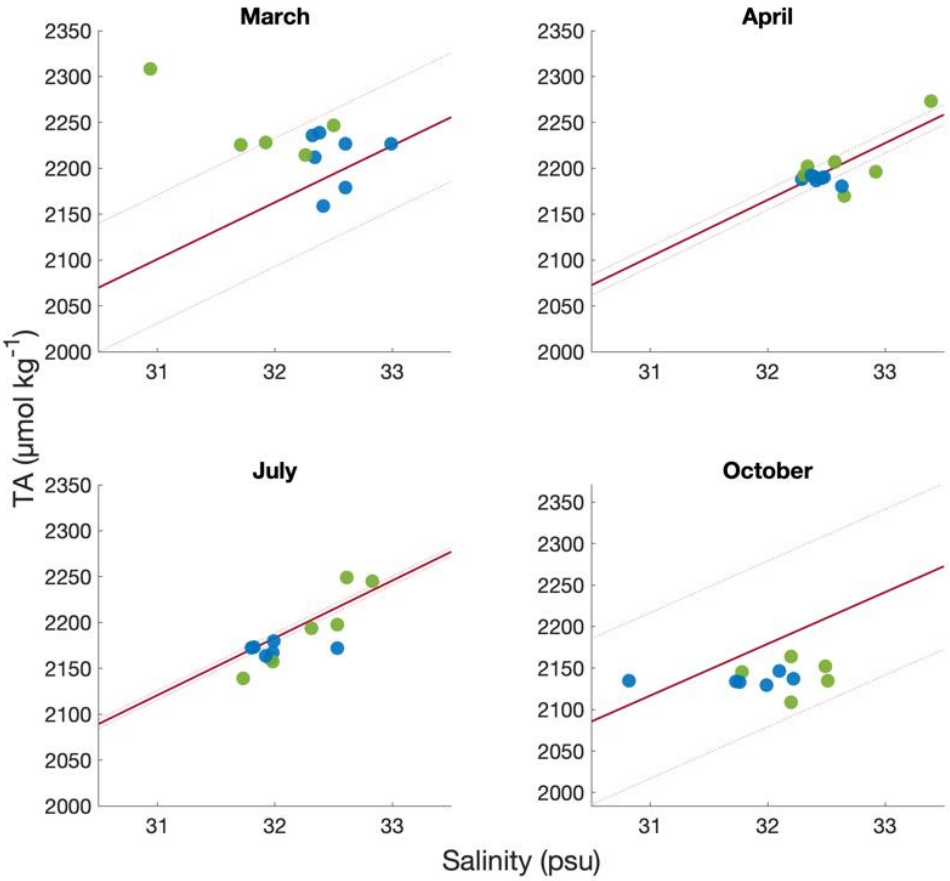

Figure 6: TA and salinity across the four sampling periods are plotted alongside the seasonally appropriate predicted conservative mixing line (red) with marsh adjacent sites in green and lagoonal-inlet sites in blue. Dotted red lines indicate 95% confidence intervals.

In April and July, observed TA shows agreement with TA values predicted by conservative mixing of freshwater and ocean endmembers, evidenced by low RMSE values (Figure 6; Table 3). However, there are several samples in April and July that fall outside of the TA-S model confidence intervals, both above and below the predicted TA values. Several marsh adjacent samples exceed the TA predicted by the conservative mixing line in March as well. In October, all observed TA concentrations fall within the 95% confidence intervals of the conservative mixing model. March and October TA-S model performance is better among lagoonal-inlet sites when compared to marsh adjacent sites; RMSE in March and October is 109.58 and 58.68 µmol/kg for marsh adjacent sites, respectively, and 34.58 and 40.1 µmol/kg for lagoonal-inlet sites, respectively (Table 3).

Table 3: Equations for predicted conservative mixing TA-S linear regression models for March, April, July, and October. To reflect how accurately each model fits observed data, RMSE is reported for all sites, marsh sites alone, and lagoonal-inlet sites alone.

Sampling Month	Conservative Mixing Line Equations	Mean Bias Error (MBE) (µmol/kg)	All Sites RMSE (µmol/kg)	Marsh Sites RMSE (µmol/kg)	Lagoonal Inlet Sites RMSE (µmol/kg)
March	TA = 61.9 (± 1.0) * S + 182.1 (± 28.3)	-46.92	75.50	109.58	34.58
April	TA = 61.9 (± 0.2) * S + 182.3 (± 4.5)	3.07	16.31	21.48	9.93
July	TA = 62.5 (± 0.1) * S + 182.1 (± 2.4)	10.48	20.46	20.96	20.01
October	TA = 62.4 (± 1.6) * S + 183.0 (± 41.0)	39.92	49.42	58.68	40.1

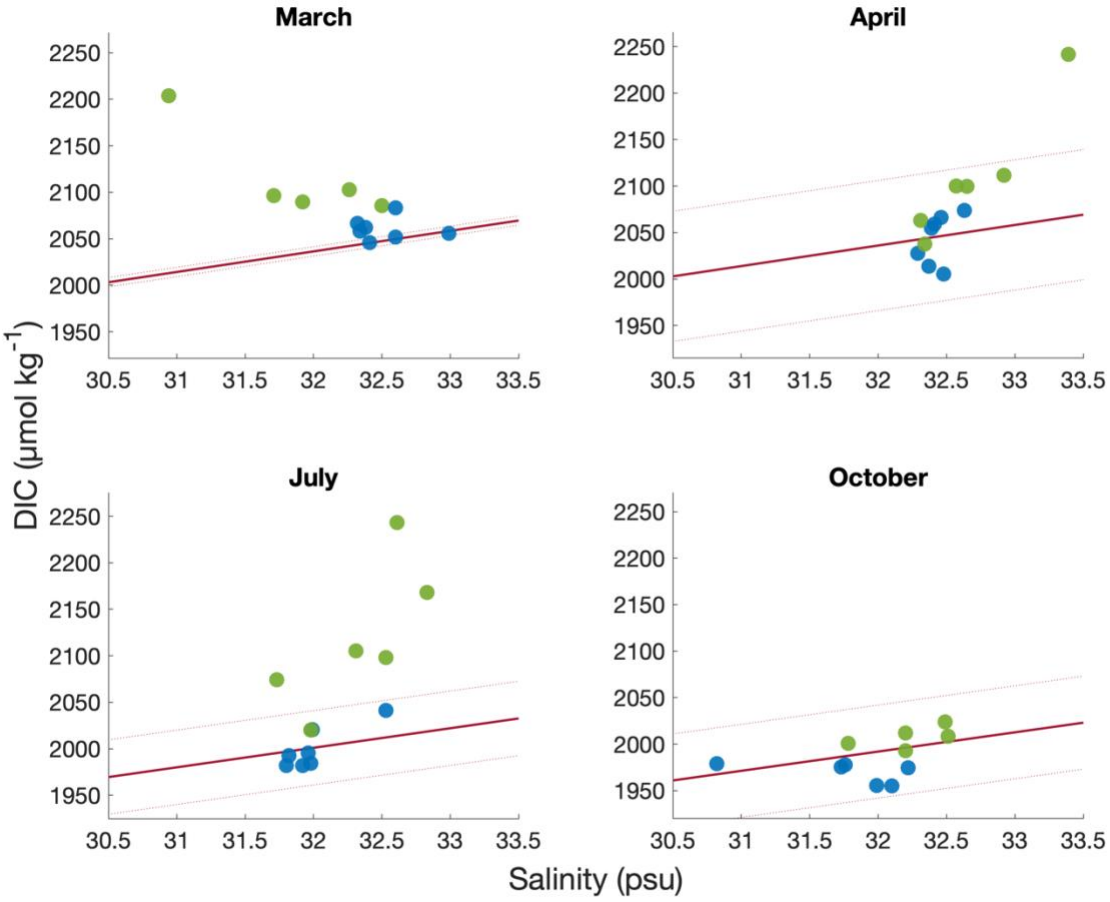

Figure 7: DIC and Salinity across the four sampling periods are plotted alongside the seasonally appropriate predicted conservative mixing line (red) with marsh adjacent sites in green and lagoonal-inlet sites in blue. Dotted red lines indicate 95% confidence intervals.

For DIC-S conservative mixing models, March, April, and July have negative bias, with mean bias error ranging from -25.11 µmol/kg (April) to -50.04 µmol/kg (July) (Table 4). October exhibits minimal, positive mean bias error (Table 4). When compared to DIC values predicted by conservative mixing of freshwater and ocean endmembers, DIC is elevated at most marsh adjacent sites in March and July sampling efforts (Figure 7). The April DIC-S conservative mixing model has high intercept error, such that only one marsh sample certainly has higher observed DIC than predicted DIC. In October, the DIC-S conservative mixing model performs well when compared to observed DIC in site types; marsh adjacent sites and lagoonal-inlet sites display low RMSE values, 13.70 and 24.69 µmol/kg, respectively (Table 4).

Lagoonal-inlet site DIC typically displays more conservative behavior than DIC at marsh adjacent sites. In March, April, and July, conservative mixing DIC-S regression models perform best among lagoonal inlet site samples, with RMSE ranging from 17.15 to 24.25 µmol/kg (Table 4). Comparatively, RMSE ranges from 80.76 to 128.09 µmol/kg when comparing observed marsh adjacent DIC values with DIC values predicted with the conservative mixing DIC-S regression models (Table 4).

Lateral mixing is an important driver of DIC and TA concentrations at VCR sites, but deviations from predicted conservative mixing lines indicate that mixing alone does not explain all of the variability seen in DIC and TA. Deviations from the predicted conservative mixing lines, especially the relatively large excess DIC observed in July, indicate potential biogeochemical influence on DIC and TA.

Table 4: Equations for predicted conservative mixing DIC-S linear regression models for March, April, July, and October. To reflect how accurately each model fits observed data, RMSE is reported for all sites, marsh sites alone, and lagoonal-inlet sites alone.

Sampling Month	Conservative Mixing Line Equations	Mean Bias Error (µmol/kg)	All Sites RMSE (µmol/kg)	Marsh Sites RMSE (µmol/kg)	Lagoonal Inlet Sites RMSE (µmol/kg)
March	DIC = (22.1 ± 0.1) * S + (1328.8 ± 2.4)	-41.67	65.35	99.05	17.71
April	DIC = (22.1 ± 0.9) * S + (1328.7 ± 26.9)	-25.11	57.68	80.76	24.25
July	DIC = (21.0 (± 0.6) * S + (1328.9 ± 17.8)	-50.04	87.93	128.09	17.15
October	DIC = (20.7 (± 0.6) * S + (1329.5 ± 16.2)	4.80	20.44	13.70	24.69

3.4.3 Spatial and Seasonal Carbonate System Patterns

*Table 5: Summary of results from statistical tests conducted to assess differences in group means and variance of DIC, TA, pCO_2, pH, and ΩAr. Treatments include site type, sampling month, marsh adjacent sites by sampling month, and lagoonal-inlet sites by sampling month. * Indicates that a significance level of $\alpha = 0.05$ was met.*

Treatment		DIC		TA		pCO_2		pH		ΩAr	
		Means	Variance	Means	Variance	Means	Variance	Means	Variance	Means	Variance
By Site-Type	Statistical Test Conducted	MWU	Levene's Test	Student's T-test	Levene's Test	MWU	Levene's Test	Student's T-test	Levene's Test	Student's T-test	Levene's Test
	p-value	< 0.001*	0.098	0.1414	0.053	< 0.001*	0.74	0.002*	0.75	< 0.001*	0.64
By Sampling Month	Statistical Test Conducted	ANOVA	Levene's Test	ANOVA	Levene's Test	KW	Levene's Test	ANOVA	Levene's Test	ANOVA	Levene's Test
	p-value	< 0.001*	0.02*	< 0.001*	0.2937	0.20	0.28	0.42	0.24	0.38	0.008*
Marsh sites by Sampling Month	Statistical Test Conducted	ANOVA	Levene's Test	ANOVA	Levene's Test	ANOVA	Levene's Test	ANOVA	Levene's Test	ANOVA	Levene's Test
	p-value	0.023*	0.22	0.0024*	0.5990	0.48	0.42	0.31	0.60	0.044*	0.26
Lagoonal-Inlet Sites by Sampling Month	Statistical Test Conducted	ANOVA	Levene's Test	ANOVA	Levene's Test	ANOVA	Levene's Test	ANOVA	Levene's Test	ANOVA	Levene's Test
	p-value	< 0.001*	0.017*	< 0.001*	< 0.001*	0.13	0.21	0.17	0.28	0.27	0.097

*Table 6: Summary of results from statistical tests conducted to assess differences in group means and variance of DIC, TA, pCO_2, pH, and ΩAr between Marsh Adjacent (M) sites and Lagoonal-Inlet (LI) sites in March, April, July, and October. * Indicates that a significance level of α = 0.05 was met.*

Treatment	DIC		TA		pCO_2		pH		ΩAr	
	Student's T-test	Levene's Test	Student's T-test	Levene's Test	Student's T-test	Levene's Test	Student's T-test	Levene's Test	Student's T-test	Levene's Test
March: M vs. LI	0.094	0.0472*	0.1802	0.8467	0.7684	0.4316	0.0829	0.6859	0.5547	0.9861
April: M vs. LI	0.0819	0.2846	0.2303	0.0652	0.1063	0.3498	0.0273*	0.5569	0.1428	0.8063
July: M vs. LI	0.0209*	0.0391*	0.1644	0.0125*	0.0389*	0.0471*	0.8497	0.0488*	0.0065*	0.0892
October: M vs. LI	0.0177*	0.8064	0.6692	0.0521	0.1431	0.2496	0.0525	0.3358	0.0684	0.1848

3.4.3a DIC patterns

When considering all sites, DIC peaks in March and decreases in subsequent sampling efforts, ranging from a maximum mean DIC of 2083. 5 ± 16.5 µmol/ kg in March to a minimum mean DIC of 1986.8 ± 17.2 µmol/ kg in October (Figure 8; Table 7). ANOVA results show that mean DIC differences between March, April, and July are not statistically significant. However, mean October DIC is significantly lower than all other seasons (p-value < 0.05).

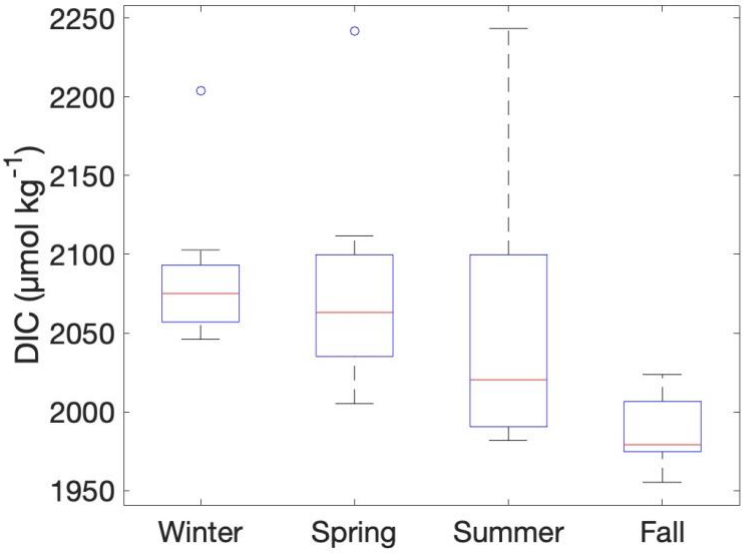

*Figure 8: Box and Whisker plot summarizing DIC concentrations across all sites in March, April, July, and October. Red lines correpond to the group median and the box limits represent the Interquartile Range (IQR) where the bottom of the box is the 25th Percentile or Quartile 1 (Q1), and the top of the box is located at the 75th Percentile or Quartile 3 (Q3). Lower whiskers correpond to the group "Minimum", which is defined as Q1 - 1.5*IQR, while upper whiskers denote the group "Maximum", defined as Q3 + 1.5*IQR. Circles correspond to outliers that are below the set minimum or above the set maximum.*

Student's t-test results indicate that DIC among marsh adjacent sites is significantly higher than DIC in lagoonal-inlet sites across all seasons (Table 6). In March and April, the mean DIC in marsh adjacent sites exceeds that of lagoonal-inlet sites by 55.2 ± 21.2 and 65.9 ± 32.1 µmol/ kg, respectively (Table 7). The difference between site type mean DIC is largest in July, with mean marsh adjacent DIC surpassing the lagoonal-inlet mean by 118.4 ± 30.9 µmol/ kg (Table 7). October has the smallest difference between site type means, at 38.0 ± 10.0 µmol/ kg (Table 7).

Observed seasonal patterns in DIC varied between marsh adjacent and lagoonal-inlet sites (Figure 9). With a mean of 2118.1 ± 23.0 µmol/ kg, July constitutes the season with the maximum mean DIC for marsh adjacent sites. However, DIC in marsh adjacent sites did not exhibit statistically significant seasonal differences between samples collected in March, April, and July. Only October DIC was significantly lower than the other three sampling periods (Student's t-test, p-values < 0.06).

Among Lagoonal-Inlet sites, maximum mean DIC was observed in March. While March and April lagoonal-inlet DIC means were similar, results from Student's t-tests show that July and October lagoonal-inlet DIC means were significantly different from all other sampling time periods (p-values < 0.05). For both site types, the sampling month with the lowest mean DIC is October, with a seasonal mean of 2007.6 ± 5.0 µmol/ kg for marsh adjacent sites and 1969.6 ± 5.0 µmol/ kg for Lagoonal-Inlet sites.

In March and July, Levene's test results show that within-group variance of marsh adjacent sites was statistically significantly higher than within-group variance of Lagoonal-Inlet Sites (Table 6). Marsh adjacent samples exhibited the greatest within-group variance in DIC in April and July, with Levene's test results signifying significantly larger variance than marsh adjacent samples collected in March or October (p-values < 0.1). Lagoonal-inlet samples also show the most within-group DIC variance in April and July, which was significantly higher than the variance of samples collected in March and October (Levene's test; p-values < 0.1). Both site types exhibit a pattern of high variance in April and July sampling, suggesting there may be seasonal controls on DIC variance in spring and summer.

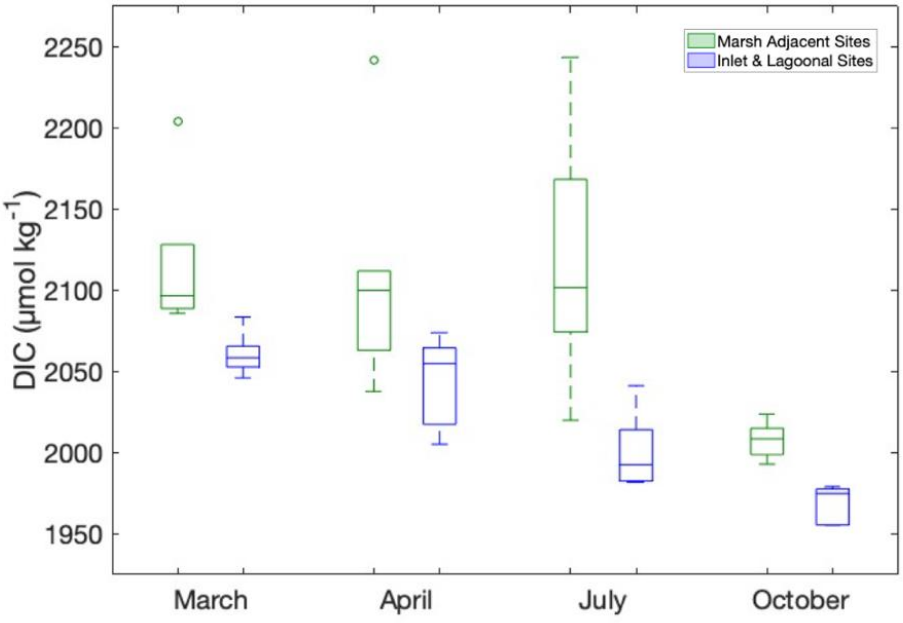

Figure 9: Box and whisker plot summarizing DIC in March, April, July, and October in marsh adjacent sites (green, left bars) and lagoonal-inlet sites (blue, right bars).

Overall, when compared to DIC observed in marsh adjacent sites, lagoonal-inlet samples exhibited more distinct differences in DIC between seasonal sampling efforts, lower within-group July DIC variance, and different timing of maximum observed DIC. Among marsh adjacent sites, there is a low correlation between DIC and salinity, pointing to greater non-conservative drivers of DIC ($R^2 = 0.1$). DIC positively correlates with salinity among lagoonal-inlet sites, reflecting the role of conservative mixing among lagoonal-inlet samples ($R^2 = 0.4$). DIC negatively correlates with DO across all seasons, following an expected pattern of increasing respiration and utilization of oxygen leading to a subsequent increase in respiratory carbon in the form of DIC. High R^2 values indicate that the relationship between DIC and DO was strongest in March and July sampling (Both R^2=0.7). March and July also represent the maximum and minimum DO observed across the four sampling efforts, reflecting seasonal differences in respiration. In July, DIC positively correlates strongly with NH_4 ($R^2 = 0.8$) and nitrate plus nitrite ($R^2 = 0.5$), corresponding with maximum observed NH_4 levels which also occur in July. There are also positive correlations between DIC and TDN and PO_4 in each season.

Table 7: Mean DIC reported with standard deviation (SE) and DIC variance for March, April, July, and October. DIC means and variance are reported for all sites, among marsh adjacent sites only, and among lagoonal-inlet sites only.

Sampling Time Period	Mean DIC & SE (µmol/ kg)	Variance, All Sites (µmol/ kg)^2	Mean DIC & SE Marsh Adjacent (µmol/ kg)	Variance, Marsh Adjacent Sites (µmol/ kg)^2	Mean DIC & SE Lagoonal-Inlet (µmol/ kg)	Variance, Lagoonal-Inlet Sites (µmol/ kg)^2
March (3/2022)	2083.5 ± 14.5	1785.6	2115.7 ± 15.9	2469.8	2060.5 ± 5.3	146.9
April (4/2023)	2073.4 ± 20.2	3618.8	2108.9 ± 22.0	4996.5	2043 ± 10.1	731.9
July (7/2022)	2054.3 ± 24.6	6558.6	2118.1 ± 23.0	6056.7	1999.7 ± 7.9	513.3
October (10/2022)	1986.8 ± 9.0	510.5	2007.6 ± 5.0	136.2	1969.6 ± 5.0	123.2

3.4.3b Total Alkalinity patterns

Of the four sampling periods, March exhibits the highest mean TA, at 2225.1 ± 12.5 µmol/ kg, and October exhibits the lowest mean TA, at 2138.1 ± 6.6 µmol/ kg (Figure 10). Based on results from Student's t-tests, there is no evidence of differing TA between marsh adjacent site means and lagoonal-inlet site means, a pattern which persists across each individual season (Table 6). However, there is significantly higher variance among marsh adjacent sites when compared to lagoonal-inlet sites in April, July, and October (Table 6). July is the sampling period with the highest variance in TA among marsh adjacent sites, and also displays the largest difference in variance between site types (Table 8).

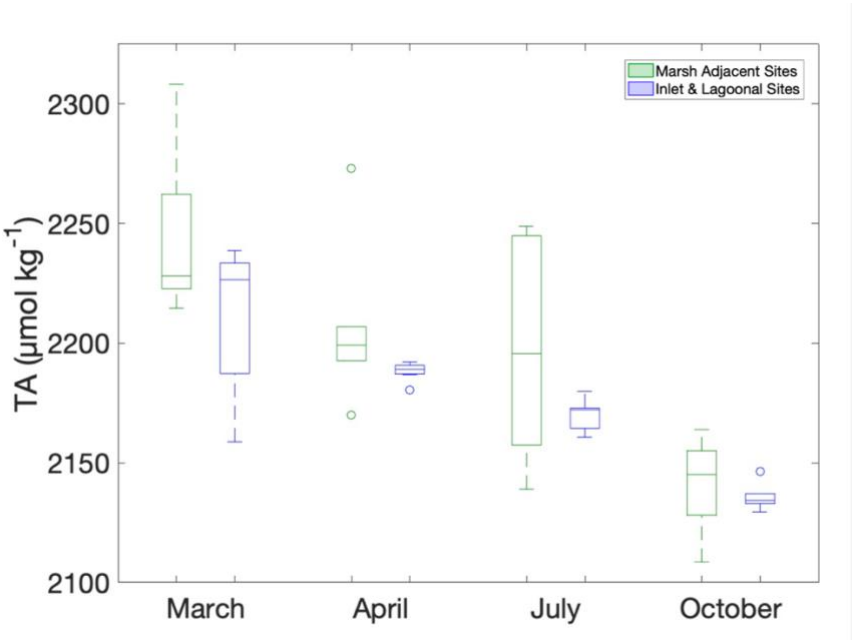

Figure 10: Box and whisker plot summarizing TA in March, April, July, and October in marsh adjacent sites (green, left bars) and lagoonal-inlet sites (blue, right bars).

Seasonal differences between sampling efforts are more evident among lagoonal-inlet mean TA concentrations than in the marsh adjacent TA concentrations. While April and July have similar TA concentrations, March and October are statistically significantly different than all other seasons (Student's t-tests; p-value < 0.1). This is in contrast to seasonal patterns at marsh adjacent sites, where March, April, and July have statistically similar TA concentrations

and only October TA is significantly lower than the other sampling periods (Student's t-tests; p-value < 0.1).

For the most part, variance among lagoonal-inlet sites did not differ by season, with the exception of March, which had statistically significantly higher variance than all other seasons (Levene's test; p-value < 0.01). March variance seems to be driven by two sites (NM and MI). While typically higher than lagoonal-inlet variance, marsh adjacent variance did not differ by season according to Levene's test results (Table 5).

When compared to DIC variance, variance of TA is lower across sites and seasons, likely owing to the more conservative nature of TA. This is especially evident when examining the difference in variance among Lagoonal-Inlet sites and Marsh Adjacent sites; the higher variance in TA and DIC among the marsh adjacent sites points to marsh-specific processes driving carbonate system variability.

In July, TA exhibits positive correlations with temperature ($R^2 = 0.5$) and NH_4 ($R^2 = 0.5$). In April and July, TA is weakly negatively correlated with DO (Both $R^2 = 0.3$). No significant correlations were found between TA and nitrate + nitrite, PO_4, or chlorophyll-a. Overall, DIC exhibits stronger correlations (i.e. higher R^2) with non-conservative parameters than TA.

Table 8: Mean TA reported with standard error (SE) and TA variance for March, April, July, and October. TA means and variance are reported for all sites, among marsh adjacent sites only, and among lagoonal-inlet sites only.

Sampling Time Period	Mean TA & SE, All Sites (µmol/ kg)	Variance, All Sites (µmol/ kg)^2	Mean TA & SE Marsh Adjacent (µmol/ kg)	Variance, Marsh Adjacent Sites (µmol/ kg)^2	Mean TA & SE, Lagoonal-Inlet Sites (µmol/ kg)	Variance, Lagoonal-Inlet Sites (µmol/ kg)^2
March (3/2022)	2225.1 ± 12.5	1317.8	2244.7 ± 12.1	1398.4	2211.1 ± 10.5	936.1
April (4/2023)	2196.9 ± 9.0	607.5	2206.8 ± 11.2	1217.3	2188.3 ± 2.6	15.3

July (7/2022)	2182.4 ± 11.2	1046.0	2196.9 ± 13.7	1986.6	2169.9 ± 3.6	42.3
October (10/2022)	2138.1 ± 6.6	198.9	2140.9 ± 8.3	438.5	2135.8 ± 3.0	32.8

3.4.3c Assessment of Potential Biogeochemical Drivers of DIC and TA

Deviations from the VCR conservative mixing TA-S and DIC-S regression models indicate some non-conservative behavior of TA, with the largest excess of DIC occurring in July sampling (Figure 12). Further investigation of DIC and TA spatial and seasonal trends reveal heightened TA and DIC variability in July, along with elevated July DIC in marsh adjacent sites relative to lagoonal inlet sites. The July sampling coincides with seasonally heightened biological activity in salt marshes that likely mediates carbonate system trends in nearby waters. To determine the potential biological drivers of carbonate system variability, we assessed stoichiometric relationships between biological processes and observed DIC and TA, with a particular focus on July trends.

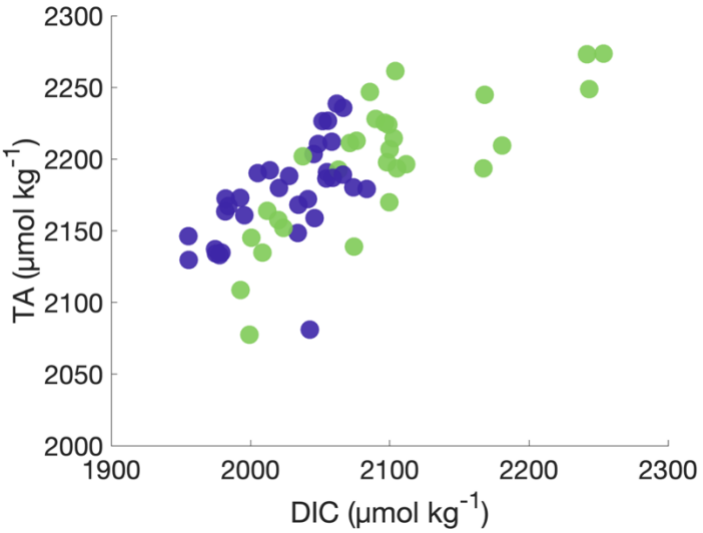

Figure 11: Marsh adjacent sites (green) exhibit a wider range of DIC and TA conditions than lagoonal-inlet sites (blue), with high DIC values driving down the TA:DIC ratio seen at marsh adjacent sites.

In July, TA:DIC ratios are lowest in marsh adjacent sites (< 1.07), while lagoonal-inlet sites are typically above a ratio of 1.07 (Figure 11). Looking across all seasons, the pattern persists with the majority of marsh adjacent samples having a TA:DIC ratio < 1.08 and most lagoonal-inlet sites > 1.08. With a range of ~0.02, July TA:DIC ratios among lagoonal-inlet sites also exhibit less variability than those in marsh adjacent sites, with a range ~0.07. As there was no significant difference between TA in marsh adjacent and lagoonal-inlet sites in July, the spatial variation seen in TA:DIC ratios is primarily driven by DIC differences. TA-DIC and TA:DIC exhibit similar patterns.

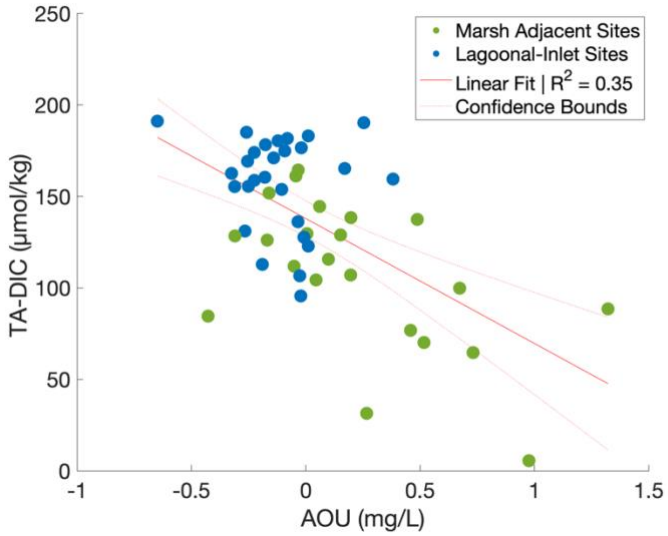

Figure 12: A linear regression of TA-DIC on AOU shows a weak negative relationship, with marsh adjacent sites comprising samples with the highest AOU and lowest TA-DIC.

Sample AOU is skewed toward oversaturation with respect to oxygen, indicating net autotrophy, especially among lagoonal-inlet sites. The majority of positive AOU values can be attributed to marsh adjacent samples. AOU shows a weak negative relationship with TA-DIC and TA:DIC, in which samples with the highest AOU were collected at marsh adjacent sites. When oxygen is used for aerobic respiration, DIC increases and there are minimal effects to TA, resulting in lower TA:DIC ratios corresponding to positive AOU values (Figure). While a negative relationship between AOU and TA-DIC is evident, especially at marsh adjacent sites, the low R^2 signifies that aerobic respiration and photosynthesis are not the only carbonate system drivers at play.

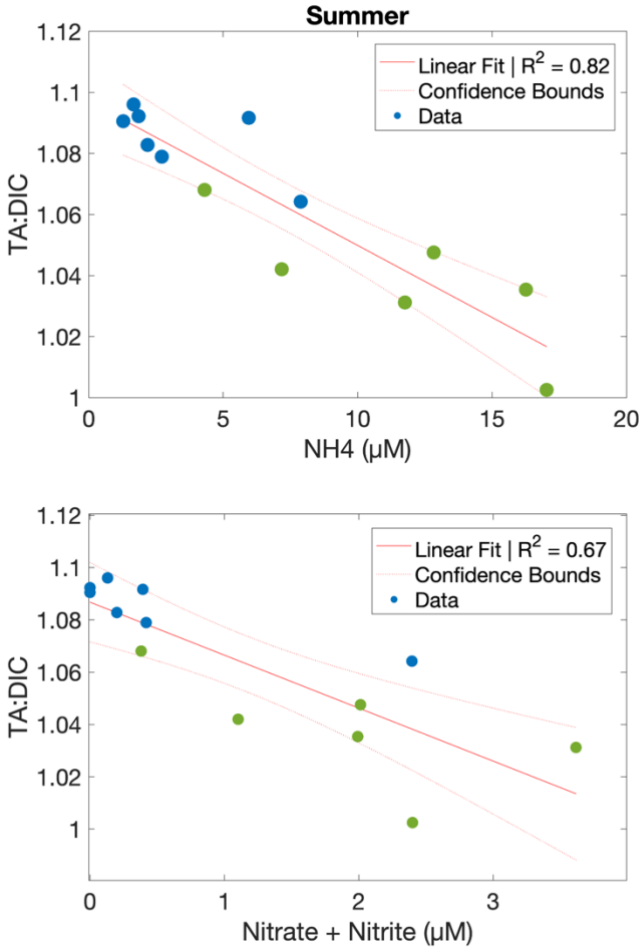

Figure 13: July DIC:TA vs. NH4 and Nitrate + Nitrite

In July, strong negative correlations were observed between NH_4 and TA:DIC and nitrate + nitrate and TA:DIC, with the highest levels of NH_4 and nitrate + nitrite occurring in marsh adjacent sites (Figure 13). Heightened summertime concentrations of NH_4 in marsh adjacent sites point toward higher rates of a combination of processes: 1) aerobic remineralization, which produces TA and DIC in a 0.14:1 ratio and 2) denitrification which produces TA and DIC in an 0.8:1 ratio.

There is also a positive correlation between NH_4 and nitrate + nitrite in July ($R^2 = 0.69$). The higher NH_4 availability paired with relatively high levels of nitrate + nitrite in July marsh adjacent sites could indicate the potential for nitrification, a process that decreases TA.

As ecosystems of heightened productivity, marshes are considered producers and exporters of both DIC and TA, with DIC exports exceeding TA exports. TA:DIC ratios, most often exhibited in marsh adjacent sites, correspond with relatively high AOU values and net heterotrophy which drives higher DIC export than TA export from the marshes. Biologically driven relationships in marsh adjacent sites are most evident in the July.

3.4.3d pCO_2: Spatiotemporal patterns, drivers, and air-sea gas exchange

While sites do not exhibit seasonal differences in pCO_2 means, there are statistically significant differences between site type pCO_2. Mean pCO_2 is higher in marsh adjacent sites than in lagoonal inlet sites, with a statistically significant difference between site types observed in July (Figure 14; Table 6). During July sampling, a significant difference between site type variance was also observed, in which marsh adjacent sites had higher variance than lagoonal inlet sites (Table 6).

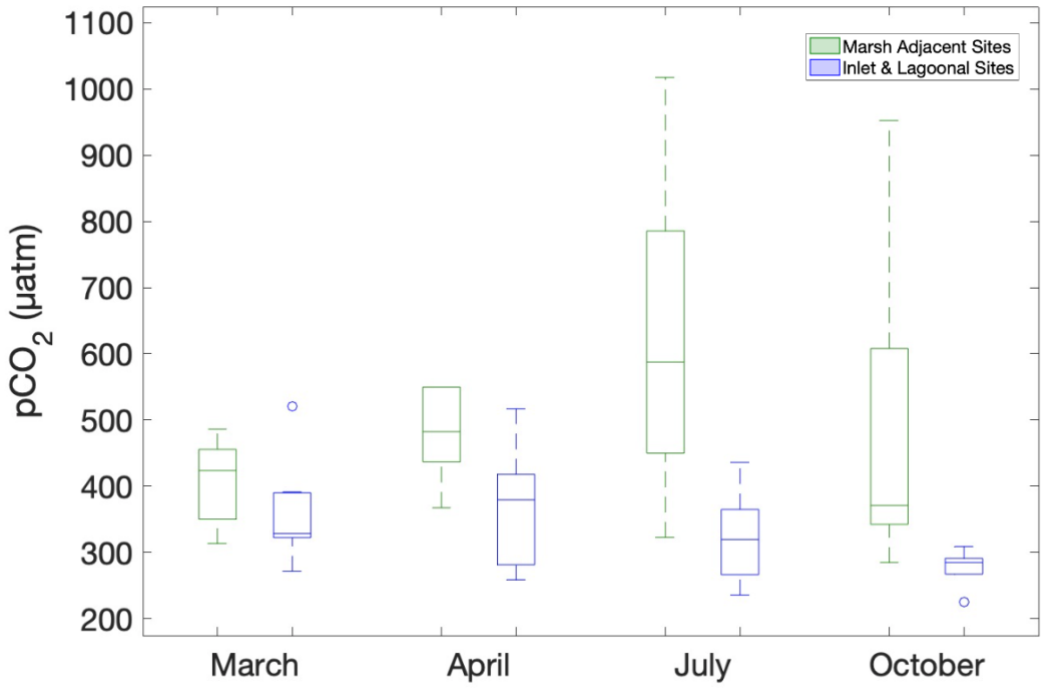

Figure 14: Box and whisker plot summarizing pCO_2 in March, April, July, and October in marsh adjacent sites (green, left bars) and lagoonal-inlet sites (blue, right bars).

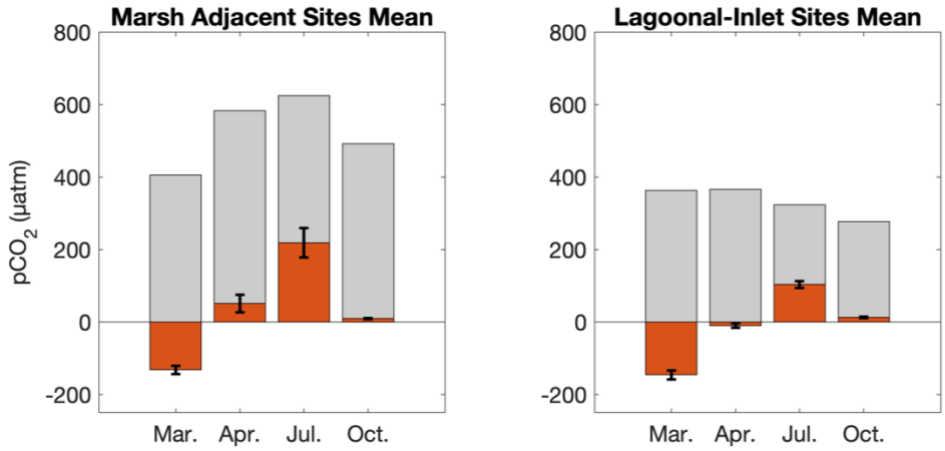

Figure 15: Mean $\Delta pCO_{2(thermal)}$ (visualized in red) is plotted alongside observed mean pCO_2 for marsh adjacent sites (left plot) and lagoonal-inlet sites (right plot). Error bars show standard error of mean pCO_2.

Relative to site-specific mean annual temperatures, lower temperatures in March serve to decrease total pCO_2 at all sites, while higher temperatures in July serve to increase total pCO_2. The April sampling effort captures the transition from cooler winter water temperatures to warmer summer water temperatures, in which marsh adjacent sites have already crossed into higher temperatures, yielding a small positive effect on pCO_2. Maximum annual temperatures at inlet sites are both lower and lag those at marsh adjacent sites (Brahmey et al., 2024), which may contribute to the small negative thermal impact on pCO_2 seen at several sites closest to inlets in April (i.e., MI, QI, SH). As temperatures fall from July to October sampling, the thermal impact on pCO_2 decreases as well, with most sites exhibiting a slight positive thermal effect on pCO_2 relative to the annual mean temperature baseline (Figure 15).

Thermal drivers contribute to the high pCO_2 observed in marsh adjacent sites in July (Figure 15). July sampling captured near-maximum annual temperatures in the VCR, which typically occur in early August (Brahmey et al., 2024). In July, thermal influences on marsh adjacent pCO_2 surpass those present in lagoonal-inlet sites (Student's t-test; p-value < 0.05). Previous work in the VCR has shown that annual maximum temperatures are higher among the VCR marsh adjacent sites compared to lagoonal-inlet sites, likely due to shallow conditions and less frequent flushing with relatively colder ocean water (Brahmey et al., 2024). The high

temperatures observed in marshes during the July sampling period lend themselves to higher thermal influences on pCO_2 in marsh adjacent sites relative to lagoonal-inlet sites. Regional and VCR-specific studies have observed long-term trends of increasing sea surface temperature and increased frequency of marine heat waves (Brahmey et al., 2024; Wiberg, 2023). These trends may lead to shifting thermal influences on pCO_2, with higher summertime temperatures and heat waves working to increase total pCO_2.

pCO_2 negatively correlates with DO across all seasons, with the strongest correlation in July ($R^2 = 0.64$). A weaker, positive relationship between pCO_2 and AOU ($R^2 = 0.49$) helps to parse out ecosystem metabolism effects on pCO_2 from any gas solubility effects. The correlation between pCO_2 and AOU is demonstrative of the biological controls on pCO_2, wherein AOU represents the photosynthetic production and respiratory consumption of oxygen and pCO_2 reflects the inverse. In July, sample pCO_2 also has a positive correlation with nitrate + nitrite ($R^2 = 0.52$) and NH_4 ($R^2 = 0.77$). pCO_2 doesn't show any significant relationships with chlorophyll-a.

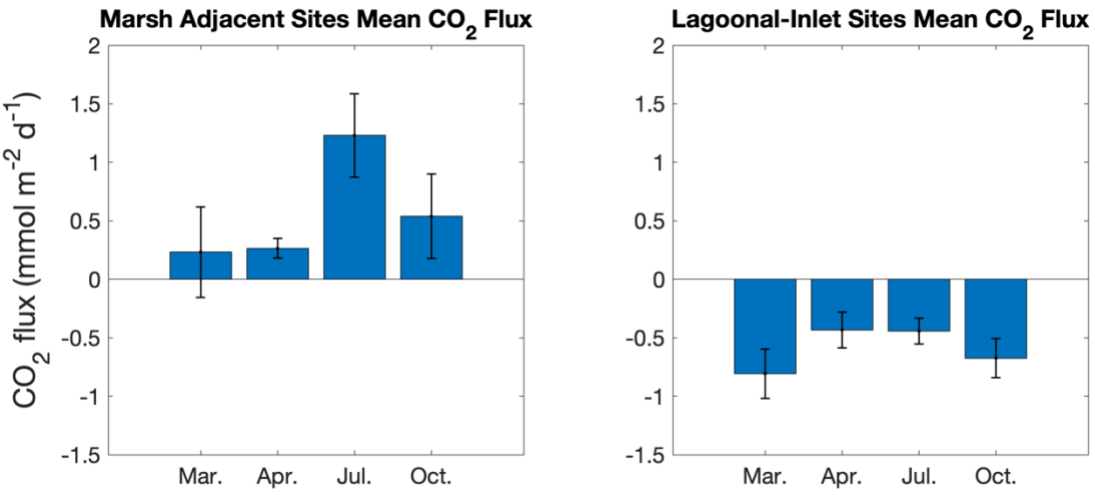

Figure 16: Mean CO_2 flux among all marsh adjacent sites (left) and lagoonal-inlet sites (right) for March, April, July, and October. Positive values indicate a CO_2 source to the atmosphere, while negative values indicate a CO_2 sink. Error bars reflect propagated error from CO2SYS pCO_2 estimations and flux calculations.

On average, marsh adjacent sites acted as sources of CO_2 to the atmosphere during the April, July, and October collection times (Figure 16). In March, the direction of mean marsh

adjacent CO_2 flux was uncertain due to error estimates spanning positive and negative values (Figure 17). At 1.23 ± 0.36 mmol/m^2/day, the July sampling effort exhibited the highest mean CO_2 flux. Lagoonal-inlet mean CO_2 fluxes were negative across all four sampling events, indicating oceanic uptake of CO_2. March and October fluxes were the largest in magnitude, at -0.81 ± 0.21 mmol/m^2/day and -0.67 ± 0.17 mmol/m^2/day. In April and July, results from Student's t-tests show that marsh adjacent sites exhibit significantly different CO_2 fluxes than lagoonal-inlet sites (Table 9). During these sampling periods, marsh adjacent sites were more likely to be a source of CO_2 to the atmosphere, whereas lagoonal-inlet sites were more likely to act as CO_2 sinks (17).

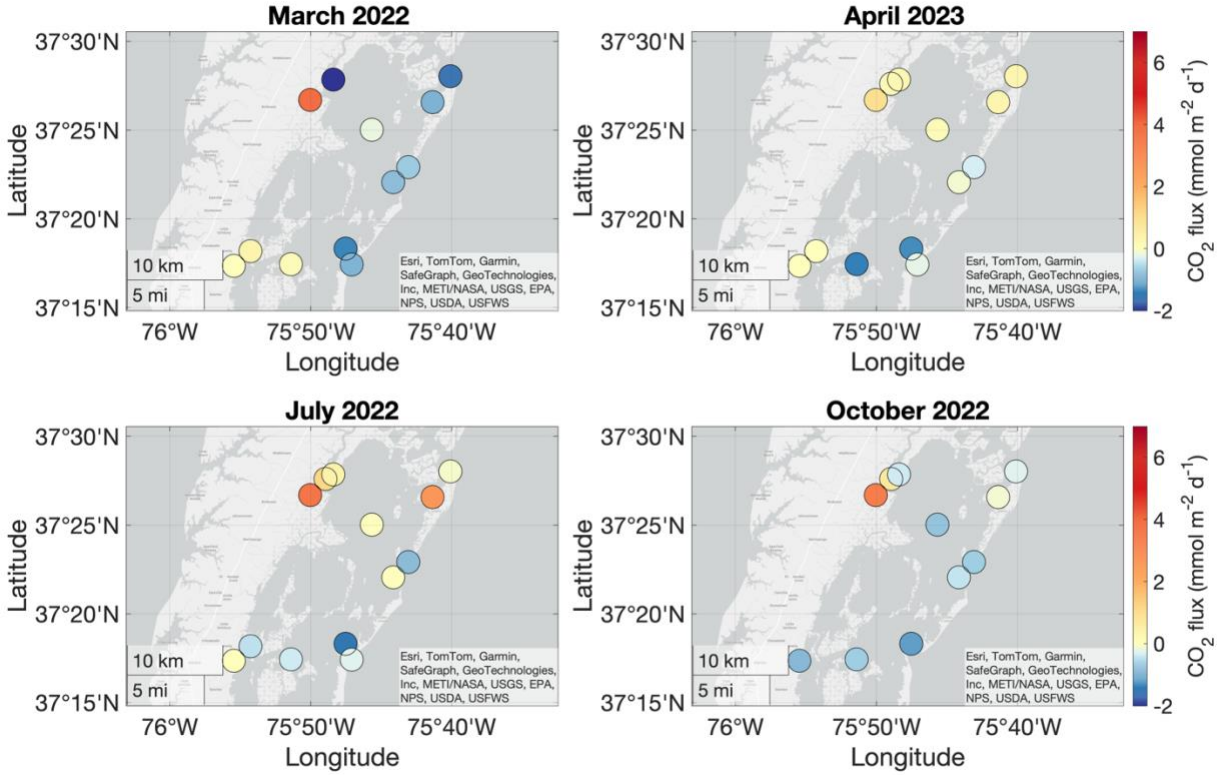

Figure 17: Maps of CO_2 flux at each lagoonal-inlet site in March, April, July, and October. Positive values indicate a CO_2 source to the atmosphere, while negative values indicate a CO_2 sink.

CO_2 flux patterns of individual sites revealed high spatial variability in both the direction and magnitude of fluxes (Figure 17). Spatial variance in CO_2 flux was higher than seasonal variance (spatial = 1.60 (mmol/m^2/day)^2; seasonal = 0.61 (mmol/m^2/day)^2). When flux variance was assessed by site type, spatial variability still surpassed seasonal variability among both

marsh adjacent sites and lagoonal-inlet sites. However, marsh adjacent sites exhibited higher variability by both metrics than lagoonal-inlet sites: seasonal variance among marsh sites was 1.05 $(mmol/m^2/day)^2$ and spatial variance was 2.72 $(mmol/m^2/day)^2$ while seasonal variance among lagoonal-inlet sites was 0.24 $(mmol/m^2/day)^2$ and spatial variance was 0.31 $(mmol/m^2/day)^2$.

All sampling was done on low wind, fair-weather days. As the magnitude of flux can change substantially at high wind speeds or during storm events (Granville, 2024), trends observed during these sampling periods are only representative of the fair-weather conditions in which they were observed. While consistently low, surface wind speed did vary between sites and sampling days, ranging from 0.1 to 4.9 m/s. To assess the impact of variability in wind speed on CO_2 flux estimations, flux was computed at a constant wind speed (2.1 m/s) in addition to observed wind speeds. Wind speed differences between sites and sampling days resulted in small differences in gas transfer velocity, and therefore CO_2 flux.

Table 9: Results from Student's t-tests assessing the difference in CO_2 fluxes between marsh adjacent (M) and lagoonal-inlet (LI) sites in March, April, July, and October.

Student's t-test Treatment:	CO_2 Flux (p-value)	CO_2 Flux normalized wind speed (p-value)
March: M vs. LI	0.5021	0.7582
April: M vs. LI	0.0295*	0.0995
July: M vs. LI	0.0462*	0.0371*
October: M vs. LI	0.1707	0.1392

Table 10: Resulting p-values from each Student's T-test treatment, in which thermal drivers of pCO_2 were compared between Marsh Adjacent (M) sites and Lagoonal-Inlet (LI) sites in March, April, July, and October.

Student's T-test Treatment:	pCO_2 Thermal Effects (p-value)
March: M vs. LI	0.2674

April: M vs. LI	0.0852
July: M vs. LI	0.0474*
October: M vs. LI	0.1162

Table 11: Mean thermal drivers of pCO_2 for Marsh Adjacent (M) sites and Lagoonal-Inlet (LI) sites in March, April, July, and October.

Month	Site Type	Mean $\Delta pCO_{2(thermal)}$ with Standard Error
March	M	-131.9 ± 7.8
	LI	-145.6 ± 9.1
April	M	51.2 ± 16.7
	LI	-9.4 ± 4.9
July	M	218.9 ± 27.8
	LI	103.8 ± 7.0
October	M	9.6 ± 1.3
	LI	13.4 ± 1.4

Table 12: Mean pCO_2 reported with standard error (SE) and TA variance for March, April, July, and October. TA means and variance are reported for all sites, among marsh adjacent sites only, and among lagoonal-inlet sites only.

Sampling Time Period	Mean pCO_2, SE (µatm)	Variance, all sites ($µatm^2$)	Mean pCO_2, SE Marsh Only (µatm)	Variance, Marsh Only ($µatm^2$)	Mean pCO_2, SE LI Only (µatm)	Variance, LI Only ($µatm^2$)
March (3/2022)	373.7 ± 56.9	557.1	398.0 ± 108.6	459	356.4 ± 27.3	6312
April (4/2023)	458.5 ± 54.7	5396.2	574.4 ± 99.1	8961.6	359.1 ± 27.3	8268.5

July (7/2022)	454.8 ± 54.7	5131.7	615.1 ± 99.1	6029.1	317.5 ± 27.3	4722.5
October (10/2022)	368.9 ± 59.4	4239.7	486.6 ± 108.6	7322.2	270.8 ± 29.5	802.8

3.4.3e pH and ΩAr: spatial and seasonal patterns and implications for marine species

Spatial patterns in ΩAr become evident when comparing marsh adjacent sites with lagoonal-inlet sites. Mean ΩAr among lagoonal-inlet sites exceed those in marsh adjacent sites in all sampling months, with statistically significant disparities between site types occurring in July and October (Figure 18; Table 6). At marsh adjacent sites, ΩAr was lowest in April and July with a mean April ΩAr of 1.24 ± 0.11 and a mean July ΩAr of 1.09 ± 0.11 (Table 14). Mean marsh adjacent ΩAr peaked in October at 1.53 ± 0.12, and similar conditions were observed in March. No statistically significant seasonal patterns emerged among lagoonal-inlet sites (Table 5). Contrasting marsh adjacent sites, July marked the sampling effort with the maximum ΩAr values in lagoonal-inlet sites, with a July mean of 1.83 ± 0.09.

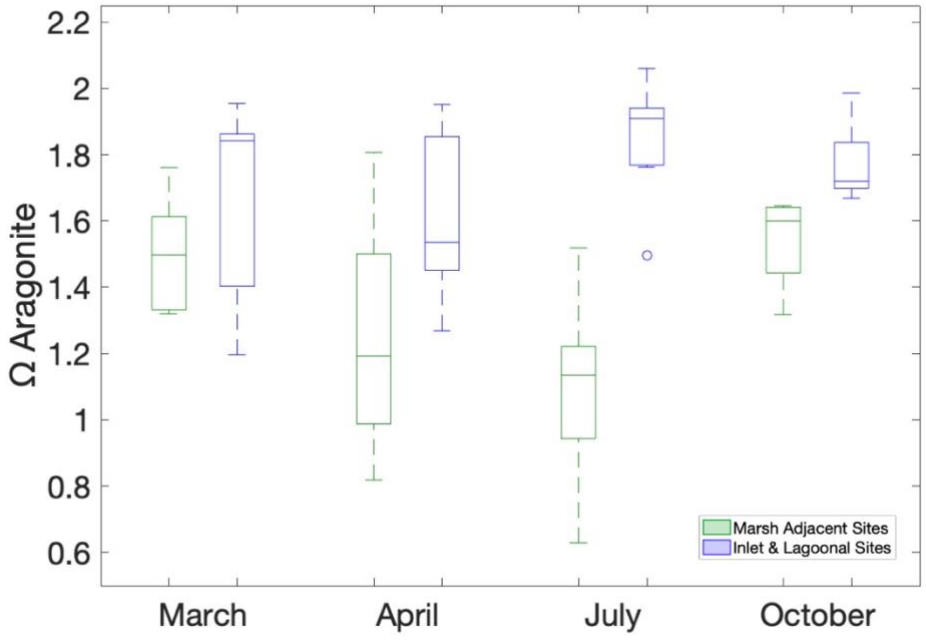

Figure 18: Box and whisker plot summarizing Ω Aragonite in March, April, July, and October in marsh adjacent sites (green, left bars) and lagoonal-inlet sites (blue, right bars).

Among marsh adjacent sites, a significant difference was found between July and October in which July means were smaller than October means (Student's t-test; p-value < 0.06). The lack of ΩAr seasonality in all but the marsh-adjacent sites may indicate seasonal biogeochemical controls on aragonite saturation state that are particular to the processes occurring near marshes.

pH, as estimated by CO2SYS, shows significantly lower values in marsh adjacent sites when compared to lagoonal-inlet sites (p-value = 0.002). July and October display the highest variability in the pH of marsh adjacent sites. There is, however, no significant seasonal pattern evident in pH (Figure 19).

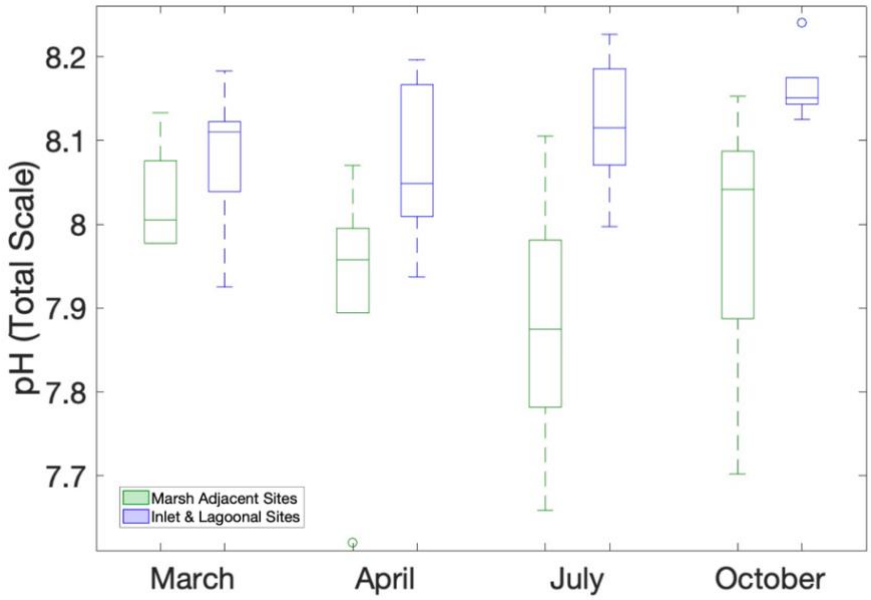

Figure 19: Box and whisker plots summarizing pH estimated with CO2SYS in marsh adjacent sites (green, left) and lagoonal-inlet sites (blue, right) in March, April, July, and October.

In July, pH positively correlates with DO and negatively correlates with nitrate + nitrite. pH also exhibits a negative correlation with NH_4, showing the strongest relationship in July (R^2 = 0.85). As expected, many of these patterns closely match relationships exhibited between nutrients and DIC, TA, and pCO_2. Ultimately, the hydrogen ion concentration of each sample is directly governed by the balance of carbonate and charged species in the water column.

Table 13: Mean pH reported with standard error (SE) and TA variance for March, April, July, and October. TA means and variance are reported for all sites, among marsh adjacent sites only, and among lagoonal-inlet sites only.

Sampling Time Period	Mean pH, SE	Variance	Mean pH, SE Marsh Only	Variance, Marsh Only	Mean pH, SE LI Only	Variance, LI Only
March (3/2022)	8.0644 ± 0.0408	0.0058	8.0419 ± 0.066	0.0042	8.0805 ± 0.03	0.007
April (4/2023)	8.0029 ± 0.039	0.022	7.917 ± 0.06	0.0250	8.0766 ± 0.03	0.0094
July (7/2022)	8.0101 ± 0.039	0.0291	7.8807 ± 0.06	0.0246	8.1211 ± 0.03	0.0066
October (10/2022)	8.0841 ± 0.043	0.0224	7.9835 ± 0.066	0.0308	8.1679 ± 0.033	0.0017

Because of the disparate responses to OA across species and life stages, we assess critical OA thresholds as defined by several levels of ΩAr reported in the literature (Table 14). While high pCO_2 and low pH can pose challenges at the organismal level, such as acid-base dysregulation, ΩAr is the best indicator of larval shell development. Here, site conditions are assessed based on four levels of ΩAr: ≤ 1 = severe, 1-1.5 = high, 1.5-2 = moderate-high, ≥ 2 = moderate. Waldbusser and colleagues (2015) report sub-lethal effects caused by short-term exposure of vulnerable life stages to ΩAr between 1.2 and 1.5 and others have reported a sublethal Ωarag threshold of 1.9 for *C. virginica* when exposure is chronic (Talmage & Gobler, 2010).

Table 14: Levels of OA Severity based on ΩAr biological thresholds for C. virginica and M. mercenaria as reported in the literature.

OA Severity (based on ΩAr)	ΩAr	Consequences within range	Results: April
Severe	≤ 1	Thermodynamic threshold below which dissolution of aragonite is favored over precipitation	2 sites

High	1 - 1.5	Acute exposure of 1.2 - 1.5 ΩAr leads to sub-lethal larval effects (Waldbusser et al., 2015)	6 sites
Moderate-high	1.5 - 2	Chronic exposure at 1.9 ΩAr or lower leads to sub-lethal larval effects for *C. virginica* (Talmage & Gobler, 2010)	5 sites
Moderate	≥ 2		0 sites

When assessed by level of OA severity, April had the most sites under an ΩAr of 1.5, with 6 sites experiencing high and 2 sites experiencing severe exposure to low ΩAr. April PCM and RB were the sites with the lowest ΩAr, with ΩAr of 0.81 and 0.97 respectively.

Across all samples, only one exceeds an ΩAr of 2. Long-term exposure to ΩAr of 1.9 has been cited as a threshold at which *C. virginica* begins to experience stress, thus indicating a possible cause for concern for eastern oysters in the VCR (Talmage & Gobler, 2010). It is, however, important to note that while the sampling scheme of this study allows us to glean a better understanding of spatial dynamics and general seasonal patterns, it does not provide the finer detail necessary to draw conclusions about shorter term variability in ΩAr and other carbonate system parameters.

Six sites exhibit ΩAr under 1.5 for two or more consecutive seasons (OH, RB, CSM, CRM, PCM, SS), indicating the possibility of chronic exposure to moderately low ΩAr at these sites (Figure 20). While five of these sites are marsh adjacent, one site, SS, is located in a shallow intertidal mudflat in central Hog Island Bay. Few other water quality sites share these characteristics with SS (no marsh, high mudflat proportion, far from inlet), so we are unable to discern a pattern in this study regarding mudflat carbonate chemistry in the VCR. However, as a large proportion of the VCR is dominated by intertidal mudflats, a more thorough investigation of ΩAr dynamics in future would allow a more comprehensive understanding of carbonate system differences across key VCR ecosystems.

While few sites fall below the critical threshold of ΩAr < 1, they do so in April during a period of heightened vulnerability due to widespread reproduction and larval growth and

development. In April, 8 of 13 sites are experiencing high or severe levels of undersaturation with respect to aragonite (ΩAr < 1.5). July has the largest range of ΩAr, and the proportion of sites experiencing high or severe undersaturation drops to just below 50%.

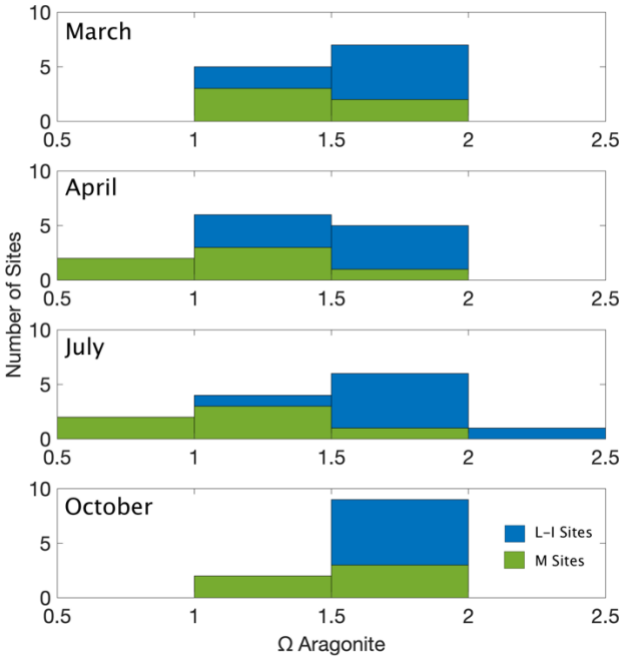

Figure 20: Bar graph depicting number of sites at each level of OA severity as defined in Table 14. Proportion of total sites that are marsh adjacent (M) sites are shown as green bars and lagoonal-inlet (LI) sites are shown as blue bars.

Table 14: Mean ΩAr reported with standard error (SE) and TA variance for March, April, July, and October. TA means and variance are reported for all sites, among marsh adjacent sites only, and among lagoonal-inlet sites only.

Sampling Time Period	Mean ΩAr, SD	Variance	Mean ΩAr, SD Marsh Only	Variance, Marsh Only	Mean ΩAr, SD LI Only	Variance, LI Only
March (3/2022)	1.59 ± 0.10	0.0694	1.48 ± 0.12	0.0326	1.66 ± 0.09	0.0902
April (4/2023)	1.44 ± 0.09	0.1218	1.24 ± 0.11	0.1311	1.60 ± 0.09	0.0638

July (7/2022)	1.49 ± 0.09	0.2029	1.09 ± 0.11	0.0879	1.83 ± 0.09	0.0332
October (10/2022)	1.66 ± 0.10	0.0294	1.53 ± 0.12	0.0200	1.76 ± 0.09	0.0142

3.5 Conclusions

In the nearshore coastal environment, spatial heterogeneity of seawater inorganic carbonate system parameters is controlled by physical, thermodynamic, and biological drivers. In the VCR, conservative mixing, thermal drivers, and biogeochemical processes exert varying degrees of control on local seawater carbonate system conditions dependent on location and season. Across all months, conservative mixing explained more of the variance at lagoonal-inlet sites when compared to marsh adjacent sites. Observed DIC and TA at lagoonal-inlet sites exhibited better agreement with values predicted by seasonal conservative mixing models than marsh adjacent sites did. Due to diverse biogeochemical processes, salt marshes can act as sources of DIC and TA to adjacent waters. Compared to lagoonal-inlet sites, marsh adjacent July measurements exhibit significant differences in DIC and pCO_2, heightened variability in TA, and non-conservative additions to DIC. While July TA is not significantly elevated among marsh adjacent sites in comparison to lagoonal-inlet sites, high TA variance observed in marsh adjacent sites in the summer point to spatially distinct biogeochemical processes with variable impacts on TA. Biogeochemistry is not the only non-conservative driver of spatial differences in seawater carbonate chemistry in July: marsh adjacent sites exhibit significantly higher thermal impacts on pCO_2 variability than lagoonal-inlet sites. Driven by higher residence times, mainland marsh sites exhibit higher temperatures than inlet sites, resulting in increased thermal influence on pCO_2. Variability in VCR seawater carbonate chemistry resulted in variation in the direction and magnitude of CO_2 air-sea gas flux, with marsh adjacent sites more likely to act as sources of CO_2 to the atmosphere than lagoonal-inlet sites. We also observed spatially diverse pH and ΩAr, with conditions occasionally crossing biological thresholds for locally important marine species, especially in spring and summer at marsh adjacent sites. Overall, fluctuations in drivers highlight the importance of considering the spatially explicit seasonality of local physical and biological drivers.

3.6 References

Accomack-Northampton Planning District Commission and the Eastern Shore of Virginia Groundwater Committee (2013). Eastern Shore of Virginia Groundwater Resource Protection and Preservation Plan.

An, S., & Joye, S. B. (2001). Enhancement of coupled nitrification-denitrification by benthic photosynthesis in shallow estuarine sediments. *Limnology and Oceanography*, *46*(1), 62-74.

Boulais, M., Chenevert, K. J., Demey, A. T., Darrow, E. S., Robison, M. R., Roberts, J. P., & Volety, A. (2017). Oyster reproduction is compromised by acidification experienced seasonally in coastal regions. Scientific Reports, 7(1), 13276.

Brahmey, E. I., McGlathery, K. J., & Doney, S. C. (2024). Quantifying seasonal to multi-decadal signals in coastal water quality using high- and low-frequency time series data, *Cambridge Prisms: Coastal Futures, in press*. https://doi.org/10.1017/cft.2024.6

Brenner, H., Braeckman, U., Le Guitton, M., & Meysman, F. J. (2016). The impact of sedimentary alkalinity release on the water column CO_2 system in the North Sea. *Biogeosciences*, *13*(3), 841-863.https://doi.org/10.5194/bg-13-841-2016

Cai, W. J., Hu, X., Huang, W. J., Jiang, L. Q., Wang, Y., Peng, T. H., & Zhang, X. (2010). Alkalinity distribution in the western North Atlantic Ocean margins. *Journal of Geophysical Research: Oceans*, *115*(C8).

Cai, Wei-Jun, Richard A. Feely, Jeremy M. Testa, Ming Li, Wiley Evans, Simone R. Alin, Yuan-Yuan Xu et al. "Natural and anthropogenic drivers of acidification in large estuaries." *Annual Review of Marine Science* 13 (2021): 23-55.

Cai, W. J., Hu, X., Huang, W. J., Murrell, M. C., Lehrter, J. C., Lohrenz, S. E., ... & Gong, G. C. (2011). Acidification of subsurface coastal waters enhanced by eutrophication. *Nature geoscience*, *4*(11), 766-770.

Cai, W. J., Wang, Y., Krest, J., & Moore, W. S. (2003). The geochemistry of dissolved inorganic carbon in a surficial groundwater aquifer in North Inlet, South Carolina, and the carbon fluxes to the coastal ocean. Geochimica et Cosmochimica Acta, 67(4), 631-639.

Dickson, A. G. (1990). Thermodynamics of the dissociation of boric acid in synthetic seawater from 273.15 to 318.15 K. Deep Sea Research Part A: Oceanographic Research Papers, 37(5), 755–766. https://doi.org/10.1016/0198-0149(90)90004-F

Doney S. C., Fabry V. J., Feely R. A., Kleypas J. A. (2009). Ocean acidification: the other CO_2 problem. *Annu.Rev. Mar. Sci.* 1, 169–192. doi:10.1146/annurev.marine.010908.163834

Doney, S. C., Mahowald, N., Lima, I., Feely, R. A., Mackenzie, F. T., Lamarque, J. F., & Rasch, P. J. (2007). Impact of anthropogenic atmospheric nitrogen and sulfur deposition on ocean

acidification and the inorganic carbon system. *Proceedings of the National Academy of Sciences*, *104*(37), 14580-14585.

Emerson, S., & Hedges, J. (2008). *Chemical oceanography and the marine carbon cycle*. Cambridge University Press.

Eastern Oyster Biological Review Team (EOBRT). Status review of the eastern oyster (Crassostrea virginica). Report to the National Marine Fisheries Service, Northeast Regional Office. 2007. NOAA Tech. Memo. NMFS F/SPO-88, 105 p. Available: http://www.nmfs.noaa.gov/pr/species/Status%20Reviews/eastern_oyster_sr_2007.pdf

Feely, R. A. *et al*. The combined effects of ocean acidification, mixing, and respiration on pH and carbonate saturation in an urbanized estuary. *Estuar. Coast. Shelf Sci.* 88, 442–449 (2010).

Fennel, K., Wilkin, J., Previdi, M., & Najjar, R. (2008). Denitrification effects on air-sea CO2 flux in the coastal ocean: Simulations for the northwest North Atlantic. *Geophysical Research Letters*, *35*(24).

Gobler, C. J., & Talmage, S. C. (2014). Physiological response and resilience of early life-stage Eastern oysters (Crassostrea virginica) to past, present and future ocean acidification. Conservation Physiology, 2(1), cou004.

Granville, K. E. (2024). Gas exchange, carbon flows, and ecosystem metabolism over a temperate seagrass meadow, Ph.D Dissertation, University of Virginia, Charlottesville, VA. 2024.

Greiner, J. T., McGlathery, K. J., Gunnell, J., & McKee, B. A. (2013). Seagrass restoration enhances "blue carbon" sequestration in coastal waters. *PloS one*, *8*(8), e72469.

Gruber N., Clement D., Carter B. R., Feely R. A., van Heuven S., Hoppema M., et al. (2019). The oceanic sink for anthropogenic CO_2 from 1994 to 2007. *Science* 363, 1193–1199. doi: 10.1126/science.aau5153

Heinze, C., Meyer, S., Goris, N., Anderson, L., Steinfeldt, R., Chang, N., ... & Bakker, D. C. (2015). The ocean carbon sink–impacts, vulnerabilities and challenges. *Earth System Dynamics*, *6*(1), 327-358.

Herrmann, M., Najjar, R. G., Kemp, W. M., Alexander, R. B., Boyer, E. W., Cai, W. J., ... & Smith, R. A. (2015). Net ecosystem production and organic carbon balance of US East Coast estuaries: A synthesis approach. *Global Biogeochemical Cycles*, *29*(1), 96-111.

James, R. K., van Katwijk, M. M., van Tussenbroek, B. I., van Der Heide, T., Dijkstra, H. A., van Westen, R. M., ... & Bouma, T. J. (2020). Water motion and vegetation control the pH dynamics in seagrass-dominated bays. *Limnology and Oceanography*, *65*(2), 349-362.

Kirwan, M. L., & Guntenspergen, G. R. (2015). Response of plant productivity to experimental flooding in a stable and a submerging marsh. Ecosystems, 18, 903-913.

Kirwan, M. L., & Megonigal, J. P. (2013). Tidal wetland stability in the face of human impacts and sea-level rise. *Nature*,
504, 53–60. https://doi.org/10.1038/nature12856

Koch, M. S., Maltby, E., Oliver, G. A., & Bakker, S. A. (1992). Factors controlling denitrification rates of tidal mudflats and fringing salt marshes in south-west England. *Estuarine, Coastal and Shelf Science*, *34*(5), 471-485.

Lan, X., J.W. Mund, A.M. Crotwell, M.J. Crotwell, E. Moglia,
M. Madronich, D. Neff and K.W. Thoning (2023), Atmospheric Carbon Dioxide Dry Air Mole Fractions from the NOAA GML Carbon Cycle Cooperative Global Air Sampling Network, 1968-2022, Version: 2023-08-28, https://doi.org/10.15138/wkgj-f215

Lewis, E., Wallace, D. W. R., 1998. Program Developed for CO2 System Calculations. ORNL/CDIAC-105. Carbon Dioxide Information Analysis Center, Oak Ridge National Laboratory, Oak Ridge, TN.

Martínez-Espinosa, C., Sauvage, S., Al Bitar, A., Green, P. A., Vörösmarty, C. J., & Sánchez-Pérez, J. M. (2021). Denitrification in wetlands: A review towards a quantification at global scale. *Science of the total environment*, *754*, 142398.

McGlathery, K.J. and RR. Christian. 2024. Water Quality Sampling - integrated measurements for the Virginia Coast, 1992-2023. Virginia Coast Reserve Long-Term Ecological Research Project Data Publication knb-lter-vcr.247.18 (doi:10.6073/pasta/2bd65ce4cd152eb069f510d12a19520d).

Millero, F. J., Lee, K., & Roche, M. (1998). Distribution of alkalinity in the surface waters of the major oceans. *Marine Chemistry*, *60*(1-2), 111-130.

Miller, K. G., Kopp, R. E., Horton, B. P., Browning, J. V., & Kemp, A. C. (2013). A geological perspective on sea-level rise and its impacts along the US mid-Atlantic coast. *Earth's Future*, *1*(1), 3-18.

Millero, F. J. (2010). Carbonate constants for estuarine waters. Marine and Freshwater Research, 61(2), 139–142. https://doi.org/10.1071/MF09254

Murphy, A. E., Bulseco, A. N., Ackerman, R., Vineis, J. H., & Bowen, J. L. (2020). Sulphide addition favours respiratory ammonification (DNRA) over complete denitrification and alters the active microbial community in salt marsh sediments. *Environmental Microbiology*, *22*(6), 2124-2139.

Najjar, R. G., Herrmann, M., Alexander, R., Boyer, E. W., Burdige, D. J., Butman, D., ... & Zimmerman, R. C. (2018). Carbon budget of tidal wetlands, estuaries, and shelf waters of Eastern North America. *Global Biogeochemical Cycles*, *32*(3), 389-416.

Neubauer, S. C., & Anderson, I. C. (2003). Transport of dissolved inorganic carbon from a tidal freshwater marsh to the York River estuary. *Limnology and Oceanography*, *48*(1), 299-307.

Nightingale, P. D., Malin, G., Law, C. S., Watson, A. J., Liss, P. S., Liddicoat, M. I., ... & Upstill-Goddard, R. C. (2000). In situ evaluation of air-sea gas exchange parameterizations using novel conservative and volatile tracers. *Global Biogeochemical Cycles*, *14*(1), 373-387.

Office for Coastal Management (2023). Coastal Wetlands (GUID: 50447; Version: July 24, 2023 Update) [Dataset]. NOAA National Centers for Environmental Information. https://www.fisheries.noaa.gov/inport/item/50447.

Ollivier, Q. R., Maher, D. T., Pitfield, C., & Macreadie, P. I. (2022). Net drawdown of greenhouse gases (CO2, CH4 and N2O) by a temperate australian seagrass meadow. *Estuaries and Coasts*, *45*(7), 2026-2039.

Orr, J.C., Epitalon, J.-M., Dickson, A. G., Gattuso, J.-P., 2018. Routine uncertainty propagation for the marine carbon dioxide system. Marine Chemistry 207, 84-107.

Paulsen, M. L., Andersson, A. J., Aluwihare, L., Cyronak, T., D'Angelo, S., Davidson, C., ... & Schroeter, S. (2018). Temporal changes in seawater carbonate chemistry and carbon export from a Southern California estuary. *Estuaries and coasts*, *41*, 1050-1068.

Perez, F. F., & Fraga, F. (1987). Association constant of fluoride and hydrogen ions in seawater. Marine Chemistry, 21(2), 161-168.

Porter, J.H., DO. Krovetz, WK. Nuttle and J. Spitler. 2023. Hourly Meteorological Data for the Virginia Coast Reserve LTER 1989-present. Virginia Coast Reserve Long-Term Ecological Research Project Data Publication knb-lter-vcr.25.50 (doi:10.6073/pasta/406578baa2fd3f9ff39cd56379631a4a).

Prentice, C., Poppe, K. L., Lutz, M., Murray, E., Stephens, T. A., Spooner, A., ... & Klinger, T. (2020). A synthesis of blue carbon stocks, sources, and accumulation rates in eelgrass (Zostera marina) meadows in the Northeast Pacific. *Global Biogeochemical Cycles*, *34*(2), e2019GB006345.

Redfield, A. C., B. H. Ketchum, and F. A. Richards (1963), The influence of organisms on the composition of seawater, in *The Composition of Seawater: Comparative and Descriptive Oceanography. The Sea: Ideas and Observations on Progress in the Study of the Seas*, vol. 2, edited by M. N. Hill, pp. 26–77, Interscience Publishers, New York.

Reimer, J. J., Medeiros, P. M., Hussain, N., Gonski, S. F., Xu, Y. Y., Huang, T. H., & Cai, W. J. (2024). Carbonate Chemistry and the Potential for Acidification in Georgia Coastal Marshes and the South Atlantic Bight, USA. *Estuaries and Coasts*, *47*(1), 76-90.

Reithmaier, G. M., Cabral, A., Akhand, A., Bogard, M. J., Borges, A. V., Bouillon, S., ... & Santos, I. R. (2023). Carbonate chemistry and carbon sequestration driven by inorganic carbon outwelling from mangroves and saltmarshes. Nature communications, 14(1), 8196. https://doi.org/10.1038/s41467-023-44037-w

Roobaert, A., Laruelle, G. G., Landschützer, P., Gruber, N., Chou, L., & Regnier, P. (2019). The spatiotemporal dynamics of the sources and sinks of CO2 in the global coastal ocean. *Global Biogeochemical Cycles*, *33*(12), 1693-1714.

Safak, I., Wiberg, P. L., Richardson, D. L., & Kurum, M. O. (2015). Controls on residence time and exchange in a system of shallow coastal bays. *Continental Shelf Research*, *97*, 7-20.

Santos, I. R., Chen, X., Lecher, A. L., Sawyer, A. H., Moosdorf, N., Rodellas, V., ... & Li, L. (2021). Submarine groundwater discharge impacts on coastal nutrient biogeochemistry. *Nature Reviews Earth & Environment*, *2*(5), 307-323.

Sharp, J.D., Pierrot, D., Humphreys, M.P., Epitalon, J.-M., Orr, J.C., Lewis, E.R., Wallace, D.W.R. (2023, Jan. 19). CO2SYSv3 for MATLAB (Version v3.2.1). Zenodo. http://doi.org/10.5281/zenodo.3950562

Smith, A. J., & Kirwan, M. L. (2021). Sea level-driven marsh migration results in rapid net loss of carbon. *Geophysical Research Letters*, *48*(13), e2021GL092420.

Smith, A. J., McGlathery, K., Chen, Y., Ewers Lewis, C. J., Doney, S. C., Gedan, K., ... & Kirwan, M. L. (2024). Compensatory mechanisms absorb regional carbon losses within a rapidly shifting coastal mosaic. *Ecosystems*, *27*(1), 122-136.

Soetaert, K., Hofmann, A. F., Middelburg, J. J., Meysman, F. J., & Greenwood, J. (2007). Reprint of "The effect of biogeochemical processes on pH". *Marine Chemistry*, *106*(1-2), 380-401.

Takahashi, T., Sutherland, S.C., Sweeney, C., Poisson, A., Metzl, N., Tilbrook, B., Bates, N., Wanninkhof, R., Feely, R.A., Sabine, C. and Olafsson, J. (2002). Global sea–air CO2 flux based on climatological surface ocean pCO2, and seasonal biological and temperature effects. *Deep Sea Research Part II: Topical Studies in Oceanography*, *49*(9-10), 1601-1622.

Talmage, S. C., & Gobler, C. J. (2009). The effects of elevated carbon dioxide concentrations on the metamorphosis, size, and survival of larval hard clams (Mercenaria mercenaria), bay scallops (Argopecten irradians), and Eastern oysters (Crassostrea virginica). Limnology and Oceanography, 54(6), 2072-2080.

Talmage SC & Gobler CJ (2010) Effects of past, present, and future ocean carbon dioxide concentrations on the growth and survival of larval shellfish. Proceedings of the National Academy of Sciences. 107(40): 17246-17251.

Tan, E., Zou, W., Zheng, Z., Yan, X., Du, M., Hsu, T. C., ... & Kao, S. J. (2020). Warming stimulates sediment denitrification at the expense of anaerobic ammonium oxidation. Nature Climate Change, 10(4), 349-355. https://doi.org/10.1038/s41558-020-0723-2

Tassone, S.J. Quantifying Heatwaves and Seagrass Recovery Dynamics in Aquatic Ecosystems, Ph.D Dissertation,University of Virginia, Charlottesville, VA. 2023.

van Heuven, S., Pierrot, D., Rae, J.W.B., Lewis, E., Wallace, D.W.R., 2011. MATLAB Program Developed for CO2 System Calculations. ORNL/CDIAC-105b. Carbon Dioxide Information Analysis Center, Oak Ridge National Laboratory, Oak Ridge, TN.

Waldbusser, G. G., Hales, B., Langdon, C. J., Haley, B. A., Schrader, P., Brunner, E. L., ... & Gimenez, I. (2015). Saturation-state sensitivity of marine bivalve larvae to ocean acidification. Nature Climate Change, 5(3), 273-280.

Wallace, R. B., Baumann, H., Grear, J. S., Aller, R. C., & Gobler, C. J. (2014). Coastal ocean acidification: The other eutrophication problem. *Estuarine, Coastal and Shelf Science*, *148*, 1-13.

Wang, S. R., Di Iorio, D., Cai, W. J., & Hopkinson, C. S. (2018). Inorganic carbon and oxygen dynamics in a marsh-dominated estuary. Limnology and oceanography, 63(1), 47-71. https://doi/10.1002/lno.10614

Wang, Z. A., Kroeger, K. D., Ganju, N. K., Gonneea, M. E., & Chu, S. N. (2016). Intertidal salt marshes as an important source of inorganic carbon to the coastal ocean. *Limnology and Oceanography*, *61*(5), 1916-1931.

Wanninkhof, R. (2014). Relationship between wind speed and gas exchange over the ocean revisited. *Limnology and Oceanography: Methods*, *12*(6), 351-362.

Weiss, R. (1974). Carbon dioxide in water and seawater: the solubility of a non-ideal gas. *Marine chemistry*, *2*(3), 203-215.

Wiberg, P. L. (2023). Temperature amplification and marine heatwave alteration in shallow coastal bays. *Frontiers in Marine Science*, *10*, 1129295. https://doi.org/10.3389/fmars.2023.1129295

Xue, L., Cai, W.J., Hu, X., Sabine, C., Jones, S., Sutton, A.J., Jiang, L.Q. and Reimer, J.J. (2016). Sea surface carbon dioxide at the Georgia time series site (2006–2007): Air–sea flux and controlling processes. *Progress in Oceanography*, *140*, 14-26.

Yin, H., Jin, L., & Hu, X. (2024). Interpreting biogeochemical processes through the relationship between total alkalinity and dissolved inorganic carbon: Theoretical basis and limitations. *Limnology and Oceanography: Methods*.

Chapter 4: The Impact of Marsh Lateral Exchange and Seagrass Presence on Seawater Carbonate System Spatial Variability in a Temperate Coastal Lagoon

4.1 Abstract

Nearshore marine ecosystems experience extreme spatiotemporal fluctuations in pH, mediated by hydrodynamic and biogeochemical drivers. In particular, seagrass meadows and intertidal salt marshes are marine ecosystems noted for their high rates of biological activity, which can modify local seawater carbonate chemistry, including pH. In this chapter, we assess patterns in high frequency pH measurements collected in a temperate seagrass meadow and in a nearby unvegetated lagoon located next to a salt marsh in the summer of 2022. On short time scales, hydrodynamic and biogeochemical drivers had diverging effects on pH fluctuations in a seagrass meadow and marsh adjacent unvegetated sites. In the seagrass meadow, indicators of ecosystem metabolism explained most of the variability in pH while shifting water height served to dilute or concentrate local signals. At the near marsh bare site, there was evidence of marsh DIC and TA export at low and ebb tides, which resulted in more prominent semidiurnal fluctuations in pH due to tidally-mediated delivery of acidic water to the bare site. Relationships with indicators of local ecosystem metabolism were lesser than those observed in the seagrass site, but diel fluctuations in pH were observed. Studying seawater carbonate chemistry across multiple diverse ecosystems at a larger, bay-wide scale (ie. marsh-lagoon-seagrass ecotone), rather than at an individual ecosystem scale (ie. seagrass meadow alone) can provide greater context to the range of conditions present across an embayment.

4.2 Introduction

Located at the land-ocean interface, nearshore coastal marine systems, including tidal wetlands, estuaries, and shallow bays, exhibit high seawater carbonate system variability, in part modulated by regional and temporal variations in net ecosystem metabolism (Cai et al., 2011; Lowe et al., 2019; Wallace et al., 2014). The influx of organic carbon and nutrients from terrestrial sources promotes high productivity in estuaries and coastal bays, ultimately contributing to carbon burial and export to the continental shelf (Herrmann et al., 2014; Najjar et al., 2018). Inorganic carbon cycling is also impacted by biological activity, with respiration and

primary production directly affecting concentrations of dissolved inorganic carbon (DIC), aqueous pCO_2, total alkalinity (TA), and pH (Gattuso et al., 1999; Lowe et al., 2019). In addition to biogeochemical forcing, hydrodynamic factors act as drivers of seawater carbonate chemistry in shallow subtidal marine systems (Ricart et al., 2021; Wang and Cai, 2004). Tidal exchange and currents can facilitate exchange between systems with variable local signatures of DIC and TA while water height controls the dilution of existing conditions (Cyronak et al., 2018; James et al., 2020).

Further complicating an already variable system, coastal carbon cycles are undergoing rapid shifts in response to ongoing anthropogenic disturbances, including nutrient pollution, climate change, and ocean acidification (Borges and Gypens, 2010; Feely et al., 2010; Wallace et al., 2014; Resplandy et al., 2024). As a consequence of oceanic uptake of anthropogenic CO_2, surface ocean pH and saturation state have declined relative to pre-Industrial levels (Gruber et al., 2023; Jewett and Romanou, 2017; Khatiwala et al., 2013). Ocean acidification is expected to escalate if anthropogenic emissions continue to rise, with projections for 2100 predicting an additional decrease of 0.04-0.3 pH units under low to high emissions scenarios (Gattuso et al., 2015). Ocean acidification can lead to detrimental outcomes for marine species, ecosystems, and reliant coastal communities, especially when working in consort with other climate stressors (Doney et al., 2020). Given the context of global and local human perturbations to coastal carbon cycles, recent work has sought to understand the magnitude and mechanisms of variability in dynamic nearshore coastal systems, and the active role these ecosystems play in local alteration of seawater inorganic carbonate chemistry (Cyronak et al., 2018; Ricart et al., 2021; Wang et al., 2016).

Seagrass meadows and tidal salt marshes are integral components of temperate nearshore coastal systems with divergent effects on seawater acid-base chemistry. Seagrasses are marine flowering plants that take up carbon dioxide during photosynthesis, serving to increase pH locally (Hendriks et al., 2014; Ricart et al., 2021). Photosynthetic carbon uptake peaks during daylight hours in the spring and summer, driving seasonal and diel patterns in temperate seagrass meadow seawater inorganic carbonate systems (Lowe et al., 2019). Seagrasses are also valued for their ecosystem services; they act as nursery habitats for fish and shellfish, attenuate wave

action, and protect coastlines from erosion and flooding (Waycott et al., 2009). As "blue carbon" habitats, enhanced sedimentation of organic material in seagrass meadows sequesters carbon in sediments, locking away carbon on the order of hundreds of years (Fourqurean et al., 2012; Pacella et al., 2018). Through blue carbon burial and direct uptake of CO_2 via photosynthesis, seagrasses serve to mitigate ocean acidification and reduce ocean pCO_2 locally, by facilitating carbon drawdown. Production of alkalinity through enhanced denitrification in seagrass sediments provides an alternative pathway for anaerobic biochemical control of seagrass meadow pH (Aoki and McGlathery, 2018).

While several studies have observed heightened pH in seagrass meadows relative to nearby unvegetated sites, uncertainties remain regarding the efficacy of seagrasses as an ocean acidfication mitigation strategy (Groner et al., 2018, Pacella et al., 2018). Hydrodynamic setting, residence time, and depth can impact the pH range in seagrass meadows, sometimes pushing meadows into more acidic conditions than neighboring unvegetated systems (Cyronak et al., 2018; Koweek et al., 2018). As ecosystem engineers, seagrasses influence their hydrodynamic setting; high seagrass shoot density has been shown to slow mean water flow, attenuate wave height, and increase residence time relative to unvegetated ecosystems (Gambi et al., 1990; Reidenbach and Thomas, 2018). In South Bay of the Virginia Coast Reserve, seagrass meadows reduce flow velocity and flushing from tidal exchange by up to 70% in summer, coinciding with peak seagrass density and shoot heights (Zhu et al., 2021). Under higher residence times, limited flushing allows the local metabolic influence of both primary production and respiration to persist for extended periods of time (Cyronak et al., 2018). In seagrass meadows, this serves to amplify the diel pH range, resulting in more pronounced pH extremes (Cyronak et al., 2018).

Along temperate coastlines, seagrass meadows can be found closely coupled, geographically, with salt marshes. As biological hotspots, salt marshes thrive in the coastal intertidal zones of middle to high latitudes, and are often situated in low-energy, protected shorelines like estuaries, bays, and lagoons (Barbier et al., 2011). As producers and exporters of dissolved inorganic carbon, salt marshes can amplify acidification in the coastal ocean through delivery of low pH, high pCO_2, and high DIC water (Reimer et al., 2024; Wang et al., 2016). In the U.S. Southeast, there is an estimated net export of 700,000 metric tons of marsh-derived DIC

to the coastal ocean per year, nearly matching DIC export from rivers to the coastal ocean (Wang and Cai, 2004). Not only are salt marshes facilitators of carbon sequestration and transport, but they also provide numerous ecosystem services such as erosion control, water purification, and fishery and biodiversity maintenance (Barbier et al. 2011).

Many physical and biological processes occurring in seagrass meadows and marshes are inextricably linked across the seagrass-lagoon-salt marsh ecotone, including sediment transfer, trophic interactions, and organic carbon exchange (Irlandi et al., 1997; Huxham et al., 2018; Plumlee et al., 2020; Renzi et al., 2019; Zhu and Wiberg, 2024). In this chapter, we assess spatial and temporal water column carbonate chemistry dynamics across a temperate seagrass-lagoon-salt marsh ecotone. In a dynamic coastal setting, lateral exchange of DIC and TA between a patchwork of ecosystems including seagrass meadows, salt marshes, mudflats, and oyster reefs, can confer extreme spatiotemporal variability in coastal carbonate chemistry. We seek to examine patterns in seagrass meadow pH relative to a near-marsh bare site to understand the full range of pH conditions present across a small, shallow bay.

4.3 Methods

4.3.1 Study Site

The Virginia Coast Reserve (VCR) is a back-barrier island lagoonal system located on the Atlantic-facing eastern coast of Virginia's Eastern Shore. The VCR is the site of the world's largest seagrass restoration project, with vegetated area extending across 3,612 hectares of the VCR's shallow lagoons (Orth et al., 2020). *Zostera marina* was historically abundant in coastal Virginia's back-barrier lagoons, but the combined effects of a noxious slime mold and a hurricane in the early 20th Century resulted in dramatic loss of seagrass extent. After the discovery of several naturally occurring seagrass patches, a restoration effort began in 2001 with the goal of re-establishing the once-prominent seagrass meadows in the VCR (Orth et al., 2020). South Bay, the focus of this chapter, boasts the largest proportion of the VCR's current seagrass area, with over 2,028 hectares of restored seagrass meadow (Orth et al., 2020). Regionally and within the VCR, peak shoot densities of *Zostera marina* occur in late June to July (Oreska et al., 2017; Orth and Moore, 1986). High water temperatures in August prompt seagrass senescence and a sharp reduction in above seabed biomass (Orth and Moore 1986; Rheuban et al. 2014a).

South Bay (Figure 1) is bounded by a barrier island, Wreck Island, on its eastern side which is primarily comprised of sandy dune and shrub-scrub habitat. North and south inlets provide tidal flushing with coastal ocean water, and dictate net flow directionality in South Bay, which primarily follows a south to north trajectory (Zhu et al., 2021). On the western boundary of South Bay is New Marsh, a salt marsh tidal creek complex vegetated with *Spartina alterniflora*. The South Bay lagoon has an average depth of 1.2 meters and is inundated twice daily with semidiurnal tides with a mean tidal range of 1 meter (Safak et al., 2015). Sediments underlying both vegetated and unvegetated sites are siliciclastic with negligible $CaCO_3$ contributions (Oreska et al., 2020). South Bay acts as a representative setting similar to other coastal bays on the U.S. East Coast and other temperate coastal systems where seagrass meadows exist not in isolation but are closely coupled with other ecosystems like salt marshes, open lagoonal waters, and barrier islands. This chapter aims to understand the combined effects of multiple interconnected ecosystems on the spatiotemporal variability in South Bay's seawater carbonate system.

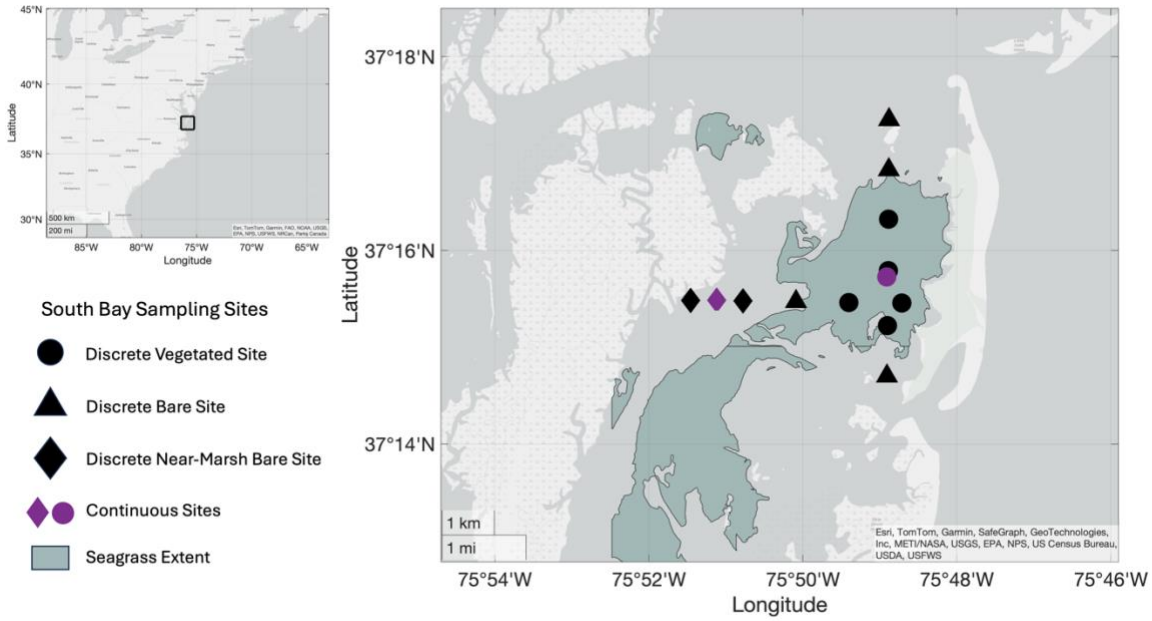

Figure 15: South Bay is a sheltered back-barrier lagoon located on the Atlantic-facing coast of Virginia's Eastern Shore. Discrete samples (black circles) were collected in June, July, and October of 2022 at 11 sites, both vegetated and unvegetated. SeapHOx continuous pH sensors were deployed at a central seagrass meadow site and a near-marsh bare site (purple). Dark grey background indicates water while white indicates land.

4.3.2 Data Collection

Two Sea-Bird Shallow SeapHOx V2 sensors were deployed in South Bay from June to July of 2022. Each instrument package consisted of a SeaFET pH sensor with an ion-sensitive field effect transistor (ISFET) sensing element and an SBE-37-ODO MicroCAT measuring temperature, salinity, optical dissolved oxygen, and pressure (SBE-37-ODO intake 0.635 meters from seafloor). Samples were collected at ten-minute intervals. One sensor was deployed in the central seagrass meadow while the other was deployed at an unvegetated site near New Marsh on the western boundary of South Bay (Figure 1). Prior to deployment, SeapHOx sensors were conditioned for 8-10 days in a tank receiving estuarine water from the York River, which exhibited natural daily fluctuations in pH. Following the conditioning period, a shore-side calibration was conducted with a series of spectrophotometric pH measurements with *m*-cresol dye (SOP 6b; Dickson et al., 2007). All discrete samples used for instrument calibration had errors of around ± 0.01 pH units. Benchmark discrete water samples were collected at sensor deployment sites at the beginning and end of monthly deployments. To discourage biofouling, instrument bodies were coated with copper tape and a copper mesh cage surrounding the ISFET sensor (Rivest et al., 2016). Data quality of SeapHOx pH data was assessed in accordance with best practices, and each timeseries was cleaned of periods of potential drift, biofouling, or instrument failure (Bresnahan et al., 2014; Rivest et al., 2016). At the end of the deployment, biofouling on sensors and instrument bodies was not observed, but biocalcification was present on the pvc structure supporting the instrument in the bare site. To account for potential effects of calcification on local pH, the latter half of the bare site timeseries was disregarded in analysis.

For continuous pH measurements, the instrument accuracy and precision was ± 0.05 pH units, as reported by Sea-Bird. Continuous dissolved oxygen (DO) and temperature measurements had reported accuracies of ± 3 µmol/kg and ± 0.002 ºC, respectively. Unless otherwise stated, error reported throughout the chapter is standard deviation plus the propagated instrument error assuming that each measurement was statistically independent. A pressure to depth conversion was applied using methodology presented in Application Note 69 from Sea-Bird (https://www.seabird.com/application-notes).

To understand spatial variability in South Bay's seawater carbonate system, discrete water samples were collected at 11 sites spaced one kilometer apart across two transects: a north-south transect spanning the distance between the two inlets, and an east-west transect across a seagrass to marsh gradient (Figure 1). Five sites were vegetated with *Zostera marina* and six sites were unvegetated, with two unvegetated sites located in the outflow zone of a New Marsh tidal creek. Discrete samples were collected at transect sites on June 2nd, July 8th, and October 7th of 2022 to capture sites during seagrass growing season, peak seagrass density, and minimum densities post-senescence. Discrete sampling on June 2nd, 2022 was conducted over a 1.75-hour sampling period, from 07:58 to 09:43 local time, during a rising mid-tide. Sampling on July 8th, 2022 took place in two parts: the three bare sites to the west of the seagrass meadow were sampled from 09:28 to 10:00 local time shortly after low tide and the remaining sites were sampled from 12:25 to 13:18, on a rising mid-tide. On October 7, 2022, samples were collected between 10:05 and 10:45 local time on a falling mid-tide. All discrete samples collected in the field were immediately poisoned with a mercuric chloride solution and stored between 2-4 ºC until laboratory analysis of DIC and TA could be conducted. Water samples were collected alongside discrete handheld YSI measurements of temperature and salinity.

DIC concentrations of water samples collected in South Bay were determined using a laser-based Apollo SciTech AS-C3 DIC analyzer connected with a Licor LI-7000 CO_2/H_2O analyzer (Neubauer and Anderson, 2003). Each sample was measured in triplicate. At the beginning of each day of sample processing, Certified Reference Material was used to produce a standard curve. Potential instrument drift was assessed by running Certified Reference Material every 10-15 samples, and corrected for. The total alkalinity of water samples was determined using open-cell potentiometric titration using certified titrant (0.1 M HCl acid in 0.6 M NaCl; A. Dickson laboratory) and an automatic titrator, the Metrohm 855 Robotic Titro. Two replicates per bottle sample were assessed and Certified Reference Material was used to ensure accuracy of titrations. In order to counteract any acidification effects from the addition of mercuric chloride, a correction was applied to attain the final TA values.

The MATLAB package CO2SYS v3.1.1 was used to estimate pH, pCO_2, and aragonite saturation state (ΩAr) with *in situ* temperature, salinity, DIC, and TA (Lewis and Wallace, 1998;

Orr et al. 2018; Van Heuven et al., 2011). The constants used in the CO2SYS estimations were Millero's (2010) K1 and K2 dissociation constants for carbonic acid and bicarbonate, Dickson's (1998) KSO4 dissociation constant, and the KF dissociation constant from Perez and Fraga (1987) (Lewis and Wallace, 1998; Orr et al. 2018; Sharp et al., 2023; Van Heuven et al., 2011).

Statistical tests were performed with respect to an $\alpha = 0.05$. pH data were non-normal according to Shapiro-Wilkes tests for normality and visual inspection of Q-Q plots. As such, distributions were assessed with a Mann-Whitney-U test or a Levene's test for variance.

4.4 Results

4.4.1 Site Characteristics

At the continuously measured vegetated site salinity ranged from 29.35 to 32.02 psu in the June to July deployment. Sharp declines in salinity were seen coinciding with periods of rain in late June (Porter et al., 2023). The bare site was less saline than the vegetated site and experienced more pronounced tidally driven salinity fluctuations. Water height and temperature were similar between the two sites, with a mean water height of 1.3 meters during the June-July deployment (Figure 2). Water temperatures ranged from 20.87 to 30.00º C during the study period, with only one day in early July in which mean daily temperature exceeded the temperature threshold at which seagrasses begin to exhibit thermal stress (28º C) (Berger et al., 2020; Wiberg, 2023). During the study period, sunrise occurred between 05:42-05:50 local time in the morning and sunset was between 20:18-20:28 local time in the evening.

Across the June-July deployment, the mean pH in the vegetated site was 8.12 ± 0.17 (SD) while the mean bare site pH was 7.75 ± 0.11 (SD) (Figure 2). pH was significantly higher at the seagrass site than the bare site during the study period (p-value < 0.001). Both sites exhibited high variability over the course of the deployment, especially on daily time scales. pH variance at the bare site is significantly lower than at the seagrass site (Levene's Test; p-value < 0.001). This is also reflected in the daily range of pH at each site, which was higher in the seagrass meadow and displayed a near-significant difference (p-value = 0.07). The mean daily range of pH at the seagrass site was 0.44 ± 0.14 while the mean daily range of pH in the bare site was 0.39 ± 0.12.

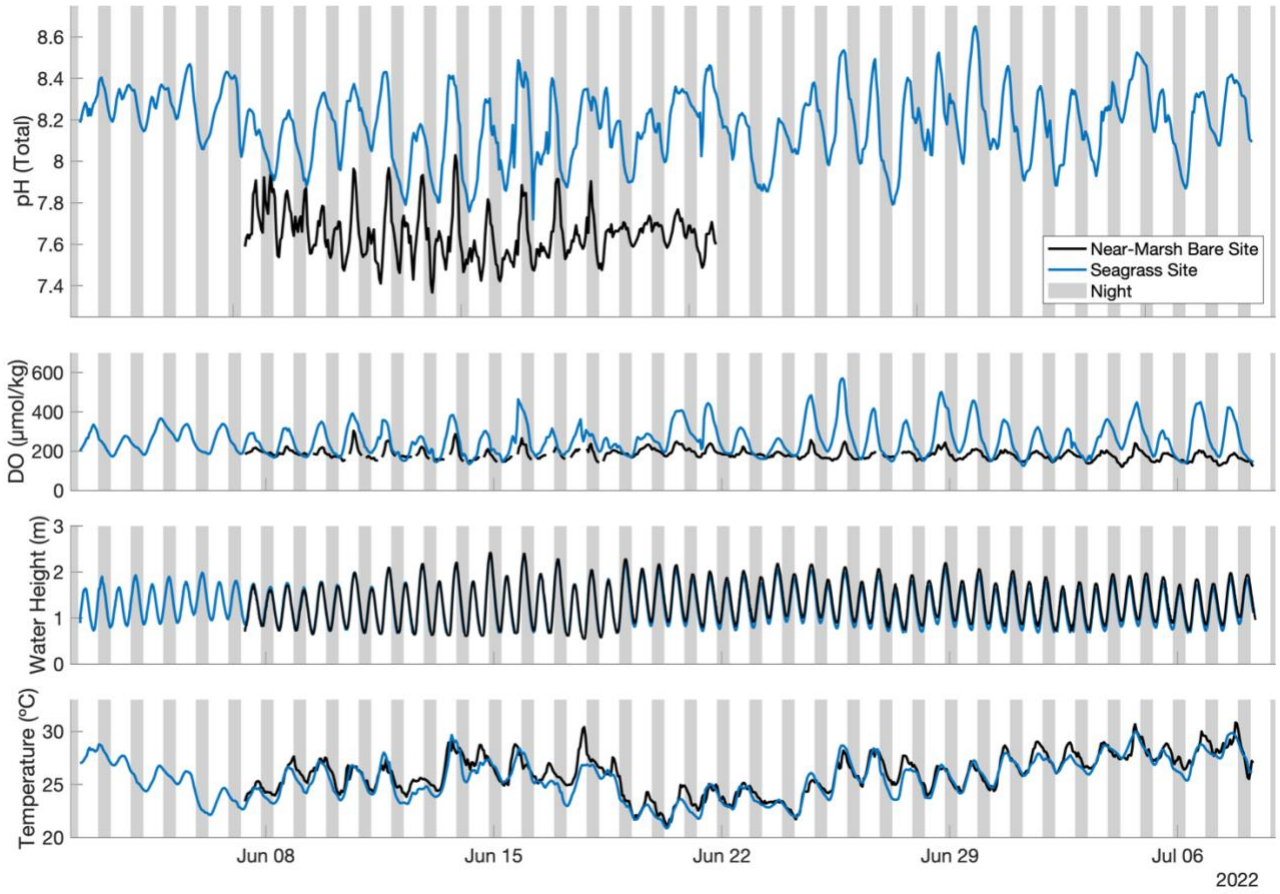

Figure 16: Hourly bins of pH, DO, water height, and temperature at the South Bay seagrass site (blue) and near-marsh bare site (black) from early June to early July, 2022. Grey bars in the background represent the hours between sunset and sunrise.

4.4.2 Diel Variability in pH

In the seagrass meadow, the mean of the pH daily minima was 7.89 ± 0.12 and typically occurred several hours after sunrise, at a mean time of 7.7 ± 1.4 decimal hours (Figure 3). Daily pH minima were preceded by AOU maxima, which occurred at a mean time of 6.2 ± 2.2 decimal hours. The timing of daily pH minima and AOU maxima were significantly different, with pH minima occurring after maximum AOU was reached (p-value = 0.002). Following a morning minimum, pH increased throughout daylight hours until reaching a mean daily maximum of 8.32 ± 0.12 pH units shortly before sunset. Occurring at a mean decimal hour of 17.5 ± 2.3, pH daily maxima coincided with daily AOU minima (p-value = 0.46; difference between times *not* statistically significant).

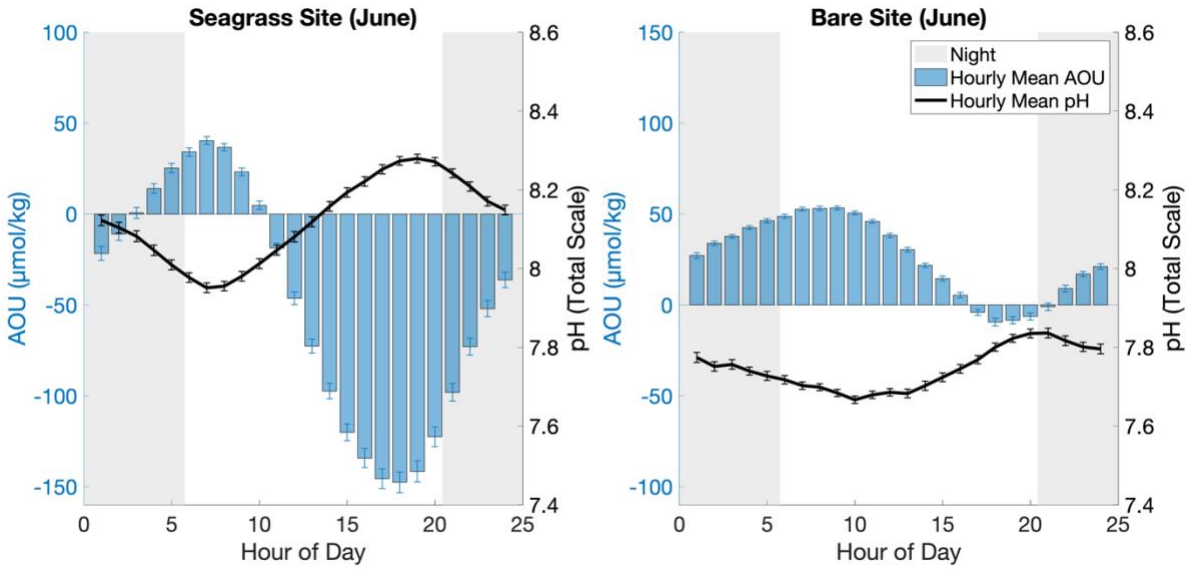

Figure 17: June AOU and pH data binned and averaged by hour of day, with the black line representing the mean 24-hour pattern in pH and blue bars showing the mean hourly AOU at the seagrass site (left) and the near-marsh bare site (right). Error bars represent standard error of the mean plus propagated instrument uncertainty.

Seagrass meadow AOU is negative for 66% of the June deployment, indicating a net autotrophic system during the study period. The mean of AOU daily maxima was 47.25 ± 19.60 µmol/kg while the mean of AOU daily minima was -173.0 ± 83.3 µmol/kg. While AOU typically exhibits daily excursions above zero, there are several instances in which AOU remains negative for over a 24-hour period. On June 5th, June 21st, and July 5th, DO produced during daytime photosynthesis was high enough for the meadow to remain oversaturated with respect to oxygen throughout the night. AOU and pH exhibit a non-linear negative relationship with an R^2 of 0.68 (best fit 4th-degree polynomial), therefore explaining 68% of the variance in seagrass meadow pH (Figure 4).

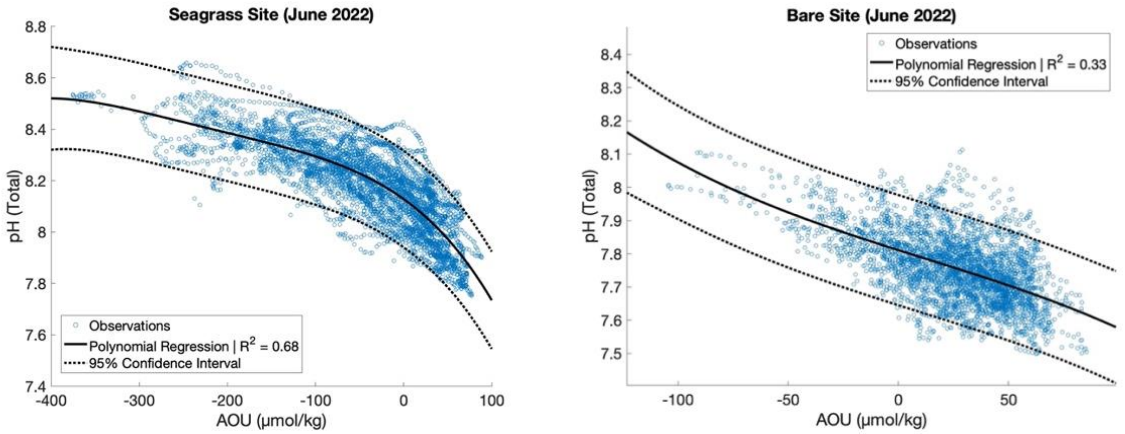

Figure 18: The left panel shows the relationship between AOU and pH at the seagrass site, fitted with a 3rd degree polynomial, which provided the best fit to the data with an R^2 of 0.68. The right panel shows AOU vs. pH at the bare site, fitted with a 3rd degree polynomial with an R^2 value of 0.33.

At the bare site, the mean of the daily pH minima was 7.59 ± 0.08 pH units. Daily pH minima occurred at a mean time of 9.5 ± 4.8 decimal hours during the study period. The mean of daily maximum pH at the bare site was of 7.97 ± 0.08 pH units (Figure 3). Bare site pH daily maxima, which occurred at an average time of 18.5 ± 5.7 decimal hours, did not significantly differ from AOU daily minima times (p-value = 0.47).

The bare site was net heterotrophic during the study period, exhibiting positive AOU for 74% of the deployment. A maximum AOU of 55.7 ± 9.3 µmol/kg occurs several hours after sunrise at an average time of 7.1 ± 2.4 decimal hours, while the mean of daily minimum AOU, -32.8 ± 31.2 µmol/kg, occurs on average at 18.5 ± 2.7 decimal hours. pH negatively correlates with AOU at the bare site, but exhibits a weaker R^2 (0.33) than pH and AOU at the seagrass site (Figure 4).

The timing of the bare site pH daily minima and maxima had higher temporal variability relative to the seagrass site, with standard deviations ranging from 4.8 to 5.7 hours. In addition to this, bare site pH often exhibited twice-daily minima and maxima corresponding to both tidal and diel cycles. Comparatively, the seagrass meadow only exhibited once-daily maxima and minima. To understand tidal drivers of pH daily variability in the bare site, data are binned by tidal stage. Here, high tide and low tide are defined temporally as the time of water height local

maxima (or minima) ± 1 hour. Bare site pH is significantly higher at high tide than at low tide, with a mean high tide pH of 7.81 ± 0.11 and a mean low tide pH of 7.68 ± 0.09 (p-value < 0.001). Additionally, mean AOU at high tide is significantly lower than AOU at low tide, with respective means of 16.1 ± 34.0 and 31.8 ± 24.6 µmol/kg (p-value < 0.001). At high tide, bare site pH and AOU exhibit a stronger negative correlation (R^2 = 0.47) than at low tide (R^2 = 0.27). In contrast, there is not a significant difference between pH at high and low tide at the seagrass site (p-value = 0.09). The same is true for AOU (p-value = 0.92). At the seagrass site, pH and AOU exhibit stronger negative correlations than at the bare site, with the R^2 at low tide (R^2 = 0.66) exceeding that at high tide (R^2 = 0.56).

4.4.3 Diel water column pH variations

To understand finer details regarding the diel relationship of pH with water height and AOU, data were binned by hour of day. In the seagrass site, hourly binning of pH data reveals AOU and to a lesser extent, water height, are key predictors of pH (Figure 5). When assessed across 24 hour-of-day bins, pH regressed on AOU is better correlated than pH regressed on water height in the seagrass site (p-value < 0.001) (Appendix 1). Much like the deployment-wide relationship (Figure 4), AOU and pH exhibit a negative, non-linear correlations across each hour of day (mean R^2 = 0.59). In contrast, the R^2 for the relationship between pH and water height is consistently low in each hour of day (mean R^2 = 0.09). The curvature and sign of the polynomial fit for pH and water height change hourly over the mean 24-hour period, experiencing transitions from a positive to negative relationship after sunrise (hour 6-7), in the mid-afternoon (hour 15-16), and after sunset (hour 21-22).

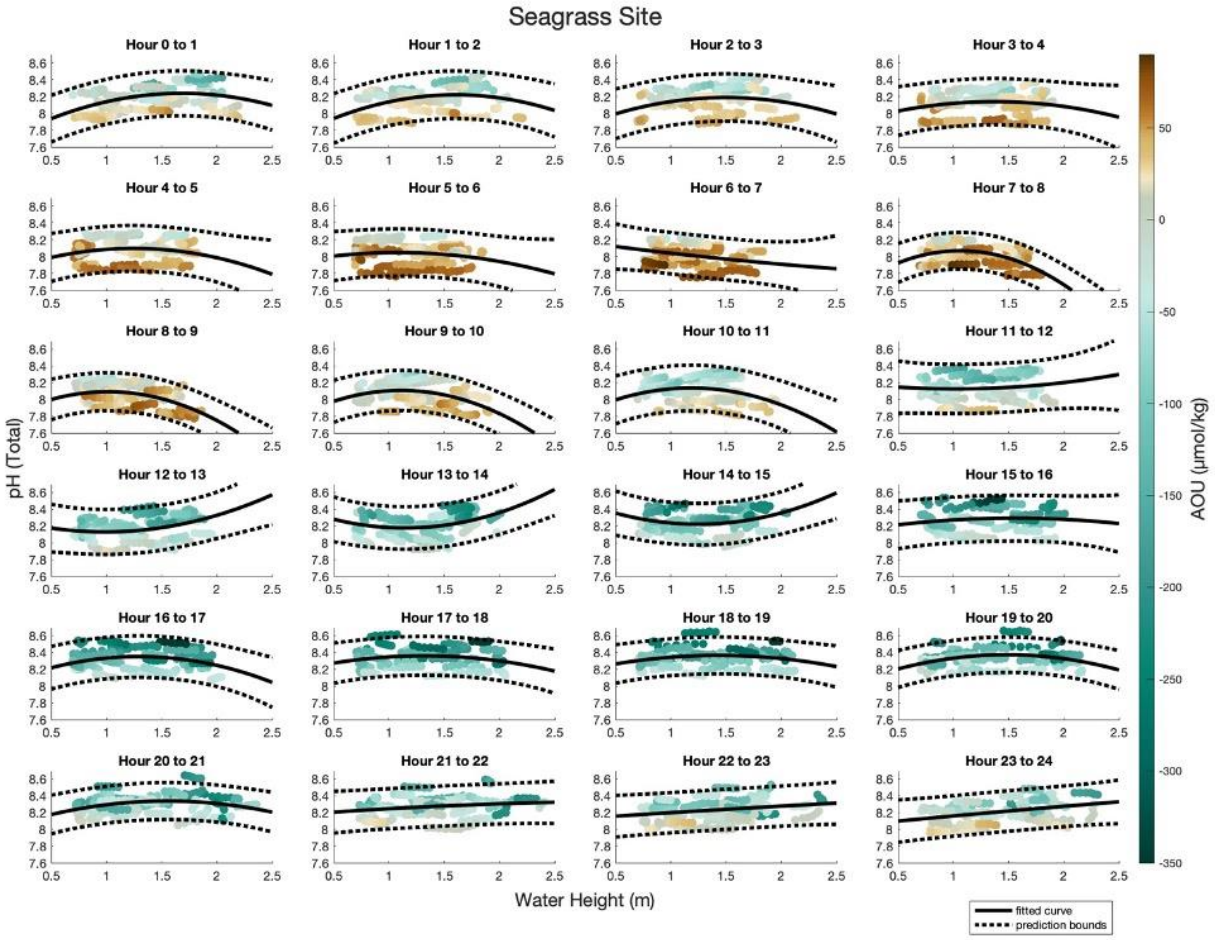

Figure 19: Hourly bins of water height vs pH in the seagrass meadow, fitted with 3rd degree polynomial curves and colored by AOU.

At the bare site, hourly bins of water height exhibit a stronger correlation with pH than AOU does with pH (p-value = 0.005). AOU is negatively correlated with pH across all time bins (mean $R^2 = 0.29$). When comparing pH AOU regressions between seagrass and bare sites, significantly less variance in pH is explained by AOU in the bare site (p-value < 0.001). Across most hours, there is a positive correlation between pH and water height at the bare site (mean $R^2 = 0.37$) (Figure 6). The strength of the relationship between pH and water height varies throughout the day. The weakest correlations occur in the morning between hours 7-10, when R^2 dip below 0.2. The highest R^2 values are above 0.5, and occur at hours 1-2, 13-14, and 21-22.

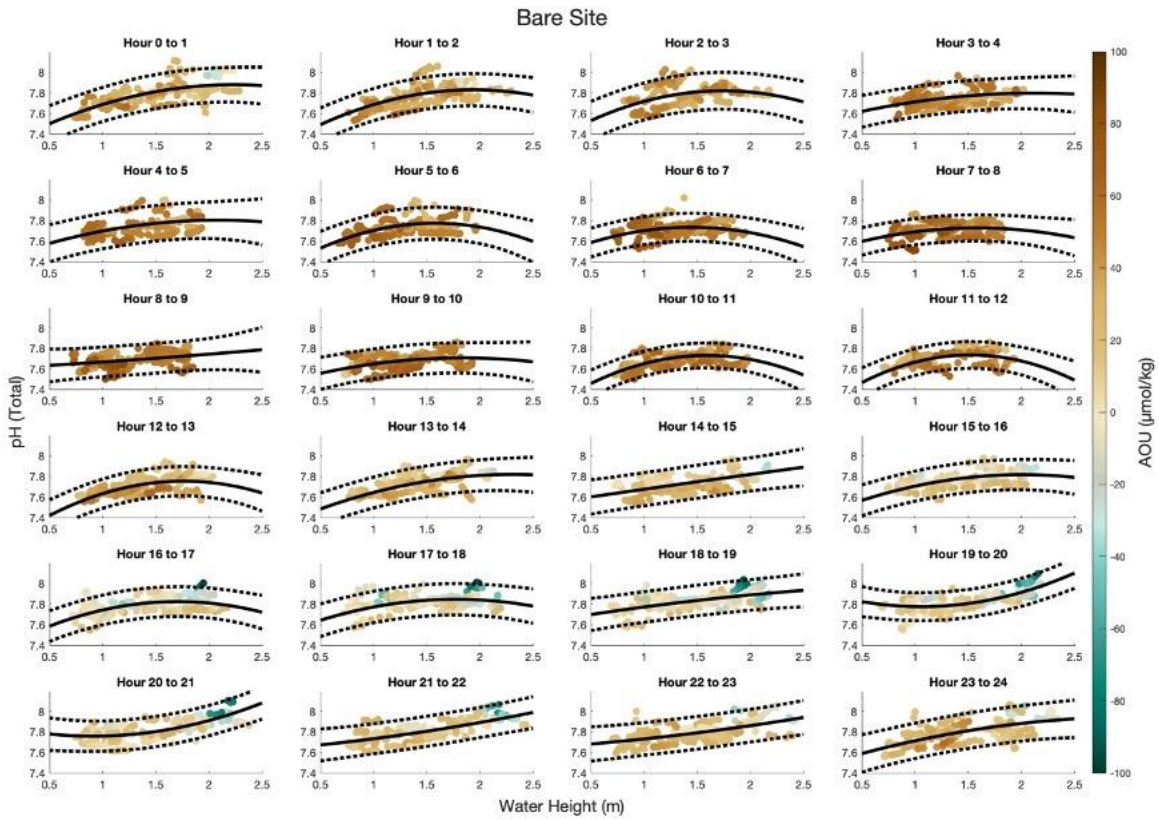

Figure 20: Hourly bins of water height vs pH at the near marsh bare site, fitted with 3rd degree polynomial curves and colored by AOU.

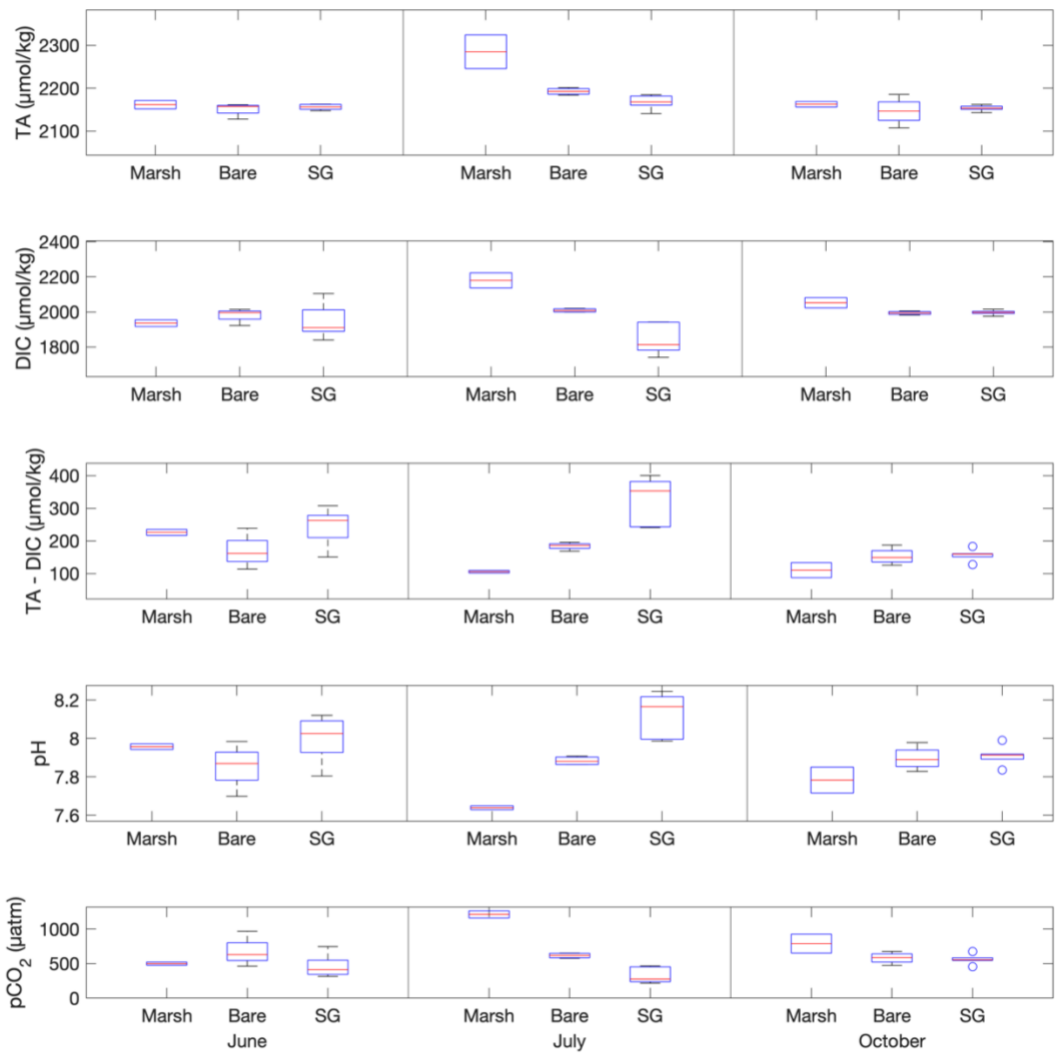

Figure 7: Boxplots summarizing discrete samples collected in near-marsh bare sites (n= 2), bare sites (n= 4), and seagrass sites (SG, n = 5), in June, July, and October of 2022. From top to bottom, plots show measured Total Alkalinity (µmol/kg), measured DIC (µmol/kg), computed pH, and computed pCO_2 (µatm).

4.4.4 Spatial Carbonate System Patterns: Discrete Sampling

Discrete sampling conducted at 11 sites across South Bay revealed seasonal and spatial patterns in water column carbonate chemistry across seagrass vegetated sites, bare sites, and near-marsh bare sites (Figure 7). Although sampling typically took place within a 1-2 hour period to minimize temporally driven differences in pH, some of the observed spatial variability is likely a result of differences in sampling time and aliasing of diel and tidal variability. Mean June DIC among the seagrass sites was 1944.3 ± 96.9 µmol/kg, with 4 of the 5 sites exhibiting a

depletion of DIC relative to the expected DIC conservative mixing line for the coastal-groundwater end members (LaRoche, 2024) (Figure 8). Mean TA minus DIC concentrations (TA–DIC), an approximate measure of seawater carbonate ion concentration, in the near marsh bare sites and typical bare sites are 226.1 ± 13.2 µmol/kg and 169.0 ± 51.7 µmol/kg, respectively. Driven by the low DIC observed in the seagrass meadows, TA–DIC means are slightly higher at 243.9 ± 58.8 µmol/kg. pH follows a similar pattern with seagrass means of 8.0 ± 0.12 compared to bare site means of 7.86 ± 0.12 and 7.96 ± 0.02 (near-marsh bare).

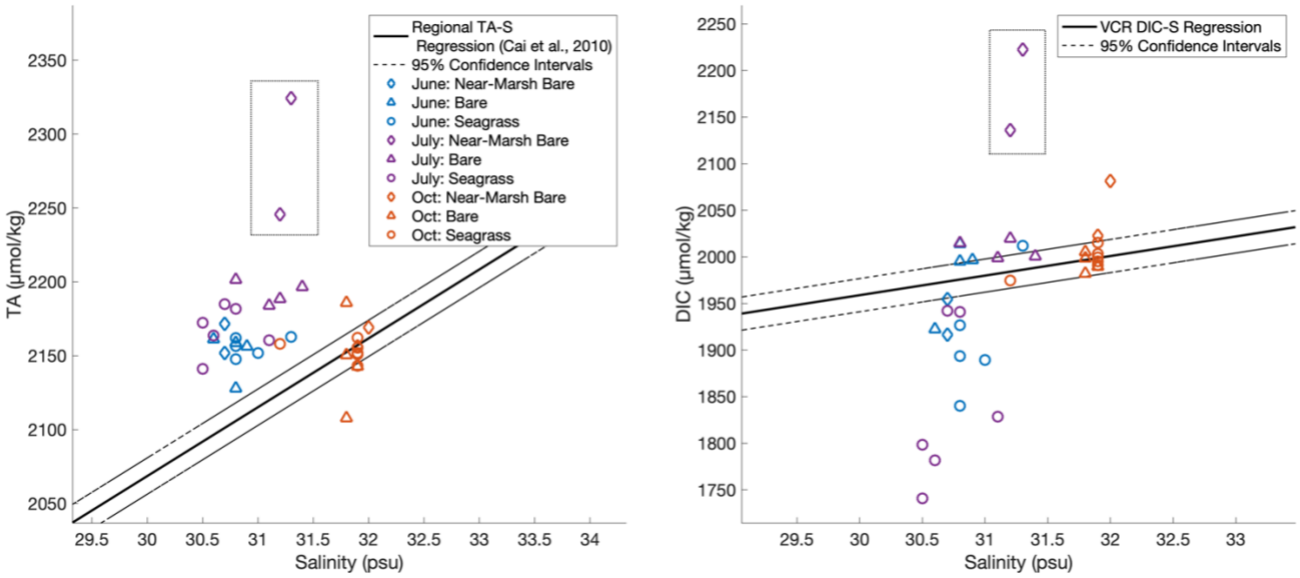

Figure 8: In the left panel, the linear regression representing the conservative mixing relationship between total alkalinity (µmol/kg) and salinity (psu) for the Mid-Atlantic Bight (Cai et al., 2010) is plotted alongside discrete measurements in South Bay, Virginia Coast Reserve. In the right panel, the DIC-S conservative mixing linear regression as defined in Chapter 3 of this dissertation (LaRoche, 2024) is plotted with South Bay discrete sampling data. Discrete samples collected in near-marsh bare sites (diamond), bare sites (triangle), and seagrass sites (circle), in June (blue), July (purple), and October (orange) of 2022. All samples were collected at mid-tide, with the exception of 2 near-marsh bare site samples (called out in dotted box) and one bare site.

South Bay exhibits the largest spatial variability in pH in July (Figure 9), with high pH observed in the seagrass meadow interior and the lowest pH observed in the two near-marsh bare sites. This is in part due to differences in sampling time; the three bare sites west of the seagrass meadow were sampled ~3 hours closer to sunrise and low tide than the other discrete samples, coinciding with a period typically characterized by very low pH in the continuously sampled near-marsh bare site. Because of this, the difference in pH between those sites and the other

vegetated and inlet-adjacent bare sites is temporally mismatched. Seagrass sites in July were consistently below the DIC-S conservative mixing line (Figure 8), with a mean DIC concentration of 1838.8 ± 84.5 µmol/kg.

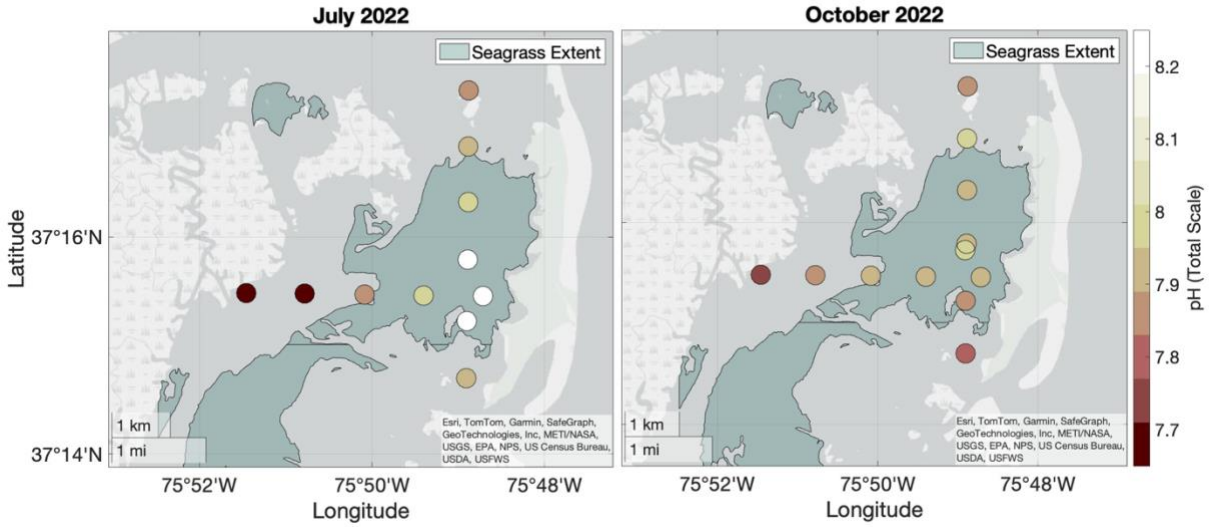

Figure 9: Map of South Bay discrete sampling sites, with circle colors representing pH in July (left) and October (right).

The seagrass sites also exhibit the lowest observed values of TA and DIC (Figure 12) but maintain the highest TA–DIC among South Bay sites, with a mean TA–DIC concentration of 328.6 ± 70.8 µmol//kg (Figure 10). The pH in the bare sites north and south of the seagrass meadows and close to ocean inlets (Figure 9) is lower than in the seagrass sites, with an average of 7.88 ± 0.02 compared to 8.13 ± 0.11. With sample collection occurring shortly after low tide, the two near-marsh bare sites exhibit the highest values of TA and DIC observed in this study. Measured DIC and TA values far exceed values predicted by conservative mixing (Figure 10), with a mean DIC of 2179.2 ± 41.6 µmol//kg and mean TA of 2162.7 ± 9.1 µmol//kg. Despite high TA and DIC concentrations, TA–DIC is lower than other sites in July at 105.8 ± 5.6 µmol/kg (Figure 8).

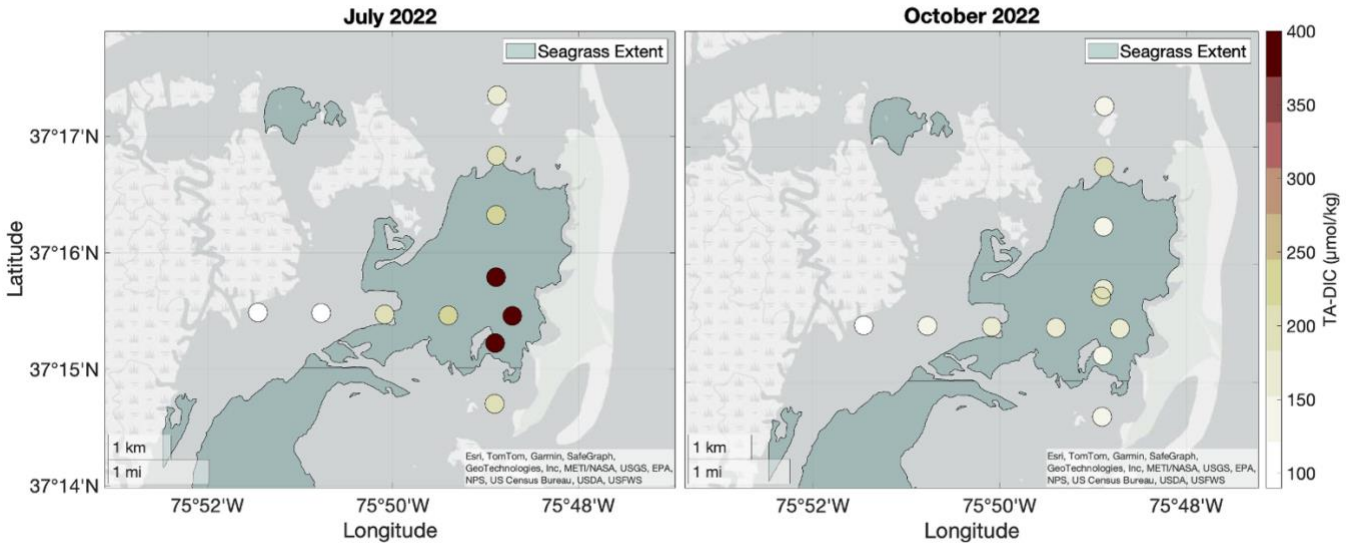

Figure 10: Map of South Bay discrete sampling sites, with circle colors representing TA – DIC (µmol/kg) in July (left) and October (right).

In October, after seagrasses have senesced, seawater carbonate system parameters in bare sites and seagrass sites exhibit similar values, while near-marsh bare sites remain elevated in DIC and pCO_2. Of all the discrete sampling months, the October samples had the best agreement with the DIC-S and TA-S conservative mixing lines (Figure 10). Among seagrass meadow sites, this is a departure from previous months, in which June and July TA was higher and DIC was typically lower than values predicted by the conservative mixing line. In the seagrass meadow, mean TA–DIC concentrations were 157.2 ± 17.9 µmol/kg and mean pH was 7.91 ± 0.05 (Figures 11 and 12). Both TA–DIC and pH were lower and less variable in October than in the previous two sampling months. An exception to the October data's general alignment with conservative mixing lines was the two near-marsh bare sites which, with a mean concentration of 2052.0 ± 41.6 µmol/kg, were in excess of DIC predicted by the conservative mixing line. Overall, October near-marsh sites had lower pH and TA–DIC and higher DIC and pCO_2 when compared to all other sites.

4.5 Discussion

4.5.1 Seagrass Meadow pH: Regulated by Net Ecosystem Metabolism

Factors aligning with net ecosystem metabolism, including time of day and AOU, are the best predictors of water column pH in the South Bay seagrass meadow during the study period. Across all data points, AOU accounts for 68% of the variability in seagrass water column pH. A diel pattern emerges in which pH minima typically occur after sunrise and pH maxima occur around sunset. During the day, photosynthesis consumes dissolved inorganic carbon and produces oxygen, driving down H^+ ion concentrations. As a primarily autotrophic system during the June-July study period, the majority of the day has negative AOU, wherein the effects of community photosynthesis exceed aerobic respiration. After sunset, when photosynthetically active radiation drops to zero, seagrass photosynthesis stops but respiration continues overnight, resulting in a buildup in the water column of CO_2 and H^+ ions and a reduction in seawater pH.

The strong relationship between seawater pH and AOU in the South Bay seagrass meadow align with findings of previous studies which report indicators of net ecosystem metabolism as key predictors of seagrass meadow pH (Lowe et al., 2019; Hendriks et al., 2014). Studies have found positive correlations between pH and daylength, light availability, leaf area index, and shoot density, all of which are drivers or indicators of seagrass metabolism (Hendriks et al., 2014). Factors that augment photosynthesis will increase seagrass uptake of CO_2, leading to a local increase in pH. Alternatively, increases in respiration within a seagrass meadow reduce local pH.

During most days of the study period, water column pH continued to decline for several hours after sunrise. Later pH minima occur due to a continued imbalance of respiration and photosynthesis that persists past sunrise. At both sites, AOU typically continues to increase after sunrise (occurring at hour 5.7) before reaching a maximum at a mean time of 6.2 ± 2.2 decimal hours in the seagrass site and 7.1 ± 2.4 decimal hours in the bare site. Daily pH minima follow AOU maxima in both the seagrass meadow and the bare site, and are offset from maximum AOU by an average of 1.7 ± 2.2 hours and 1.8 ± 4.2 hours, respectively. The offset between peak AOU and sunrise is likely a reflection of fluctuating respiration rates throughout the day. In the

South Bay seagrass meadow, declining respiration rates have been observed in conjunction with decreasing oxygen availability overnight (Juska and Berg, 2022). After sunrise, increased oxygen availability from photosynthesis boosts respiration rates (Juska and Berg, 2022). The continued increase in AOU and decrease in pH for several hours after sunrise are in agreement with accelerated rates of respiration outpacing photosynthetic oxygen production in the early morning. The daily lag observed between peak AOU and minimum pH indicates the contribution of drivers besides aerobic net ecosystem metabolism. Denitrification occurring in seagrass meadow sediments is a potential contributor to pH dynamics that would be decoupled with AOU. As enhanced denitrification rates have been observed in South Bay's seagrass meadows (Aoki and McGlathery, 2018), denitrification is a potential contributor to pH diel patterns that would be decoupled with AOU.

Previous work in *Zostera marina* seagrass meadows has documented negative relationships between ΔpH (here, ΔpH = seagrass – source water) and water height and RMS velocity, two indicators of flushing rates in the seagrass system (Ricart et al., 2021). Water velocity in the South Bay seagrass meadow is lowest at high and low slack tides, resulting in decreased flushing (Carr et al., 2016). Depending on the time of day and the current balance of photosynthesis and respiration, this could result in increases or decreases in pH.

Water height and tidal stage can be indicators of several mechanisms that have varying effects on seawater carbonate chemistry: 1) dilution, 2) residence time, and 3) lateral transport. Low dilution at low tide increases water column signals from local biogeochemical processes while high dilution at high tide can dilute water column signals and decrease the difference in seawater pH between the local and source waters. For example, when low water height coincides with periods of high respiration, respiratory products are more concentrated in the water column, resulting in lower pH values. Increased residence time, too, serves to enhance water column signals in seawater carbonate chemistry while increased flushing rates would dampen local signals. Rising and falling tides also introduce water from external sources via lateral transport that bring with them their own unique biogeochemical makeup.

At the seagrass site, water height serves primarily as an indicator of residence time and dilution. While water height explains some variation in water column pH (2-26%), the relationship is non-linear and highly variable over an average 24-hour day both in strength and sign. Overnight, there is a positive relationship between pH and water height. This transitions to a negative relationship after sunrise wherein lower water heights correspond with higher pH. Lower pH produced by respiration occurring overnight is modified by water height, where higher water produces greater dilution of existing conditions. These observations of time-dependent pH tidal fluctuations align with previous work in seagrass meadows (Cyronak et al., 2018). In addition to the dilution mechanism, tidal fluctuations may also impact seagrass meadow pH via mixing with source/ inlet water. In this particular study, source water pH was not measured continuously so we are unable to estimate the impact of source water mixing directly. However, discrete samples collected north of the meadow near the inlet exhibited lower pH than the seagrass meadow during daytime sampling, providing some context for source water values.

4.5.2 Seagrass Meadow pH: Spatial and Seasonal Variability

Across discrete sampling efforts, the highest water column pH values were observed within the seagrass meadow during the early July sampling effort, coinciding with peak seagrass density in the VCR. Ranging from 8.0 to 8.25 pH units, July pH was not uniform across the five sampling sites within the seagrass meadow (Figure 8). This pH range is in approximate agreement with the highest spatial range of pH observed in a *Z. marina* meadow in Mission Bay, San Diego, California (Cyronak et al., 2018). Seawater carbonate system spatial variability within the seagrass meadow as seen in July can be the result of several mechanisms, including variability in net ecosystem metabolism and hydrodynamic setting. First, spatial variability in net ecosystem metabolism can drive impacts on DIC, TA, and pCO_2, and subsequently pH. On short time scales, previous work in South Bay showed heightened primary production under high light availability and current flow (Rheuban et al., 2014b). Even subtle differences in environmental conditions like water clarity, light availability, current velocity, shoot density, and more can lead to local variation in gross primary productivity (Hendriks et al., 2014). Spatial variation in respiration, calcification, and benthic biogeochemical processes can also impact spatial heterogeneity of water column pH within the seagrass meadow.

Second, differences in residence time and depth among seagrass sites can impart variability in the longevity of water column metabolic signals (Cyronak et al., 2018). The central seagrass meadow is shallower compared to the outer seagrass meadow. As lower water height and longer residence times serve to amplify metabolic signals, the shallow central site may experience a wider daily range of pH, including higher daytime pH than deeper sites. Discrete samples collected in July demonstrate that pH is higher in the central seagrass meadow relative to other meadow sites, but it is possible that this does not represent a constant pH elevation in the central meadow. Higher residence time and lower water height in the central meadow may confer greater variability to pH in the central meadow, with daytime pH exceeding edge meadow sites but nighttime pH falling below edge sites.

Typically, by October, rates of primary production and respiration in the South Bay seagrass meadow have declined from summertime maxima (Berger et al., 2020). A decline in primary production would align with the lower daytime water column pH observed across the seagrass meadow in October. After seagrass senescence, hydrodynamic regimes in seagrass meadows shift as well, resulting in higher current velocities coinciding with lower seagrass densities and shoot lengths (Zhu et al., 2021). However, even seagrass at minimal heights can impart velocity reductions in the seagrass meadow (Zhu et al., 2021). In winter, the seagrass meadow in South Bay continues to reduce water velocity by 40% relative to nearby bare sites (compare to 60% in summer) (Hansen and Reidenbach, 2013). The continuation of velocity reduction in seagrass meadows after senescence poses a question of whether temperate seagrass meadows retain elevated water column pH year-round relative to source waters, or if increased residence times result in reduced geographic pH differences after senescence. In future, more work could be done to discern how the timing of seasonal shifts in residence time and net ecosystem metabolism interact to effect seagrass meadow seawater carbonate system dynamics.

4.5.3 Near-marsh bare site: lateral mixing

Coupling of water column pH signals and tidal stage at the continuous near marsh bare site suggest the influence of lateral exchange from nearby marshes, inlets, and other nearby systems. Water column pH exhibits a higher correlation with water height than AOU, with low water height at any given hour of day consistently coinciding with low pH and high water height

corresponding with relatively higher pH. Bare site conditions varied with tidal stage, showing lower pH and higher AOU at low tide (± 1 hour) than high tide (± 1 hour) (p-value < 0.001) while also exhibiting a weaker correlation between pH and AOU at low tide. In conjunction, these low tide conditions suggest that biogeochemical signals from marsh exports are a key contributor to water column pH for a bare site that was marsh adjacent; note that other bare sites away from marshes and closer to ocean inlets may not follow the same pattern.

Marsh exports of DIC and TA are known to peak at low tide, resulting in delivery of low pH, high DIC water to adjacent systems via lateral tidal flow (Tamborski et al., 2021; Wang et al., 2016). According to July discrete samples collected at the bare near-marsh sites near low tide, DIC and TA were in excess of expected values for conservative mixing of coastal-groundwater end members alone, indicating the potential for TA and DIC added via local biogeochemical pathways. The continuously sampled bare site exhibits fluctuating correlation strength between pH and AOU, with overall lower R^2 values than seen for the same relationship in the seagrass site. As AOU only captures aerobic metabolism, anaerobic respiration may also contribute to heightened DIC and TA, as well as decreased pH signals with low correlation to AOU. High TA values indicate the occurrence of biogeochemical processes that are acting as sources of alkalinity, which include denitrification or other anaerobic pathways. Previous work has estimated denitrification rates in South Bay mudflats, and denitrification was found to be minimal compared to rates occurring in nearby seagrass meadows (Aoki and McGlathery, 2018). Limited contributions from local denitrification would indicate signals of anaerobic activity are likely being imported from marshes, which are hotspots of anaerobic activity (Martínez-Espinosa et al., 2021). This, paired with the stark differences observed between near marsh bare sites and other bare sites, suggests that the difference in seawater carbonate chemistry observed near the marshes is indeed a signal of additional marsh-related TA and DIC loading. Despite having higher alkalinity concentrations than sites without marsh influence, alkalinity levels in near-marsh bare sites are not sufficiently high to counteract the DIC export from marshes, leading to low TA–DIC values in the July low tide sampling.

Around high tide, conditions in the continuous near marsh bare site become less acidic and exhibit lower AOU, likely as the result of tidal flushing enriching the system with more

oxygenated, higher pH source water. In this case, the source water entering the bare site on a rising tide is likely coming from the ocean inlets via the nearby channel. While lateral transport of water from the nearby seagrass meadows is possible during a rising tide, the high residence time in the seagrass meadow and the dominant flow direction in South Bay would dictate delivery of water to the bare site is primarily coming directly from the channel and inlet, rather than transiting through the seagrass meadow.

Overall, the observed relationships of pH with water height, AOU, and low/high tide suggest that lateral transport of water masses with divergent seawater carbonate system characteristics is a key control on the near-marsh bare site pH dynamics, with low tide bringing in more acidic water from the nearby marsh, and high tide bringing in high pH water from other nearby systems. However, any changes in pH and AOU at the bare site derived from lateral transport of aerobic biogeochemical signals may also be subject to transformation during transit.

In July and October discrete sampling, a gradient of low to high pH along the west-east transect between the marsh and the seagrass meadow suggests DIC is being exported from marshes. Other studies have documented heightened DIC export from marshes occurring in seasons of high productivity (Schiebel et al., 2019; Wang and Cai, 2004). In the Southeastern U.S., exports of marsh DIC are highest in the summer and fall and lowest in the spring (Wang and Cai, 2004). Fall inorganic carbon export from marshes is dominated by organic matter decomposition occurring in sediments, and lateral transport is mediated by vertical supply fluxes within the marsh by pore water drainage (Schiebel et al., 2019). We observe a similar seasonal pattern in the near-marsh sites in this study in which DIC and pCO_2 in October exhibit continued elevation relative to seagrass and bare sites without marsh influence. DIC and pCO_2 peak in the July sampling, coinciding with a low tide, and are lower in October, sampled on a falling mid-tide. The difference between sampling months likely lies, at least in part, in the difference in tidal stage.

4.5.4 Further Potential Impacts of Residence Time

Depth measurements between the two sites with continuous measurements show that they experience nearly identical water height and timing of tides throughout the deployment period.

However, there are likely differences in residence time and flushing between the two sites. There are twice daily fluctuations in salinity and pH at the near marsh bare site, the timing of which are in alignment with semidiurnal tides. In contrast, the seagrass meadow exhibits salinity and pH patterns that do not have pronounced semidiurnal fluctuations. The seagrass site sees greater change to pH on diurnal rather than semidiurnal time scales. Flow attenuation from seagrass shoots increases water residence time in the seagrass site, allowing for greater buildup of locally generated biogeochemical signals. Unlike the seagrass meadow, the near-marsh bare site has little in the way of flow attenuation, with lower residence time and more frequent flushing. This is reflected in the more pronounced semidiurnal fluctuations in pH and salinity. Because of the lower residence time, any locally generated biogeochemical signals are more likely to be transported out of the bare site, allowing for the import of external signals at high and low tide.

4.6 Conclusion

In the nearshore marine environment, spatial coupling of diverse ecosystems yields substantial spatial and temporal heterogeneity in seawater carbonate chemistry. Across a marsh-lagoon-seagrass ecotone, we observed high temporal pH variability over short time scales (diel, tidal) in the water column over both a seagrass vegetated site and unvegetated near marsh site. While seawater pH at both locations varies on diel and tidal time scales, seagrass site pH is primarily controlled by local metabolism, exhibiting large diel fluctuations and high negative correlation with AOU. This chapter only characterizes seawater pH conditions during the seagrass growing season up to around peak shoot density, but further exploration of pH patterns in temperate seagrass meadows during different stages of seagrass growth, including after peak density and post-senescence, would fill in key knowledge gaps about seasonal transitions in temperate meadows. The near marsh bare site experienced semidiurnal swings in pH mirroring local tidal cycles, wherein DIC and TA exports from the nearby marsh at low tide result in periods of low pH and flushing at high tide results in periods of relatively high pH. Studying seawater carbonate chemistry across multiple diverse ecosystems at a larger, bay-wide scale (i.e., marsh-lagoon-seagrass ecotone), rather than at an individual ecosystem scale (i.e., within the seagrass meadow alone) can provide greater context to the range of conditions present across an embayment and the critical influence of lateral transport. Integration of seawater pH variability across adjacent ecosystems can help to improve our understanding of highly variable nearshore

coastal systems, like seagrass meadows, salt marshes, and lagoons, and resolve uncertainties regarding the carbon cycle connectivity between these evolving systems (Smith et al., 2024).

4.7 Appendix

Table 15: Binned by hour of day, the R^2 of 3rd degree polynomial relationships between pH regressed on water height and pH regressed on AOU in the continuous near marsh bare site and the continuous seagrass site.

Hour of Day	Bare Site		Seagrass Site	
	R^2: Water Height vs pH	R^2: AOU vs. pH	R^2: Water Height vs pH	R^2: AOU vs. pH
1	0.54	0.34	0.18	0.70
2	0.50	0.19	0.13	0.67
3	0.35	0.05	0.06	0.59
4	0.26	0.10	0.02	0.56
5	0.30	0.30	0.02	0.59
6	0.33	0.29	0.02	0.61
7	0.19	0.30	0.11	0.60
8	0.17	0.36	0.26	0.50
9	0.11	0.23	0.24	0.52
10	0.17	0.26	0.15	0.58
11	0.40	0.18	0.06	0.63
12	0.32	0.13	0.01	0.65
13	0.50	0.39	0.11	0.56
14	0.53	0.29	0.11	0.56
15	0.38	0.41	0.06	0.66
16	0.46	0.27	0.01	0.70
17	0.41	0.28	0.05	0.67
18	0.29	0.44	0.03	0.54
19	0.34	0.32	0.03	0.55
20	0.48	0.43	0.07	0.52
21	0.51	0.40	0.06	0.49
22	0.51	0.33	0.05	0.58
23	0.37	0.31	0.07	0.60
24	0.44	0.27	0.14	0.64

4.8 References

Aoki, L. R., and McGlathery, K. J. (2018). Restoration enhances denitrification and DNRA in subsurface sediments of Zostera marina seagrass meadows. *Marine Ecology Progress Series*, *602*, 87-102.

Barbier, E. B., Hacker, S. D., Kennedy, C., Koch, E. W., Stier, A. C., and Silliman, B. R. (2011). The value of estuarine and coastal ecosystem services. *Ecological monographs*, *81*(2), 169-193.

Berg, P., Delgard, M. L., Polsenaere, P., McGlathery, K. J., Doney, S. C., and Berger, A. C. (2019). Dynamics of benthic metabolism, O2, and pCO2 in a temperate seagrass meadow. *Limnology and Oceanography*, *64*(6), 2586-2604.

Berger, A. C., Berg, P., McGlathery, K. J., and Delgard, M. L. (2020). Long-term trends and resilience of seagrass metabolism: A decadal aquatic eddy covariance study. *Limnology and Oceanography*, *65*(7), 1423-1438.

Borges, A. V., and Gypens, N. (2010). Carbonate chemistry in the coastal zone responds more strongly to eutrophication than ocean acidification. *Limnology and Oceanography*, *55*(1), 346-353.

Bresnahan Jr, P. J., Martz, T. R., Takeshita, Y., Johnson, K. S., and LaShomb, M. (2014). Best practices for autonomous measurement of seawater pH with the Honeywell Durafet. *Methods in Oceanography*, *9*, 44-60.

Buapet, P., L. M. Rasmusson, M. Gullström, and M. Björk. 2013. Photorespiration and carbon limitation determine productivity in temperate seagrasses. *PLoS One* **8**: e83804. doi:10.1371/journal.pone.0083804

Cai, W. J., Hu, X., Huang, W. J., Jiang, L. Q., Wang, Y., Peng, T. H., and Zhang, X. (2010). Alkalinity distribution in the western North Atlantic Ocean margins. *Journal of Geophysical Research: Oceans*, *115*(C8).

Cai, W. J., Hu, X., Huang, W. J., Murrell, M. C., Lehrter, J. C., Lohrenz, S. E., ... and Gong, G. C. (2011). Acidification of subsurface coastal waters enhanced by eutrophication. *Nature geoscience*, *4*(11), 766-770.

Carr, J. A., D'Odorico, P., McGlathery, K. J., and Wiberg, P. L. (2016). Spatially explicit feedbacks between seagrass meadow structure, sediment and light: Habitat suitability for seagrass growth. *Advances in Water Resources*, *93*, 315-325.

Cyronak, T., Andersson, A. J., D'Angelo, S., Bresnahan, P., Davidson, C., Griffin, A., ... and White, M. (2018). Short-term spatial and temporal carbonate chemistry variability in two contrasting seagrass meadows: implications for pH buffering capacities. *Estuaries and Coasts*, *41*, 1282-1296.

Dickson, A. G., Sabine, C. L., and Christian, J. R. (2007). *Guide to best practices for ocean CO2 measurements*. North Pacific Marine Science Organization.

Doney, S. C., Busch, D. S., Cooley, S. R., & Kroeker, K. J. (2020). The impacts of ocean acidification on marine ecosystems and reliant human communities. *Annual Review of Environment and Resources*, *45*, 83-112.

Feely, R. A., Alin, S. R., Newton, J., Sabine, C. L., Warner, M., Devol, A., ... & Maloy, C. (2010). The combined effects of ocean acidification, mixing, and respiration on pH and carbonate saturation in an urbanized estuary. *Estuarine, Coastal and Shelf Science*, *88*(4), 442-449.

Fourqurean, J. W., Duarte, C. M., Kennedy, H., Marbà, N., Holmer, M., Mateo, M. A., ... and Serrano, O. (2012). Seagrass ecosystems as a globally significant carbon stock. *Nature geoscience*, *5*(7), 505-509.

Gambi, M., Nowell, A., and Jumars, P. (1990). Flume observations on flow dynamics in Zostera marina (eelgrass) beds. *Marine Ecology Progress Series*, **61**, 159–169. https://doi.org/10.3354/meps061159

Gattuso, J. P., Frankignoulle, M., and Smith, S. V. (1999). Measurement of community metabolism and significance in the coral reef CO2 source-sink debate. *Proceedings of the National Academy of Sciences*, *96*(23), 13017-13022.

Gattuso, J. P., Magnan, A., Billé, R., Cheung, W. W., Howes, E. L., Joos, F., ... and Turley, C. (2015). Contrasting futures for ocean and society from different anthropogenic CO2 emissions scenarios. *Science*, *349*(6243), aac4722.

Groner, M. L., Burge, C. A., Cox, R., Rivlin, N. D., Turner, M., Van Alstyne, K. L., ... & Friedman, C. S. (2018). Oysters and eelgrass: potential partners in a high pCO 2 ocean. *Ecology*, *99*(8), 1802-1814.

Gruber, N., Bakker, D. C., DeVries, T., Gregor, L., Hauck, J., Landschützer, P., ... and Müller, J. D. (2023). Trends and variability in the ocean carbon sink. *Nature Reviews Earth and Environment*, *4*(2), 119-134.

Hansen, J. C., and Reidenbach, M. A. (2013). Seasonal growth and senescence of a Zostera marina seagrass meadow alters wave-dominated flow and sediment suspension within a coastal bay. *Estuaries and coasts*, *36*, 1099-1114.

Hendriks, I. E., Olsen, Y. S., Ramajo, L., Basso, L., Steckbauer, A., Moore, T. S., ... and Duarte, C. M. (2014). Photosynthetic activity buffers ocean acidification in seagrass meadows. *Biogeosciences*, *11*(2), 333-346.

Herrmann, M., Najjar, R. G., Kemp, W. M., Alexander, R. B., Boyer, E. W., Cai, W. J., ... and Smith, R. A. (2015). Net ecosystem production and organic carbon balance of US East Coast estuaries: A synthesis approach. *Global Biogeochemical Cycles*, *29*(1), 96-111.

Huxham, M., Whitlock, D., Githaiga, M., and Dencer-Brown, A. (2018). Carbon in the coastal seascape: how interactions between mangrove forests, seagrass meadows and tidal marshes influence carbon storage. *Current forestry reports*, *4*, 101-110.

Irlandi, E. A., and Crawford, M. K. (1997). Habitat linkages: the effect of intertidal saltmarshes and adjacent subtidal habitats on abundance, movement, and growth of an estuarine fish. *Oecologia*, *110*, 222-230.

James, R. K., van Katwijk, M. M., van Tussenbroek, B. I., van Der Heide, T., Dijkstra, H. A., van Westen, R. M., ... and Bouma, T. J. (2020). Water motion and vegetation control the pH dynamics in seagrass-dominated bays. *Limnology and Oceanography*, *65*(2), 349-362.

Jewett, L., and Romanou, A. (2017). Ocean acidification and other ocean changes. *Climate science special report: fourth national climate assessment*, *1*, 364-392.

Juska, I., & Berg, P. (2022). Variation in seagrass meadow respiration measured by aquatic eddy covariance. *Limnology and Oceanography Letters*, *7*(5), 410-418.

Khatiwala, S., Tanhua, T., Mikaloff Fletcher, S., Gerber, M., Doney, S. C., Graven, H. D., Gruber, N., McKinley, G. A., Murata, A., Ríos, A. F., and Sabine, C. L.: Global ocean storage of anthropogenic carbon, Biogeosciences, 10, 2169–2191, https://doi.org/10.5194/bg-10-2169-2013, 2013.

Koweek, D. A., Zimmerman, R. C., Hewett, K. M., Gaylord, B., Giddings, S. N., Nickols, K. J., ... and Caldeira, K. (2018). Expected limits on the ocean acidification buffering potential of a temperate seagrass meadow. *Ecological Applications*, *28*(7), 1694-1714.

Lewis, E., Wallace, D. W. R., 1998. Program Developed for CO2 System Calculations. ORNL/CDIAC-105. Carbon Dioxide Information Analysis Center, Oak Ridge National Laboratory, Oak Ridge, TN.

Lowe, A. T., Bos, J., and Ruesink, J. (2019). Ecosystem metabolism drives pH variability and modulates long-term ocean acidification in the Northeast Pacific coastal ocean. *Scientific Reports*, *9*(1), 963.

Millero, F. J. (2010). Carbonate constants for estuarine waters. Marine and Freshwater Research, 61(2), 139–142. https://doi.org/10.1071/MF09254

Najjar, R. G., Herrmann, M., Alexander, R., Boyer, E. W., Burdige, D. J., Butman, D., ... and Zimmerman, R. C. (2018). Carbon budget of tidal wetlands, estuaries, and shelf waters of Eastern North America. *Global Biogeochemical Cycles*, *32*(3), 389-416.

Neubauer, S. C., and Anderson, I. C. (2003). Transport of dissolved inorganic carbon from a tidal freshwater marsh to the York River estuary. *Limnology and Oceanography*, *48*(1), 299-307.

Oreska, M. P., McGlathery, K. J., Aoki, L. R., Berger, A. C., Berg, P., and Mullins, L. (2020). The greenhouse gas offset potential from seagrass restoration. *Scientific reports*, *10*(1), 7325.

Oreska, M. P., McGlathery, K. J., and Porter, J. H. (2017). Seagrass blue carbon spatial patterns at the meadow-scale. *PloS one*, *12*(4), e0176630.

Orth, R.J., Lefcheck, J.S., McGlathery, K.S., Aoki, L., Luckenbach, M.W., Moore, K.A., Oreska, M.P., Snyder, R., Wilcox, D.J. and Lusk, B. (2020). Restoration of seagrass habitat leads to rapid recovery of coastal ecosystem services. *Science advances*, *6*(41), eabc6434.

Orth, R. J., and Moore, K. A. (1986). Seasonal and year-to-year variations in the growth of Zostera marina L.(eelgrass) in the lower Chesapeake Bay. *Aquatic Botany*, *24*(4), 335-341.

Orr, J. C., J.-P. Gattuso, and J.-M. Epitalon (2015) Comparison of ten packages that compute ocean carbonate chemistry, Biogeosciences, 12, 1483–1510, https://doi.org/10.5194/bg-12-1483-2015 .
Orr, J.C., J.-M. Epitalon, A. G. Dickson, and J.-P. Gattuso (2018) Routine uncertainty propagation for the marine carbon dioxide system, in prep. for Mar. Chem., in press, https://doi.org/10.1016/j.marchem.2018.10.006.

Pacella, S. R., Brown, C. A., Waldbusser, G. G., Labiosa, R. G., and Hales, B. (2018). Seagrass habitat metabolism increases short-term extremes and long-term offset of CO2 under future ocean acidification. *Proceedings of the National Academy of Sciences*, *115*(15), 3870-3875.

Perez, F. F., and Fraga, F. (1987). Association constant of fluoride and hydrogen ions in seawater. Marine Chemistry, 21(2), 161-168.

Plumlee, J. D., Yeager, L. A., and Fodrie, F. J. (2020). Role of saltmarsh production in subsidizing adjacent seagrass food webs: Implications for landscape-scale restoration. *Food webs*, *24*, e00158.

Porter, J.H., DO. Krovetz, WK. Nuttle and J. Spitler. 2023. Hourly Meteorological Data for the Virginia Coast Reserve LTER 1989-present. Virginia Coast Reserve Long-Term Ecological Research Project Data Publication knb-lter-vcr.25.50 (doi:10.6073/pasta/406578baa2fd3f9ff39cd56379631a4a).

Redfield, A. C., Ketchum, B. H., & Richards, F. A. (1963). The influence of organisms on the composition of seawater. *The sea*, *2*(2), 26-77.

Reidenbach, M. A., and Thomas, E. L. (2018). Influence of the Seagrass, Zostera marina, on Wave Attenuation and Bed Shear stress within a Shallow Coastal Bay. *Frontiers in Marine Science*, **5**(OCT), 397. https://doi.org/10.3389/fmars.2018.00397

Reimer, J. J., Medeiros, P. M., Hussain, N., Gonski, S. F., Xu, Y. Y., Huang, T. H., and Cai, W. J. (2024). Carbonate Chemistry and the Potential for Acidification in Georgia Coastal Marshes and the South Atlantic Bight, USA. *Estuaries and Coasts*, *47*(1), 76-90.

Renzi, J. J., He, Q., and Silliman, B. R. (2019). Harnessing positive species interactions to enhance coastal wetland restoration. *Frontiers in Ecology and Evolution*, *7*, 131.

Rheuban, J. E., Berg, P., and McGlathery, K. J. (2014a). Ecosystem metabolism along a colonization gradient of eelgrass (Zostera marina) measured by eddy correlation. *Limnology and Oceanography*, *59*(4), 1376-1387.

Rheuban, J. E., Berg, P., and McGlathery, K. J. (2014b). Multiple timescale processes drive ecosystem metabolism in eelgrass (Zostera marina) meadows. *Marine Ecology Progress Series*, *507*, 1-13.

Ricart, A. M., Ward, M., Hill, T. M., Sanford, E., Kroeker, K. J., Takeshita, Y., ... and Gaylord, B. (2021). Coast-wide evidence of low pH amelioration by seagrass ecosystems. *Global change biology*, *27*(11), 2580-2591.

Rivest, Emily B., Margaret O'Brien, Lydia Kapsenberg, Chris C. Gotschalk, Carol A. Blanchette, Umihiko Hoshijima, and Gretchen E. Hofmann. "Beyond the benchtop and the benthos: Dataset management planning and design for time series of ocean carbonate chemistry associated with Durafet®-based pH sensors." *Ecological informatics* 36 (2016): 209-220.

Ruesink, J. L., S. Yang, and A. C. Trimble. 2015. Variability in carbon availability and eelgrass (*Zostera marina*) biometrics along an estuarine gradient in Willapa Bay, WA, USA. *Estuaries Coast.* **38**: 1908–1917. doi:10.1007/s12237-014-9933-z

Safak, I., Wiberg, P. L., Richardson, D. L., and Kurum, M. O. (2015). Controls on residence time and exchange in a system of shallow coastal bays. *Continental Shelf Research*, *97*, 7-20.

Schiebel et al., 2019
Sharp, J.D., Pierrot, D., Humphreys, M.P., Epitalon, J.-M., Orr, J.C., Lewis, E.R., Wallace, D.W.R. (2023, Jan. 19). CO2SYSv3 for MATLAB (Version v3.2.1). Zenodo. http://doi.org/10.5281/zenodo.3950562

Tamborski, J. J., Eagle, M., Kurylyk, B. L., Kroeger, K. D., Wang, Z. A., Henderson, P., and Charette, M. A. (2021). Pore water exchange-driven inorganic carbon export from intertidal salt marshes. *Limnology and Oceanography*, *66*(5), 1774-1792.

van Heuven, S., Pierrot, D., Rae, J.W.B., Lewis, E., Wallace, D.W.R., 2011. MATLAB Program Developed for CO2 System Calculations. ORNL/CDIAC-105b. Carbon Dioxide Information Analysis Center, Oak Ridge National Laboratory, Oak Ridge, TN.

Wallace, R. B., Baumann, H., Grear, J. S., Aller, R. C., and Gobler, C. J. (2014). Coastal ocean acidification: The other eutrophication problem. *Estuarine, Coastal and Shelf Science*, *148*, 1-13.

Wang, Z. A., and Cai, W. J. (2004). Carbon dioxide degassing and inorganic carbon export from a marsh-dominated estuary (the Duplin River): A marsh CO2 pump. *Limnology and Oceanography*, *49*(2), 341-354.

Wang, Z. A., Kroeger, K. D., Ganju, N. K., Gonneea, M. E., and Chu, S. N. (2016). Intertidal salt marshes as an important source of inorganic carbon to the coastal ocean. *Limnology and Oceanography*, *61*(5), 1916-1931.

Waycott, M., Duarte, C. M., Carruthers, T. J., Orth, R. J., Dennison, W. C., Olyarnik, S., ... & Williams, S. L. (2009). Accelerating loss of seagrasses across the globe threatens coastal ecosystems. *Proceedings of the national academy of sciences*, *106*(30), 12377-12381.

Wiberg, P. L. (2023). Temperature amplification and marine heatwave alteration in shallow coastal bays. *Frontiers in Marine Science*, *10*, 1129295.

Zhu, Q., and Wiberg, P. L. (2024). Effects of seasonal variations in seagrass density and storms on sediment retention and connectivity between subtidal flats and intertidal marsh. *Journal of Geophysical Research: Biogeosciences*, *129*(4), e2023JG007785.

Zhu, Q., Wiberg, P. L., and Reidenbach, M. A. (2021). Quantifying seasonal seagrass effects on flow and sediment dynamics in a back-barrier bay. *Journal of Geophysical Research: Oceans*, *126*(2), e2020JC016547.

Summary

Nearshore marine systems like intertidal salt marshes, lagoons, and seagrass meadows, are characterized by high variability in seawater inorganic carbon. These systems are important players in critical climate issues like carbon burial, acidification, and CO_2 air-sea gas exchange, but uncertainties and heterogeneity in seawater carbonate system dynamics obfuscate their roles. Quantification of carbonate system dynamics across a diverse patchwork of nearshore systems can provide insight into landscape scale variability and inorganic carbon connectivity. In the work presented in this dissertation, we demonstrate spatial and temporal trends in DIC, TA, pH, and pCO_2 across multiple nearshore ecosystems. Chapters 2 and 3 demonstrated that biogeochemical controls were prominent in the summer across lagoonal marsh adjacent sites and seagrass meadow sites, with probable contributions from both aerobic and anaerobic pathways. Hydrodynamic drivers, including water height and tidal fluctuations, resulted in varying mechanisms of seawater carbonate system change, including dilution and lateral exchange. Taken together, the monitoring of nearshore marine carbonate chemistry in the VCR reveals complex and seasonally mediated interactions of ecosystem metabolism, lateral exchange, and hydrologic drivers.